Loss Modeling in Non-Ideal Transmission Lines for Optimal Signal Integrity

vorgelegt von

Master of Science

Brian Curran

aus Milwaukee

Von der Fakultät IV – Elektrotechnik und Informatik

der Technischen Universität Berlin

Zur Erlangung des akademischen Grades

Doktor der Ingenieurwissenschaften

- Dr.Ing. -

genehmigte Dissertation

Promotionsausschuss:

Vorsitzender: Prof. Dr.-Ing. Thomas Sikora
Berichter: Prof. Dr.-Ing. Dr.-Ing. E.h. Herbert Reichl
Berichter: Prof. Dr.-Ing. A. Ege Engin

Tag der wissenschaftlichen Aussprache: 16 April 2012

Berlin 2012

D83

Acknowledgements

I have learned a great deal working on this dissertation over the last four years. Direct and moral support from many people enabled me to complete the work.

First, I would like to thank Professor Dr.-Ing. Dr.-Ing. E.h. Herbert Reichl for guiding my research, offering invaluable discussions and feedback, and reviewing the final work. I must also thank Professor Dr.-Ing. Ege Engin for your important contributions and review of the final work. Thank you Dr.-Ing. Ivan Ndip, an excellent researcher and supervisor, who guided the work in detail from beginning to end, offering advice and scrutiny at every step. I appreciate the support I received from Stephan Guttowski and the entire SDI Department and RSD Research Group, especially Uwe Maas, Gerhard Fotheringham, Robert Erxleben, and Florian Ohnimus who were always willing to lend and attentive ear when I had a new idea or question.

Much of the work was completed in association with projects funded by the Fraunhofer Society, in cooperation with Fraunhofer-IZM in Munich (now Fraunhofer-EMFT) and Fraunhofer-IFAM in Bremen. Additionally, Fraunhofer-IZM Abteilung SIIT also offered valuable assistance to research in this dissertation. Only with the competent and helpful colleagues from these research groups that prepared test structures and measurements was this work possible. I am also grateful for the funding from the Fraunhofer Society.

I must also thank my wife Mareen for her encouragement and support.

Abstract

The drive toward higher integration densities of electronic devices has led to smaller transmission line conductor sizes and compound dielectric structures with multiple lossy dielectrics. The desire for higher bit-rates, upwards of 100 GBits/s, has led to increased skin-effects, proximity effects, and dielectric losses. Losses in these transmission lines are often difficult to predict due to non-ideal transmission line cross-sections, including surface roughness, edge-shape effects, and moisture absorption in organic dielectric materials.

Therefore, in this work, a methodology for modeling the conductor in transmission lines is proposed that includes the edge-shape effects and surface roughness over a wide frequency range. First, it is shown that state-of-the-art models are deficient due to limitations in their bandwidths, flexibility, and computation times. A novel model, which models the direct current (DC) resistance, skin-effect, and proximity effect together with the edge-effects and surface roughness effects, is proposed called the Adapted Filament Method. By modeling these effects together, it is possible to model extremely non-ideal transmission lines (for example, lines produces with ink-jet printing processes) where the surface roughness is a significant proportion of the conductor thickness, edge-shape effects include very narrow angles, and each conductor surface has a different roughness profile. The proposed model extends the filament method by building an inhomogeneous conductivity toward the conductor surfaces. The Adapted Filament Model offers more accurate results than the state-of-the-art models over a larger frequency bandwidth with greater physical insight. It also models proximity effects together with surface roughness effects, which is a deficiency of nearly every other model. Due to its physical insight the model is also useful for evaluation of transmission line fabrication technologies because it can determine dominant loss mechanisms in given frequency ranges.

Furthermore, state-of-the-art techniques are investigated for modeling the dielectric losses in structures where several dielectric layers, with various characteristics, contribute to the losses. The most important composite dielectric modeling techniques were investigated to determine composite material dielectric loss characteristics. Based on these, a combination of modeling techniques is developed to analytically model a complex dielectric structure, including the effects of moisture absorption. The methodology was used to investigate, analytically, for the first time, the effects of moisture absorption on the high frequency characteristics of coplanar transmission

lines. This investigation showed an increase in dielectric losses and permittivity dispersion at low frequencies.

The conductor modeling approached were verified with high frequency measurements of coplanar transmission lines. The lines were fabricated with the before mentioned innovative ink-jet micro-printing process. The modeled results correspond to the measured results within a few percent. Three different transmission lines with different dimensions and metallization conductivities were measured and modeled up to 60 GHz. Modeling shows that, for a coplanar transmission line printed with an ink-jet printing technique, edge shape effects and surface roughness became the dominant loss mechanisms at around 5 GHz and accounted for 70% of the total losses at 20 GHz. When lower conductivity ink was used (approximately 1/5 of the previous), while the skin- and proximity effect losses increased, the surface roughness and edge-shape effects only accounted for 20% of the losses at 60GHz. The composite dielectric modeling techniques were verified for a lossy dielectric encapsulation material using planar interdigital capacitors up to frequencies of 110 MHz. It is shown that the effective permittivity and dielectric loss tangent of a composite dielectric are frequency dependent at low frequencies, but this dependency stabilizes at around 200MHz.

Finally, the dielectric and conductor modeling techniques were applied together to find the broadband transmission line characteristics of a coplanar transmission line. For a typical application, the combined modeling indicates low frequency dielectric losses and characteristic impedance dispersion that stabilizes around 1 GHz.

Key Words: conductor losses, skin-effect, proximity effect, surface roughness, filament method, dielectric losses, moisture absorption, Lichtenecker equation, composite dielectric

Zusammenfassung

Der stete Trend zu höherer Integrationsdichte elektronischer Systeme führt zur Realisierung von immer kleineren Verbindungsleitungen gepaart mit zusammengesetzten dielektrischen Strukturen, die aus mehreren verlustbehafteten Dielektrika bestehen. Das Bedürfnis nach höheren Bitraten, bis zu 100 GBit/s und mehr, führt zu stark ausgeprägtem Skin- und Proximity-Effekt sowie zu erhöhten dielektrischen Verlusten. Die Verluste dieser Verbindungsleitungen sind oft schwierig vorherzusagen auf Grund ihrer nicht-idealen Querschnitte, zum Beispiel auf Grund von Oberflächenrauigkeit und Ätzeffekten an den Kanten der Leiter, sowie in Folge der Feuchtigkeitsaufnahme in organischen Dielektrika.

Deshalb wird in dieser Arbeit eine Methodologie für die Leiterbahnmodellierung unter Berücksichtigung der Kanteneffekte und Oberflächenrauigkeit vorgestellt, die für einen ausgedehnten Frequenzbereich Gültigkeit besitzt. Es wird gezeigt, dass die derzeit verfügbaren Modelle verbesserungsbedürftig sind. Sie haben Einschränkungen bezüglich ihrer Bandbreite, Flexibilität, und Rechenzeit. Dazu wurde ein neuartiges Modell, das den Gleichstromwiderstand (DC), Skin- und Proximity-Effekt zusammen mit der Oberflächenrauigkeit und den Kanteneffekten berücksichtigt, entwickelt. Es wird im Folgenden als erweitertes Filament-Modell bezeichnet. Mit der gemeinsamen Modellierung dieser Effekte wird es möglich, extrem nicht-ideale Leiterbahnen (zum Beispiel solche, die durch ein Ink-Jet- Schreibverfahren hergestellt wurden) zu modellieren, bei denen die Oberflächenrauigkeit einen erheblichen Teil der Leiterdicke ausmacht, die Leiterkanten sehr kleine Winkel aufweisen, und die Rauigkeitprofile auf jeder Oberfläche verschieden sind. Das vorgestellte Modell basiert auf einer Erweiterung der Filament-Methode. Hierbei wird die Rauigkeit durch eine geänderte Leitfähigkeit an der Oberfläche berücksichtigt. Dieses Model bietet ein höheres Maß an Genauigkeit, eine größere Bandbreite, und liefert ein größeres physikalisches Verständnis als konventionelle Modelle. Das neuartige Modell verknüpft die Rauigkeitseffekte mit den Proximity-Effekten, was fast kein anderes Modell leistet. Auf Grund seiner physikalischen Transparenz kann dieses Modell zur Bewertung von Technologien für die Herstellung von Verbindungssystemen verwendet werden, weil es die dominanten Verlustmechanismen im interessierenden Frequenzband erkennen lässt.

Des Weiteren werden konventionelle Methoden für die Modellierung von dielektrischen Verlusten in elektrischen Verbindungsstrukturen mit mehreren und gemischten Dielektrika unterschiedlicher Verlusteigenschaften untersucht, insbesondere auch die wichtigsten

theoretischen Ansätze zur Beschreibung von Verbund-Dielektrika. Darauf fußend wurde eine kombinierte Vorgehensweise für die Modellierung dielektrischer Schichten, inklusive möglicher Feuchteaufnahme, entwickelt. Zum ersten Mal wurde ein analytisches und praktisch anwendbares Modell vorgestellt, welches die Effekte der Feuchtigkeitsaufnahme auf die Hochfrequenzeigenschaften von Koplanarleitungen beschreibt. Es wurde gezeigt, dass die dielektrischen Verluste und die Dispersion der Permittivität schon bei kleineren Frequenzen mit der Feuchtigkeit ansteigen.

Der Leitermodellierungsansatz wurde mittels Hochfrequenzmessungen an koplanaren Verbindungsleitungen verifiziert. Die Leitungen wurden mit einem innovativen Mikrodruckprozess, dem schon erwähnten Ink-Jet-Verfahren hergestellt. Die Messungen weichen von den Vorhersagen der Modellierung um weniger als drei Prozent ab. Drei koplanare Leitungen mit verschiedenen Dimensionen und Metallisierungen wurden gefertigt und bis 60 GHz vermessen. Die Modellierung zeigt, dass bei einer mit dem Ink-Jet-Schreibverfahren hergestellten Koplanarleitung Kanteneffekte und Oberflächenrauigkeit schon ab 5 GHz die dominanten Verlustmechanismen bewirken, welche bei 20 GHz 70% von den gesamten Verlusten ausmachen. Verwendet man für die Koplanarleitung eine Silbertinte mit niedrigerer Leitfähigkeit (ungefähr 1/5 der ursprünglichen), so steigen die gesamten Verluste, aber Rauigkeit und Kanteneffekte bewirken nur noch 20% der gesamten Verluste bei 60 GHz. Zudem wurde der dielektrische Modellierungsansatz für ein verlustbehaftetes organischen Verkapselungsmaterial bis 110 MHz verifiziert. Die Charakterisierung erfolgte durch eine Kapazitätsmessung mit Hilfe eines planaren Interdigital-Kondensators. Es wurde gezeigt, dass effektive Permittivität und dielektrischer Verlustwinkel von einem zusammengesetzten Dielektrikum bei niedrigen Frequenzen frequenzabhängig sind; aber diese Abhängigkeit stabilisiert sich bei ca. 200 MHz.

Schlussendlich wurden die beiden Modellierungsansätze bezüglich Leiter und Dielektrikum integriert und gemeinsam angewendet, um die Transmissionseigenschaften von Koplanarleitungen über einen weiten Frequenzbereich zu berechnen. Für typische Anwendungen ergibt die gemeinsame Modellierung dielektrische Verluste bei niedrigeren Frequenzen und eine Dispersion der Wellenimpedanz, die sich um 1 GHz herum stabilisiert.

Key Words: Dämpfung, Skin-Effekt, Proximity Effekt, Oberflächenrauigkeit, Filament Methode, Dielektrische Verluste, Lichtenecker Gleichung, geschichtete Dielektrika

Chapter 1: Introduction

1.1. Motivation and Goal

Recently, there has been a demand for compact, cheaper, and higher performance electronic products, particularly in mobility, energy, health care, security, and communications. Ultra-small sensor nodes, medical monitoring and implants, RFID systems, and wireless communications are just a few applications that will require higher performance electronics [1]. Not only IC technology, but also packaging and assembly all show the trend of greater miniaturization. As a result, new technologies such as thin-film, all-silicon-system modules, system-in-package (SiP), and micro-printing processes are becoming more and more commonplace [2, 3]. In these technologies, wire diameters, interconnects pitches, PCB metallization thickness, microvias, and wafer thicknesses will continue to decrease in size [4]. The speed of electronic products has increased as well, with data rates approaching 100 Gbps.

Decreased conductor dimensions will introduce conductor losses. These losses can be exacerbated by conductors with non-rectangular cross-sections that could previously be neglected. At high frequencies or bit rates, the skin-depth decreases below the thicknesses of thin-film conductors. These higher frequencies also mean that even small surface roughness profiles can affect the signal integrity of a structure. In some cases, environmental effects, such as humidity and temperature dependencies of low-cost encapsulation and underfill polymer materials introduce further complexity. These *non-ideal transmission line characteristics*, which had previously been neglected during the design and modeling process, must now be included to predict the response of modern structures to ensure signal integrity. *Non-idealities* in this work are defined as the following phenomena:

- Conductor cross-sections that deviate from the intended shapes
- Surface roughness profiles

- Composite dielectric effects as a result of moisture absorption

Designing these systems to be capable of supporting broadband signals, while maintaining signal integrity is a complex task. The losses that play a role in these systems have several different origins and ignoring attenuation sources can result in losses beyond an acceptable margin. Frequency dependency of the complex permittivity will lead to dispersion of the delay and reflections, eroding the signal integrity of digital broadband signals. Variations in permittivtiy and characteristic impedance can also change the levels of simultaneous-switching-noise and cross-talk. Long-term reliability problems can arise from humidity or temperature influences. A trial-and-error approach to this problem is impractical because it will significantly increase the length and cost of the design cycle and can lead to "over-engineering", where the full capabilities of the fabrications technologies are not utilized. Furthermore, it is difficult, expensive, and time consuming to determine and solve these problems in the testing phase of a product. And, if the problems are not found, the product can malfunction or fail. Therefore, it is imperative that a methodology is developed that predicts the influences of transmission line non-idealities during the design phase of a package. This comprehensive methodology would determine signal-integrity (SI) problems associated with the non-idealities in the pre-layout phase to prevent SI problems before they occur.

Therefore, it is the goal of this dissertation to produce a methodology for predicting the effects of the *transmission line non-idealities* previously listed for SiP modules, all-silicon-system modules, and other high density microelectronic packages. The will be done by building accurate and reliable models that predict the influence of *transmission line non-idealities*. The models will be validated with measurements and full-wave simulations. The validated models will then be used to determine the influence of the non-idealities and verify that their influence is not critical.

Chapter 2: Analysis of State-of-the-Art Models For Lossy Transmission Lines

2.1. Conductor Skin-Effect Modeling

The distribution of a direct current (DC) over the cross-section of a conductor can be considered uniform. However, due to an effect called the skin-effect, a majority of an alternating current (AC), will only penetrate into the surface of the conductor to a certain depth, known as the skin-depth (δ). When the skin-depth is much larger than the thickness of the conductor, the resistance of the conductor can be approximated as the DC resistance. When the skin-depth is smaller than the thickness of the conductor, the resistance of the conductor increases because the current flows through only a part of the conductor cross-section. Wheeler [5] first modeled the skin-effect of a conductor with method called *The Incremental Inductance Rule*. With *The Incremental Inductance Rule*, the resistance and inductance of a conductor are determined with skin-effect considered, sometimes called the high-frequency (HF) resistance and inductance. The increment of inductance decrease is subtracted from the DC inductance for the given skin-depth at a given frequency. Then the high-frequency resistance is calculated for that inductance decrease. In multi-conductor transmission lines, additional resistance that is created by conductors in the proximity of the circuit is also considered.

At low frequencies the skin-effect resistance of a conductor can be approximated as the same as the DC resistance (when the skin-depth δ is much larger than the conductor thickness t). As frequencies increase, the penetration depth will become smaller than the dimensions of the conductor. At this frequency point, the resistance gradually becomes frequency dependent, increasing proportionally to the square-root of the frequency. Other researchers, for example Pucel[6], and Gupta [7] have modeled the skin-effect resistance for isolated conductors (without

proximity effects) and microstrip lines in the region where the depth of penetration is much smaller than the metallization thickness. These models predict the skin-effect resistance and inductance by deriving approximations beginning with the Maxwell's Equations (the penetration depth can be derived directly from Maxwell's Equations).

These models are very simple and intuitive and ideal for understanding the skin-effect. However, in modern electronics, models that accurately characterize the characteristics of a conductor from low frequencies, across a corner frequency, and into a higher frequency range are necessary. It is also necessary to model the proximity effects to nearby conductors and the non-idealities of a conductor.

2.1.1. Frequency Domain Modeling Techniques

2.1.1.1. Planar Transmission Line Skin-Effect Modeling

In the following section, skin-effect models are divided into three general classifications, namely closed-form physical, filament, and full-wave.

I. Closed-Form Physical Models

Derivations from Maxwell's equations and the *incremental inductance rule* (where the surface resistance is calculated by approximating a finite-thickness where the current propagates) have led to variations of analytical equations for the skin-effect resistance and inductance for various transmission line structures. He [8], for example, offers a method to compute the per-unit-length parameters of a microstrip line including material dispersion. A complete set of equations for the circuit parameters of parallel plate, microstrip, and stripline transmission lines are presented by Jianmin in [9] which were reconstructed using genetic algorithms, designed to include material dispersion. These equations have limitations in their bandwidth and accuracy, especially at the corner frequency – where skin-depth is equal to conductor thickness. These models are also limited in their implementation. For example, the He model only gives accurate results when the height of the microstrip is at least half of the width, and still varies from the more accurate filament model (which will be discussed in the next section) by up to 10%, as shown in Fig. 2.1.

Analytical models normally model the skin-effect only in the region where the thickness of the conductor is larger than the skin-depth, which can be thought of as R_{AC}. However, Hall [10], describes a method by which the R_{DC} and R_{AC} can be modeled together by taking the square root of the sum of their squares. This method is used to generate the He and Wheeler plots in diagram 2.1. Even within their bandwidth, their accuracy is questionable because they show discrepancies when compared to each other and other more accurate models. Two analytical skin-effect models deviate by as much as 20% from a more accurate filament model, even within their functional frequency band.

The traditional and most simplistic conductor models assume that the conductors have perfect rectangular or circular cross-sections. For planar conductors this is often not the case. The fabrication techniques can often lead to transmission lines that are trapezoidal or have rounded edges. In this work, *edge shape effects* are defined as edges of planar conductors that do not have right angles; they are either rounded or trapezoidal. Some efforts have concentrated on an analytical approach to transmission lines with *edge shape effects* – meaning that the conductor edges are not right angles. For example, Barsotti [11, 12] developed a method for calculating transmission line parameters for trapezoidal or rounded transmission lines with correction factors for "edge shape effects" using a modified incremental induction rule. This technique uses the assumption of a surface impedance boundary condition. There have also been attempts to characterize transmission lines with trapezoidal cross-sections by using Schwarz-Cristoffel conformal mapping techniques [13, 14]. Guo [15] offers an analytical approach for modeling non-rectangular conductors, but limited to conductors with trapezoidal cross-sections. The conformal mapping techniques have been successful in characterizing transmission lines, however, the characterizations seem impractical for application in circuit simulations for various reasons. In some cases they have no closed-form solution or only a very complex quasi-closed form solution and the equations are so large and complex they offer no insight into the relationships between parameters. Their error margins and bandwidth are unknown because many have not been verified by measurements. Furthermore, the existing models are limited to certain conductor geometries and cannot be applied to arbitrary profiles.

II. Filament Methods

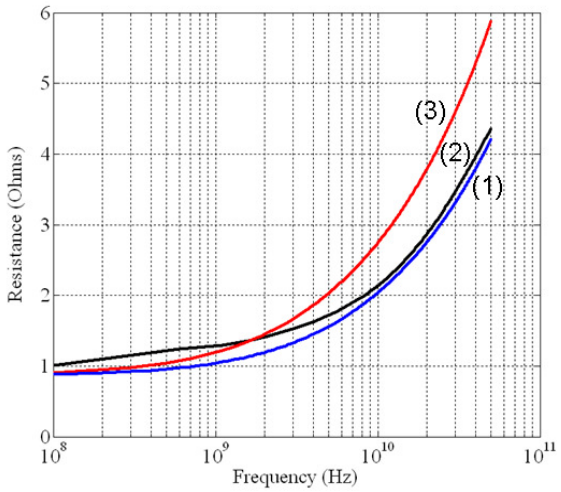

Fig.2.1. A comparison of (1) The He microstrip model (w = 10 µm, t = 2 µm, h = 8 µm), (2) The VuDinh filament model, (3) The Wheeler

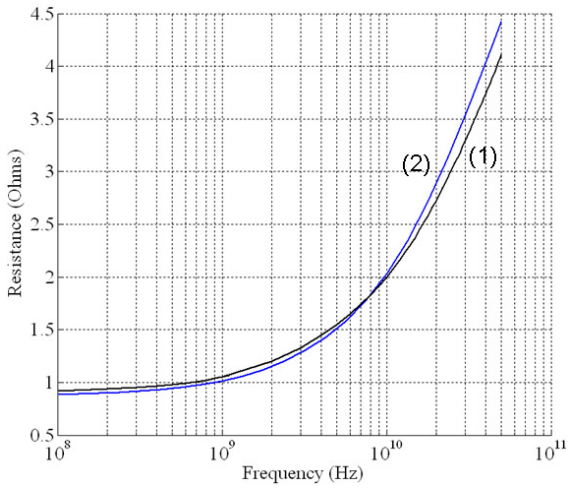

Fig. 2.2. A comparison of microstrip resistance (w = 10 µm, t = 2 µm, h = 8 µm), (1) The VuDinh filament model, and (2) A full-wave simulation using Ansoft High-Frequency Structure Simulator.

To address the limitations associated with bandwidth and proximity effects in the aforementioned models, and to improve the overall accuracy, methods have been developed that discretize the cross-section of a conductor and solve for the current within each discrete section. These models are often called filaments models. For each filament of the cross-section a resistance and an inductance are calculated, as well as mutual inductance between it and all of the other filaments. The mutual-inductances shut off the current flow in the center conductors as the frequency increases, leaving only outside layers for the current to flow. A ladder circuit can be calculated to determine the impedance at a given frequency.

VuDinh in [16, 17] developed a model that discretized the cross section of a microstrip line for both an infinite and finite ground plane respectively. Weeks [18], also proposed a filament model very similar to the Vu Dinh model. Coperich and Ruehli use a similar discretization method, using filaments and faces, to model the skin-effect and proximity effect in conductors [19]. Mei and Ismail [20] use the same concept for modeling an isolated conductor. They also extend the model by using model order reduction techniques to create a partial-element equivalent circuit ladder of only a few components so that the model could be implemented in SPICE simulations. Then, in [21], they extend the model to coplanar and coupled transmission lines. The model order reduction techniques are explained in greater detail in [20]. Their proximity effect model

can theoretically also be applied for conductors with certain non-rectangular cross-sections. Hua [22], extends the Mei model to coplanar lines with a curved cross-section; for example, a line printed on a cylinder. De Zutter tries to simplify the filament model by replacing sections of the conductor with dielectric in the model [23]. Mido attempts to simplify the filament model mathematically by approximating the cross-section of a conductor into many round filaments [24].

The filament models solve the problem of modeling the corner frequency (where the metal thickness is the same as the penetration depth). However these models require some alteration to identify the problem of skin-effect in arbitrary conductor cross-sections. The models also do not consider surface roughness. Applying these models to non-ideal conductor geometries is theoretically possible but has not been validated through measurement and published to date. For very high frequencies and larger geometries, a filament model cannot easily be used for circuit level time-domain simulations because it is too large and leads to very large computation times. One alternative is to apply model order reduction techniques to reduce the model to a more reasonable size. The model-order-reduction techniques in [20, 21] reduce the model to 1/10 the number of components, however, the model-order-reduction introduces slight inaccuracies of 2-6% at high frequencies (30 GHz and above). When compared to full-wave simulations, in Fig. 2.2, the filament models are accurate within 0-10% over the entire frequency range. The computation time for these models is between 1 and 6 minutes without any model order reduction.

The way a filament model is discretized will also have an effect on the accuracy of the results. At the highest frequency, the filament size must be smaller than the skin-depth to achieve better than 5% accuracy. As an example, the skin-effect resistance in a 20 μm x 2 μm rectangular conductor was calculated using the Vu Dinh filament method. The conductor was discretized as shown in Fig. 2.3 (a), where the cross-section was divided into rectangular filaments. The filaments were then arranged in a ladder circuit, shown in Fig. 2.3 (b), to compute the skin-effect resistance and inductance of the circuit. The resistance is shown in Fig. 2.3 (c). In this example, the smallest and second smallest discretization (black line and blue line) converge at around 20 GHz, where the skin-depth is around 0.47 μm - twice the larger discretization. Based on that, it is assumed that when the discretization size is half the skin-depth, the inaccuracy is negligible.

Comparing the curves then at 60 GHz, it becomes clearer how much inaccuracy increasing the size of the rectangles in the discretization introduces into the model. When the discretization size is approximately the same as the skin-depth, about 5% inaccuracy will be introduced. At 50% larger than the skin-depth, it exceeds 10%.

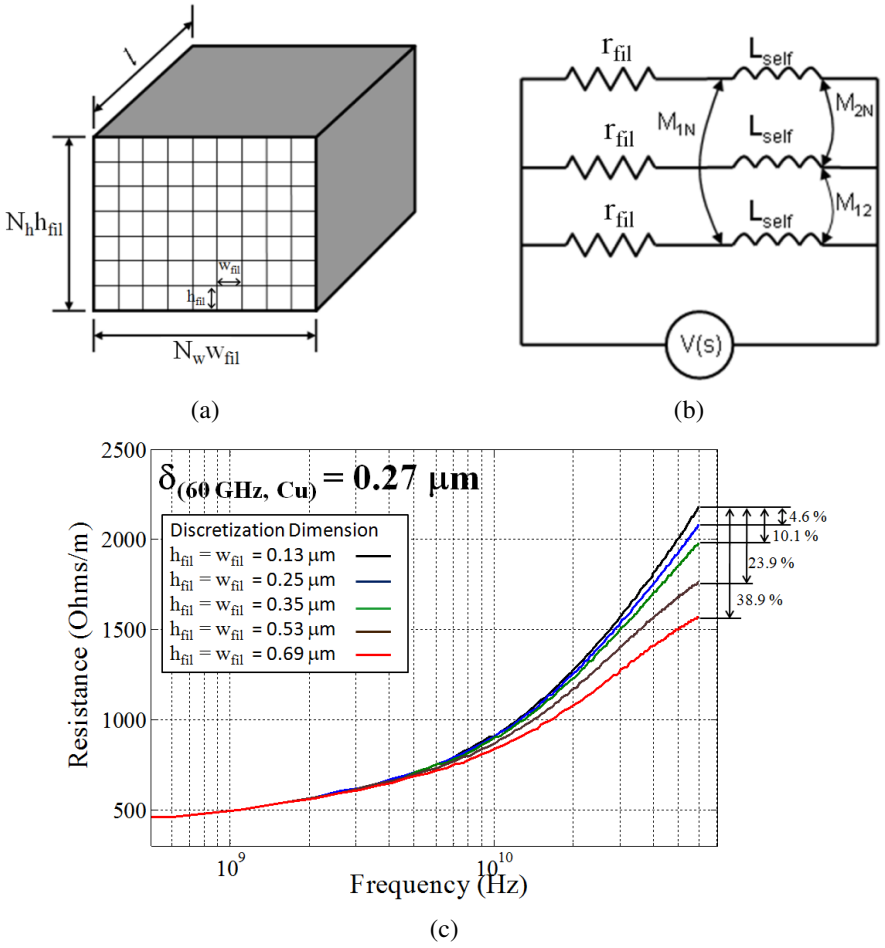

Fig. 2.3. Filament method, (a) conductor discreitzation, (b) ladder circuit, (c) skin-effect resistance for various dicretization sizes.

III. Full-Wave Numerical Models

The most accurate models for skin-effect modeling are full-wave numerical models because they solve the Maxwell's Equations for a specific structure without any quasi-static assumption. Full-wave models discretize a 3D design of a structure, generate a mesh, and then solve for Maxwell's Equations at every point in the mesh. Wang uses the Finite-Difference-Time-Domain (FDTD) technique to model the skin-effect [25]. The finite-element method was used by several authors in [26-29]. Tsuk uses a hybrid approach that calculates the low frequency resistance and inductance

with a filament approach and the high frequency parameters with a full-wave surface integral approach [30]. Wlodarczyk has also modeled the skin-effect using the boundary element method [31]. The results are compared to analytical approaches. All of these methods are very accurate and can usually be used for arbitrary cross-sections. They are, however, very time intensive. For example, the full-wave simulation for curve Fig. 2.2 (2), which was created using Ansoft HFSS which uses the Finite Element Method (FEM) method, required nearly one hour of computation time plus time to build the 3D model. And, for very complex structures, commercial full-wave simulation software may take hours or not successfully generate results because of computational limitations. These methods only apply correction for surface roughness with analytical models. They are limited then by the accuracy of the analytical surface roughness equations. It is difficult to simulate small angles (like those in some edge-effects) or large width to thickness aspect ratios with 3D numerical techniques. For small edge-effects, the mesh must be smaller than the angle, which requires a very fine mesh. For large aspect ratios, the mesh must be smaller than the height, which then requires a large mesh to span the entire width. Full-wave techniques also offer no insight into the physics of the structure. There is no clear relationship between circuit parameters and the results which can make troubleshooting and optimization difficult.

2.1.1.2. Circular Transmission Line Skin-Effect Modeling

As with planar transmission lines, analytical equations with similar limitations have been established using the incremental induction rule for the transmission line parameters of coaxial and two-wire transmission lines. Ulaby outlines some of these models in his book [32].

Skin-effect modeling of vertical interconnects requires a slightly different approach because the conductors have a circular cross-section and cannot be discretized into rectangular filaments. An alternative approach is to discretize the elements in layers radially. Yen [33] developed a model that discretizes the cross-section of a coaxial transmission line along the radius, creating a series of concentric rings. Each ring has a resistance, inductance, and mutual inductances to the other rings. Kim and Neikirk build a similar ladder circuit for coaxial transmission lines and other lines with circular cross-sections [34]. These models follow the same concept as the filament models in the previous section. However, for circular conductors, the concept has been

simplified by discretizing the transmission line into layers in the radial direction, then finding resistances and inductances for each layer. A very similar approach is made by Sen [35]. Sen's and Yen's approaches have the added advantage that they can also be used to generate PEEC models that can be implemented into circuit simulators.

The limitations are similar to those from the previous section, these models do not account for deviations in the shape of the cross-section or surface roughness on the conductors. The models are also bandwidth limited and often limited in implementation.

2.1.2. Time Domain Modeling Techniques

Time-domain modeling is important for high-speed digital products because the time-domain is where performance is ultimately measured. It is valuable to develop a circuit model for an interconnect that can be implemented in large scale circuit simulations. Three categories of time-domain skin-effect modeling are discussed in this section. These categories are inverse Fourier Transform techniques, physically based time-domain models, and non-physical analytcial models.

I. Inverse Fourier Transform Techniques

An approach that has been used in the past to model conductor losses in time-domain is to conduct all of the analysis in frequency-domain, then convert the signals to time domain using an inverse Fourier Transform. This technique was evaluated by Griffith [36], Djordjevi´c [37], and Schutt-Aine [38]. Dawoud uses a frequency dependent resistor to reduce the complexity of a Fast Fourier Transform (FFT) computation [39]. The techniques are accurate but are very expensive in terms of computation. The number of computations for a discrete Fourier Transform is N^2 and NlogN for a FFT (a FFT, however, requires a symmetry in the response), where N is the number of points. A second problem with this approach is that these responses cannot be implemented or scaled in a circuit simulator because no equivalent circuit is constructed – all computation is done in frequency domain and converted.

II. Physically Based Time Domain Models

A physically based time domain model builds a lumped element equivalent circuit, using the physical parameters and dimensions of the structure, to model the parameters of the conductor. This circuit is then implemented alone or as part of a larger circuit in a circuit simulator. A reduced filament model, for example, would fit into this category because it is physically based yet small enough to implement in a circuit simulator. Kopcsay proposes a very simple skin- and proximity-effect model that includes coupling between return current paths and adjacent transmission lines [40]. This model, however, is only adequate for single frequencies or very small frequency bands because the transmission line parameters are treated as constants. The model from Yen mentioned in the previous section is also a physical model that is implementable directly as a lumped element equivalent circuit [33]. Another frequency-domain model that can also be directly implemented in SPICE is the model from Mei, but it can normally only be implemented in SPICE for the gigahertz frequency range if model order reduction techniques are used, or else computation times become too long [20, 21]. The model from Coperich and Ruehli also includes model order reduction techniques so that it can be directly implemented in SPICE [19]. Vu Dinh has published an additional paper that applies his previous technique, at low frequencies without a model order reduction technique, in time-domain simulations including proximity effects to return current paths and adjacent transmission lines [41]. Kamon describes a generalized model order reduction technique that can be applied to all filament models with a uniform resistance in [42] and the more rigorous "Krylov-Subspace Model Order Reduction Technique" in [43] that can reduce models on the order of 10,000 to less than 10. There has also been some success modeling the skin-effect in the time-domain with a method called the "difference method" [44-46].

When these models are directly implemented as equivalent circuits, then the number of components grows as their bandwidth and accuracy increases. The model order reduction requires mathematical approximations that add inaccuracy. In the publications, the inaccuracy is completely negligible at low frequencies and climbs up to around 3-6% at higher frequencies (around 30 GHz). However, there was no examination of the accuracy of the model order reduction techniques as the model is further and further reduced, over large frequency bands, or with frequencies higher than 30 GHz. The reduced models are also not scalable after they are reduced.

III. Non-Physical Models

A non-physical model also creates a lumped element circuit model. The difference between the non-physical and physical models is that the non-physical models are not based directly on the physical aspects of the conductor and only mimic a response from a physical model so that it can be implemented as a lumped element equivalent circuit. A model called the "Continued Fraction Expansion Method" (CFE) can be used to accurately mimic a frequency domain response [47, 48]. A similar method is presented by Roy in [48] called the "Rational Polynomial Approximation" method. A method called the "Non-Uniformly Discretized-π Model" can also be used [49]. A. E. Engin provides a more in-depth investigation into these three methods in his publications [50] and [51]. Neikirk and Kim also propose a ladder model that can mimic frequency-domain response to a high accuracy [34]. This model uses a curve-fitting loop to generate ideal coefficients to match the desired measured or computed response.

As an example, the lumped element equivalent circuit model for the CFE method is shown in Fig. 2.4, where R_{ac} is the high frequency resistance at a given point f_{ac}. At low frequencies, the largest inductor (farthest left) approaches an short circuit and we only see the DC resistance. As the frequency increases, first the largest inductance L/3, then the smaller inductances (L/7, L/11, and so on) behave more and more like closed circuits, increasing the resistance to mimic the high frequency resistance of the conductor.

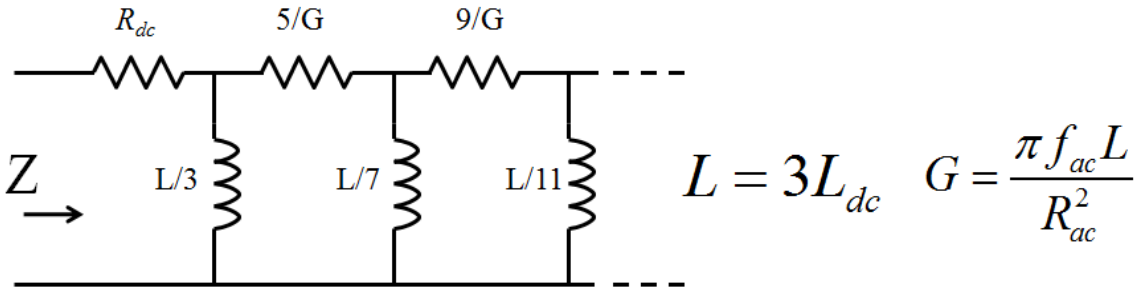

Fig. 2.4. Lumped element equivalent circuit from the CFE method.

IV. Summary

Model order reduction always introduces some inaccuracy. Likewise, using the CFE or similar methods to approximate a response will also add inaccuracy into the simulation, especially in the region of the corner frequency, which may contain the transmission frequency. That being said, generally these are negligible deviations; their deviation can easily be less than 3% over their given frequency ranges. As with the model order reduction techniques, the number of components increases as the accuracy and bandwidths increase. Unlike the reduced filament models, models like the CFE and Rational Polynomial are scalable.

2.2. Surface Roughness Modeling

In the following paragraphs, modeling of surface roughness on transmission lines will be discussed. These models have been categorized into three main types: correction factors, effective parameters and full-wave simulations. After the third technique, some other surface roughness research activities that do not qualify as one of these categories are briefly discussed. Finally, an important state-of-the-art technique for determining skin-effect resistance and inductance including surface roughness is discussed. Limitations are then summarized.

I. Accounting for Surface Roughness with Correction Factors

Until now, most surface roughness modeling in the frequency domain has used analytical equations that make a correction factor K. The correction factor, a function of skin-depth and root-mean-square (RMS) surface roughness depth, is multiplied by the attenuation to determine a more accurate attenuation including surface roughness. Four of these correction factors are compared in

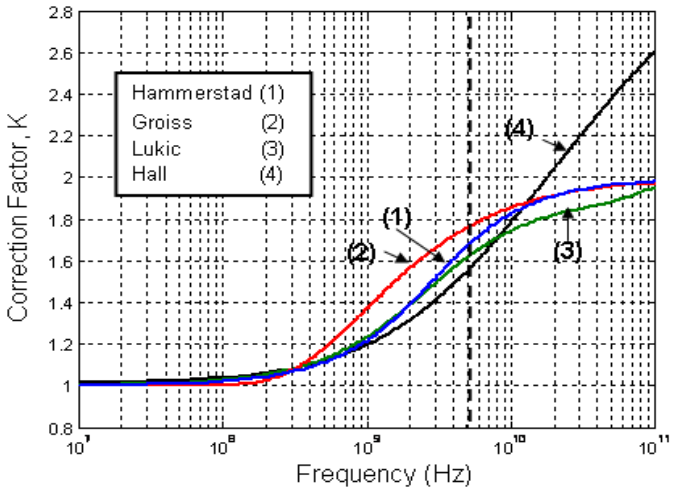

Fig. 2.5. Comparison of state-of-the-art surface roughness correction factors for roughness height of 1 μm in copper.

Fig. 2.5. The first of these correction factors was proposed by Hammerstad and Jensen [52]. This surface roughness factor accounts for the roughness by calculating an increased transmission line length that the current must flow (as it flows up and down through roughness ridges) above the frequency where the skin-depth is smaller than the surface roughness height. A similar correction factor presented by Groiss in [53] provides similar results and is sometimes used in commercial full-wave solvers including Ansys High Frequency Structure Simulator (HFSS) [54]. Stephen Hall presents a new analytical equation for the surface roughness that models the conductor surface as half ellipsoids protruding from flat rectangles [55]. The Hall equation is more accurate over a wider bandwidth but it is harder to implement because more geometrical factors have to be determined from the profile measurements of the conductor and the accuracy may only be for that specific surface roughness profile. Luki´c proposes a computer generated analytical equation that mimics results from full-wave simulations [56]. This equation is also more accurate over a slightly larger bandwidth. This equation, however, is only valid for the specific profile used in the full-wave simulations. As with all analytical approaches, these equations are bandwidth limited. A designer cannot apply different surface roughness profiles to the different faces of the conductor (in the presence of proximity effects, for example) because these correction factors are designed for the attenuation over the entire boundary.

II. Accounting for Surface Roughness with an Effective Parameter

Hall offers some alternative possibilities to characterize surface roughness in conductors by replacing a parameter of the conductor with an effective parameter that accounts for surface roughness. One possibility is to use an effective skin-depth. Skin-depth is normally inversely proportional to the square-root of the frequency. Hall suggests that it is made proportional to a slightly higher power than ½. Another suggestion is to use an effective dielectric loss tangent that is higher than the actual material dielectric loss tangent. These methods are all frequency invariant and, therefore, they will have significant inaccuracies for broadband applications. A surface roughness model must consider the frequency dependent behavior of the losses for broadband investigations [57]. Another non-traditional approach comes from Proekt. Proekt has built a formula for a frequency dependent effective conductivity of the conductor to account for surface roughness through the application of perturbation theory to find the solution for the electromagnetic fields in the vicinity of the surface roughness [58]. The model is very mathematically intensive and there is no measurement data to verify its accuracy.

III. Accounting for Surface roughness with Full-wave Simulations

Luki´c [56] and Chen [59] have presented methods to characterize surface roughness using full-wave simulations. In both cases, 3-D boxes of conductor with a surface roughness profile were simulated. Luki´c compares different types of surface roughness, specifically pyramid, hemispherical, and cubical roughness profiles. Chen simulates a pyramid profile for a specific application. While these methods can accommodate different types of surface roughness, unlike the previous methods, they are non-analytical and, in their respective publications, were only used to compare the different profiles. Applications of these full-wave techniques to transmission lines in a generic way to quantify the TML parameters have not been presented. Additionally, full-wave simulations are computationally very time consuming, in some cases taking several hours to simulate one transmission line.

IV. Miscellaneous Investigations of the Surface Roughness Effect

El-Shenawee has developed a technique designed to account for surface roughness of the dielectric under a microstrip by using an effective transmission line height based on the RMS height of the surface roughness [60]. Huray has developed an analytical model to predict additional losses from a "snowball" effect – roughness consisting of groupings of tiny spheres of conductor – with good matching to measured results [61]. Quan Chen uses stochastic integral equations to determine the effect of surface roughness if it has a random profile [62, 63]. With all of these methods, the bandwidth limitations are unclear. And, in [61-63], none of the methods were verified with measurement. Various researchers have applied the existing techniques for various applications or compared existing surface roughness techniques. Applications of the classical analytical formulas for surface roughness are compared to different types of copper foils with different roughness profiles in [64]. In [64] and [65], techniques are also discussed for reducing surface roughness during fabrication. Han uses the analytical formulas to characterize transmission lines,

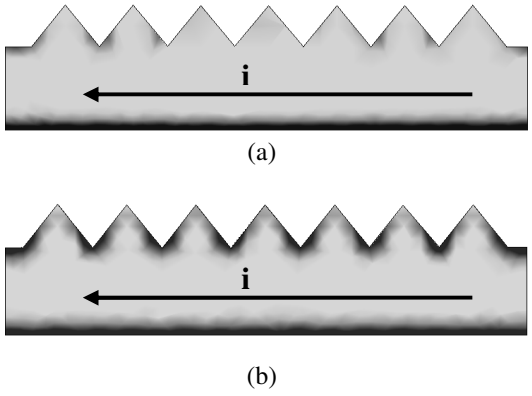

Fig. 2.6. (a) Current distribution when h = (1/3)w, (b) Current distribution when h = 3w.

including comparisons between measured fabricated transmission lines [66]. Henry [67] conducts an analysis of transmission line losses where he determines the percentage of losses from surface roughness. Chan includes surface roughness in his analysis of losses due to non-ideal effects, along with other factors like moisture effects and dielectric frequency dependence [68].

V. Time Domain Surface Roughness Modeling

Finally, Liang and Hall have published a very simple method to include surface roughness effects in the calculations of per-unit-length inductance and resistance of the conductor with frequency dependent correction factors for per-unit-length resistance and inductance for frequency domain modeling. In their technique, the HF resistance and inductance are modeled with other traditional modeling techniques [69]. While this is a step in the right direction, Liang uses the same analytical formula proposed by Hammerstad to modify the skin-effect and state-of-the-art skin- and proximity effect models. Therefore, the initial skin-effect and surface roughness models may not accurately model the skin-effect, especially at the corner frequency. That being said, the same technique could be applied to other frequency domain skin-effect resistance and inductance models to address the same problem.

VI. Summary

To summarize, some limitations of state-of-the-art surface roughness models are:

- All of the analytical models are bandwidth limited. For example, the Hammerstad model saturates as low as 5 GHz (depending on RMS surface roughness height). The Hall model extends this to around 30 GHz but only with a cost in implementation limitations and complexity [55].
- These models only account for the high frequency impact of surface roughness. Naturally, a surface roughness profile that penetrates a considerable distance into the conductor in comparison to the thickness of the conductor will also influence the DC and low frequency resistance of the conductor.
- Another limitation is that these models are not flexible enough to address different types of surface roughness profiles - different technologies may result in different surface roughness shapes.

- The state-of-the-art models are not capable of analyzing different surface roughness penetration depths on different faces of the conductors. This limitation is important because of the impact of proximity effects. In Fig. 2.6, microstrips with a strong and a weak proximity effect are compared. The distribution of the current in the conductor is strongly affected, meaning that a roughness that is only present on the top surface of the conductor will have a stronger impact when there is a smaller proximity effect. This limitation if further quantified in Chapter 3.
- The current surface roughness models do not account for surface roughness profiles on a return current path conductor.
- The final limitation identified of state-of-the-art surface roughness modeling is that it has, until now, exclusively focused on the effects of surface roughness on the conductor attenuation of a transmission line (with the exception of a small amount of research from Hall that included inductance). Modeling the effects of surface roughness on the characteristic impedance, delay, and inductance would be a valuable contribution to conductor modeling.

2.3. Dielectric Modeling

In multi-conductor transmission lines, current is attenuated in the dielectric material as well as in the conductor due to conductivity and high frequency loss characteristics of the dielectric material. Therefore, an examination of transmission line losses must also include dielectric losses.

Dielectric losses are dependent on the material characteristics of the dielectric, particularly the complex frequency dependent permittivity, ε, which is usually divided into relative permittivity, ε_r, dielectric loss tangent, $\tan(\delta)$, and conductivity σ. These characteristics are frequency dependent. The frequency dependence of the dielectric parameters is relatively well understood. Hammerstad presents an expression for the frequency dependence of the dielectric constant in [52]. This equation is further discussed by Liang in [69].

2.3.1. Frequency Domain Modeling Techniques

Conformal mapping techniques and derivations from Maxwell's Equations have been used to analytically model the dielectric losses of a transmission line. Consequently, analytical equations for the dielectric attenuation for different transmission line structures are also available in various publications. Chan conducts an investigation into stripline losses, which includes an equation for the dielectric losses [68]. Han presents an equation for the dielectric attenuation in a microstrip line [66]. Haydl conducts an investigation of coplanar and microstrip transmission line losses and presents analytical formulas for the galvanic dielectric attenuation for each structure [70]. In his book, Gupta also presents analytical equations to predict the attenuation from the dielectric in microstrip and slotline structures [71]. Wadell has created a very complete compilation of equations for the dielectric losses in many transmission line structures in [72].

These limitations of analytical dielectric models have been identified as:

- Analytical expressions for the dielectric losses are not available for every type of geometry.
- As with all analytical equations, they are bandwidth limited and assumptions are made that limit the accuracy (for example, they often assume that the conductor is infinitely thin or a perfect electrical conductor).
- Another limitation of these models is that they usually do not identify the situation of heterogeneous dielectrics, but especially heterogeneous dielectrics where the conductivity, dielectric loss tangent, and permittivity are all different. In these cases, the effective permittivity and the losses will be frequency dependent. Situations may arise in modern structures where a transmission line has several dielectric layers.

At this time, the only effective way to predict the response of these structures is through full-wave simulations. Full-wave simulations offer no physical insight into the dependencies between the geometry and response of the structure. Thin layers (for example, the SiO_2 layer often present in silicon and glass structures), although they can have a large effect on the response, can lead to long computation times and require a good understanding and attention to the construction of the 3D mesh to achieve an accurate and credible result.

2.3.2. Composite Dielectric Modeling Techniques

A composite dielectric is a dielectric with different materials, sometimes called phases, mixed into a composition. A common example in microelectronics is when moisture is absorbed into an organic dielectric. A two-phase water and polymer composite dielectric results.

It is widely known that organic dielectrics absorb water when they are kept in environments with high temperatures and humidity. Absorption of fluids into a dielectric was examined in [73]. The uptake and saturation levels were determined for various structures on FR4 epoxy with a FEM full-wave simulation and verified with measurements. The results are limited to 80°C and 85% Relative Humidity (RH) and show that the absorption is strongly dependent on the dimensions and metallization of the printed circuit board (PCB). The effects of moisture and temperature absorption on the dissipation factor, resistance, breakdown voltage, and relative permittivity for polyamide and other organic dielectric materials is shown in [74-78]. A study by Zhao shows the effect of moisture on the deterioration of the dielectric permittivity [79]. A study by Jujian investigates moisture induced breakdown and failure in dielectrics [80, 81]. Studies have also studied the effects of moisture on the mechanical properties, for example [82-84]. One concern that has been identified regarding moisture absorption is that moisture will settle on an interface between two dielectrics as the difference in expansion coefficients will form delamination and adhesion loss at the interface. This phenomenon was investigated in [85]. Monitoring of the phenomenon with a method to test the stress of a module is presented in [86]. A technique to reduce this effect was presented by Fan in [87].

The effect of moisture absorption on dielectric properties has also been a topic of research activities. The Wiener Limits say that for a dielectric composite, there are two extreme limits for the permittivity, which represent full isotropy horizontally and vertically. This is discussed in greater detail by Chowari, et. al. in [88, 89]. For example, Chan discusses an equation for the absorption dependent permittivity in [68]. Goncharenko [90] does an analysis of the state-of-the-art techniques for determining the effective permittivity when moisture is absorbed into a dielectric.

$$\varepsilon_{eff}^{\ k} = \theta\varepsilon_1^{\ k} + (1-\theta)\varepsilon_2^{\ k} \qquad \text{Eq. 2.1}$$

The Lichtenecker Equation, Eq. 2.1, is the most commonly used method. In fact, other published models can usually be simplified to this equation. The Lichtenecker equation is essentially a technique for averaging the complex permittivities of the moisture, ε_1, and the organic substrate, ε_2, dependent on a material parameter, *k*, that is related to the isotropy of the fluid in the dielectric (transitioning from -1 for entirely horizontally isotropic, 0 for anisotropic, and +1 for entirely vertically isotropic). It is averaged according to the volume fraction of moisture in the dielectric, θ. The results is an effective permittivity, ε_{eff}.

A further theoretical analysis and justification is offered by Zakri in [91] and a derivation from Maxwell's equations is presented in [92]. Kärner [93] uses the Lichtenecker Equation and theoretical absorption prediction, based on a Fick Model, to predict the relative permittivity over time. He compares the results of measurements and achieves very good correlation using this method. The Looyega model can be simplified to the Lichtenecker equation with the isotropy constant, k, of 1/3. It has been shown that the Looyega model is appropriate for composites that are porous and isotropic. The model is often used when water is the primary material and is discussed in more detail in [94-96].

State-of-the-art composite dielectric modeling, in general, has also been studied. The Mawell-Garnett theory is also used in published literature to determine the characteristics of a mixed composite. The formula is often used during analysis of mixtures where granulated media is the primary material, for example in the study from Robinson [97] or in mixtures where water is the primary material [98]. The model was also discussed in [90, 94, 99]. The Maxwell-Garnett model, treats two materials as a primary material and an infused material, and is based on an approximation that the primary material has suspended spheres of the infused material creating a composite mixture. The model is often used for the determination of optical parameters and shows limitations when the composite materials have a comparable ratio [100].

The Bruggeman model is also used to determine characteristics of composite materials. This model is demonstrated in [94, 100, 101]. The Bruggeman model is used when there are mixtures

of two or more different interdispersed materials. The model does not distinguish between the different materials as the absorber – absorbed, and therefore is often used when the mixtures have comparable percentages of both materials. The Bruggeman model also accounts for the phenomenon of grains of the material linking and forming chains in the composite, known as percolation.

A full-wave simulation method to determine the inhomogeneous absorption rates of an organic dielectric are shown in [73, 102]. A similar investigation is shown in [103]. This model was presented as a way to determine the amount of liquid absorbed in the dielectric material at different times of immersion in an environment. This is important because during the absorption process, the fluid absorbs from the outside inward. Therefore, the skin of the conductor could have a higher moisture concentration that the center. It is also possible that, when the metallization has a high aspect ratio of width to substrate height, that the moisture absorption arrives at an equilibrium and never reaches the area under the center of the metal.

Research has also examined the effects of temperature in dielectrics. For example, Jacob in [104] presents information based on measurements for various high frequency dielectrics dependent on temperature. The temperature and frequency dependency of the permittivity for organic substrates with certain impurities added is presented in [105]. A measurement method for the complex permittivity of dielectrics up to 1400°C is introduced in [106]. The effects of thermal aging, both electro-thermal and normal thermal was investigated in [107]. This study shows the effect of thermal aging on the permittivity and the loss tangent of epoxy resins.

The following problems remain:

- While the effect of humidity absorption on the permittivity of a material has been widely studied, as well as thermo-mechanical properties, the effect of humidity on transmission line parameters (α, β, Z_o, and crosstalk) has not been investigated.
- Water is known to have conductive properties but these properties are not understood across broad frequency bands when water is absorbed into an organic material. These properties are dependent on the ionization of the water in the material, which is not known for water that has been absorbed into organic dielectric materials.

- The electrical characteristics including the effects of moisture absorption, with different substrate configurations, encapsulations, and underfills have not been studied.

2.3.3. Time Domain Dielectric Modeling Techniques

Several researchers have used conformal mapping techniques, where the signal and ground plane are mapped to an equivalent parallel plate capacitor, to develop expressions for a capacitance between transmission line signal and ground planes that can be used to model the dielectric in lumped element equivalent circuits. Bogatin reviews several traditional analytical equations for microstrip capacitance from Kaupp, Schneider, Kumar, and Sakura in [108]. Bogatin then proposes an improved model for capacitance and conductance in [109]. Several equations have also been published for coplanar conductance and capacitance. Coplanar mapping techniques are used in [110-112]. Willams extends the model from [110] to include embedded coplanar lines that have two different dielectric substrate layers [113].

To predict the dielectric losses, it is necessary to model the frequency dependence of the dielectric loss tangent, $\tan(\delta)$, and the relative permittivity, ε_r. Engin does this by revisiting the "Continued Fractional Expansion Method", which he previously used to develop a lumped element equivalent circuit for the conductor, to build a lumped element equivalent circuit for dielectric loss [50, 51, 114]. A second model that Engin uses to characterize the dielectric in the time-domain is called the Debye Model, which works by giving a causal admittance function to model a constant dielectric loss tangent. The parameters of the model are extracted from two values of the complex permittivity [50, 51, 114]. Zhang also applies the Debye method as well as a similar method called the Lorenzian method to model the dielectric effects in the time-domain [9]. Coperich in [115] and Yu in [116] also use the Debye model to characterize the dielectric. Arabi models the dielectric losses by using causal analytical equations that model the frequency dependence of ε' and ε'' [117]. Vu Dinh also uses analytical equations to model the capacitance between a microstrip and ground plane [118]. Using non-physical models to model the dielectric response is a similar process to using non-physical models to model skin-effect. At corner frequencies these models must be very carefully fitted or they will introduce errors. Furthermore, the bandwidth and accuracy of the model only increases when the number of components in the model increases. And, as with the physical models, the time-domain models are not available

that model a heterogeneous dielectric with various permittivities, dielectric loss tangents, and conductivities.

Chapter 3: Modeling the Conductor in Transmission Lines with Non-Rectangular Cross-Sections and Surface Roughness

As shown in the previous chapter, many useful models already exist for the modeling of skin-effect, proximity effect, edge-effects, and surface roughness. These models can all be considered useful within their limitations. One can also view this, not simply as limitations, but advantages and disadvantages. For example, while a correction factor has the disadvantage of a bandwidth limitation, it has the advantage that it is simple and easy to implement. With different models, a designer can achieve a balance between simplicity, accuracy, computation time, and physical insight. That being said, the models are potentially misused when they are not understood, which can result in significant modeling inaccuracies.

Therefore, in this chapter, a methodology is introduced that organizes the different modeling techniques. This allows their implementation within their limitations. The methodology includes (1) all geometrical parameters, and (2) all electrical effects that affect the current distribution inside the conductor. It employs various modeling techniques of different complexities.

The methodology was constructed in a systematic way considering the limitations of not only the surface roughness modeling techniques but also the current density modeling techniques (analytic, quasi-static, full-wave). Because of this systematic approach, the methodology also identifies one case where the state-of-the-art models that were addressed in Chapter 2 do not adequately address the losses from surface roughness. A novel approach for modeling the surface roughness is presented to fill the gap.

3.1. A Methodology for the modeling of a conductor with surface roughness and a non-rectangular cross section

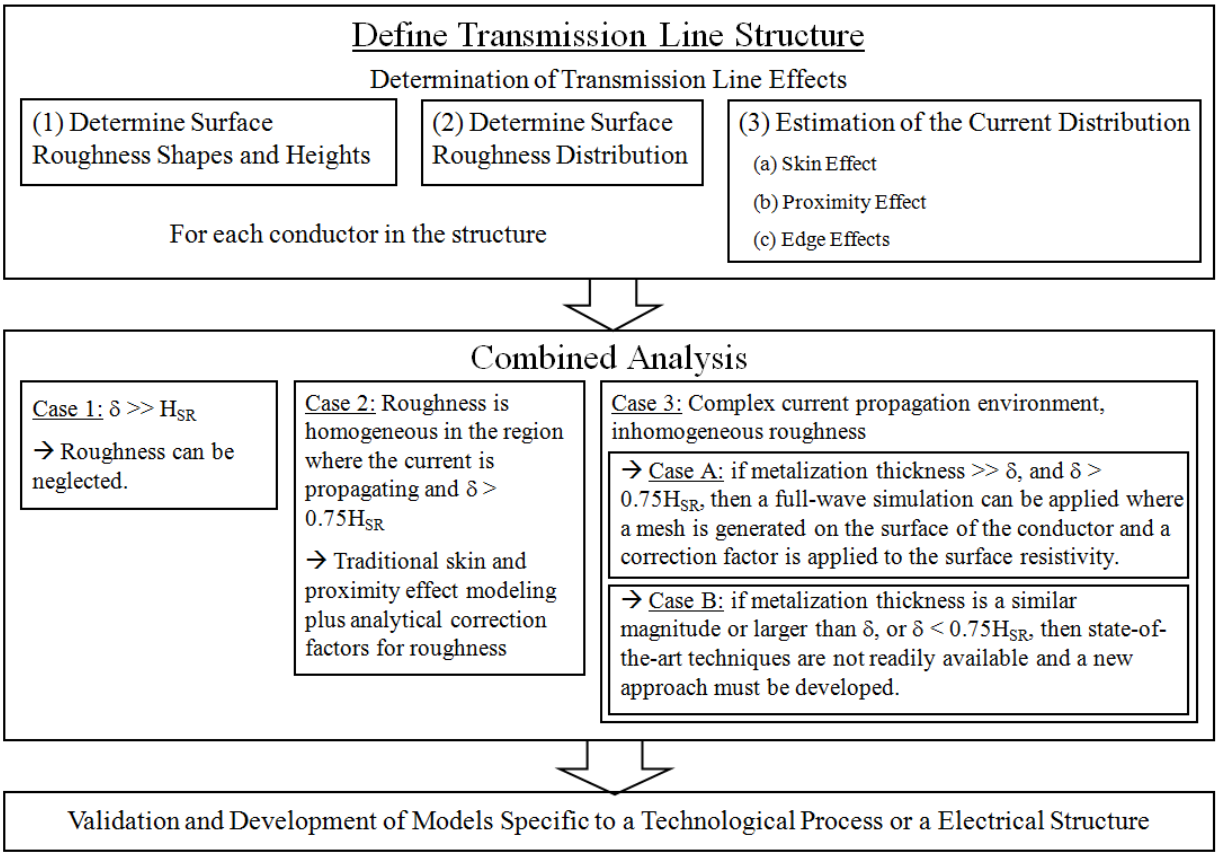

Fig. 3.1. Methodology for modeling the losses in a non-ideal transmission line.

The methodology for the modeling of losses in a non-ideal transmission line is shown in Fig. 3.1. A non-ideal transmission line, in this context, is defined as a transmission line whose cross-section deviates from an intended rectangular or circular cross-section and/or has surface roughness.

A. Define Transmission Line Structure and Determine the Transmission Line Effects

The first step to modeling a transmission line with a non-ideal conductor is to define the transmission line segment to be modeled. An input port and output port, where the model begins and ends, are assigned.

Looking at Fig. 3.2(a), the traditional transmission line approximation is of a perfectly rectangular conductor. Fig. 3.2(b) is a more realistic view. The conductor is not necessarily rectangular, there is roughness on the top, bottom, and sides ($H_{SR,top}$, $H_{SR,bottom}$, and $H_{SR,sides}$). The roughness is not evenly distributed, meaning $H_{SR,top}$, $H_{SR,bottom}$, and $H_{SR,sides}$ all have different values. The conductor is no longer perfectly rectangular, it is now trapezoidal with lower inside angles ϕ. The goal of this step in the methodology is to determine which of these effects in the transmission line segment will affect the conductor losses. Then it can be determined which approximations can be made regarding the conductor cross-section. Approximations can be made once the realistic cross-section and the current distribution in the conductor is understood.

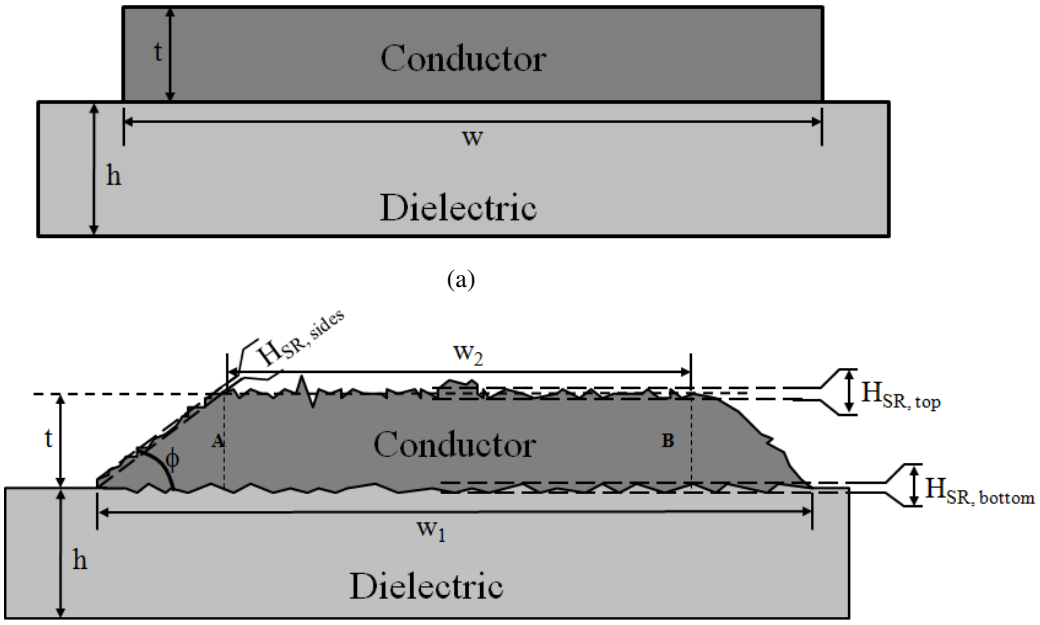

Fig. 3.2. (a) Traditional approximation of a conductor cross-section, (b) realistic conductor cross-section.

The H_{SR} values can be achieved by measurement, when appropriate measurement tools are available. When these tools are not available, published or estimated data for the characteristics can be applied instead.

(1) Determination of the Surface Roughness Heights and Shapes:

The two most common methods of expressing roughness are the arithmetic average roughness height (AARH) and the root mean square (RMS) Average. The arithmetic average roughness height is determined by measuring the peak-to-peak height of the roughness and taking an arithmetic average of the values. To determine the root mean square average, instead of averaging the peak to peak height of the roughness, the squares of the values are averaged and the square root is taken. Fig. 3.3 shows what is meant by "peak-to-peak" measurements. If we measure the vertical distance between 1 and 2, then 2 and 3, and so on, across the entire conductor, these values would be used to determine the arithmetic or root mean square average surface roughness heights.

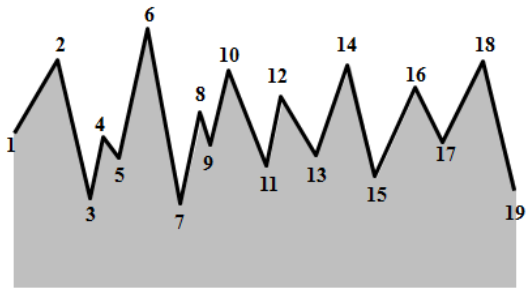

Fig. 3.3. Surface roughness on a conductor.

The shape of the roughness can be determined by looking at a cross-section or the surface of the conductor. Some technologies will result in spherical nanoparticle agglomerates on the conductor surface or some treatments will result in rounded roughness rather than jagged. An estimation of the shape is normally made through visual inspection.

(2) Estimation of Roughness Distribution:

Roughness may be measured on the top face of the conductor, which normally will not match the bottom of the conductor. For example, a printed transmission line on glass may have significant roughness on the top surface but almost no roughness on the bottom surface. In other cases, the bottom of a line may have roughness added to improve adhesion. Measurements or

approximations of the roughness on each face of the conductor must be made. The roughness distribution will play a role in its impact. Longitudinal roughness changes are also examined. Often, however, with uniform transmission line geometries, the roughness will not change in the longitudinal direction.

(3) Estimation of the Current Distribution:

In some cases, this step is very simple. With a calculation of the skin-depth at the highest operating frequency, if it is much larger than the thickness of the conductor, current distribution can be assumed to be homogeneous. Ideally, a cross sectional current distribution plot of the transmission line with the proximity effects and edge effects for the highest applicable frequency is generated. This approximation is important to determine if the roughness profiles can be ignored or approximated during the modeling.

B. Combined Transmission Line Analysis with Appropriate Techniques

Based on the information in the previous steps, a technique for transmission line analysis can be chosen. Essentially, there are three cases.

Case 1: In the case that the skin-depth is much larger than the height of the surface roughness ($\delta >> H_{SR}$) for the highest operating frequency, surface roughness can be neglected altogether. In this case, the surface roughness will have no significant effect on the transmission line parameters. Even for electrically thin conductors with significant roughness, the average height can be used to model the conductor losses. The equation for skin-depth, derived directly from Maxwell's Equations, is Eq. 3.1.

$$\delta = \sqrt{\frac{2}{\omega\mu\sigma}} \qquad \text{Eq. 3.1}$$

The Ansoft HFSS current density diagrams shown in Fig. 3.4 demonstrate this difference. The figures are a side view of a signal conductor of a microstrip TML where the current is flowing in the direction of the arrows. The darker areas indicate higher current flow and the lighter areas

lower current flow (the scale indicates the normalized current density). In Fig. 3.4(a), the current flows through the bulk of the conductor because the skin-depth, 2 μm, is about 4 times the peak-to-peak surface roughness height, 0.5 μm. In contrast, Fig. 3.4(b) shows a skin-depth that is about 1/3 the peak-to-peak surface roughness height. In Fig. 3.4(b) the roughness peaks and valleys act as discontinuities to the current propagation which will affect the conductor resistance. Therefore, when the skin-depth is on the same order or smaller than the surface roughness profile, the surface roughness must be accounted for, and another case must be examined.

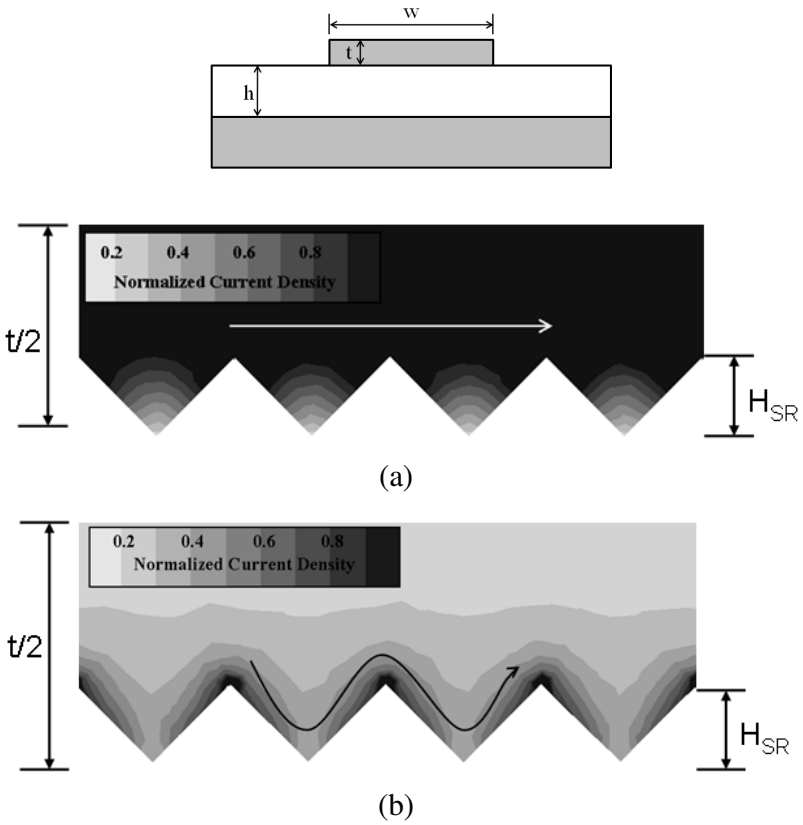

Fig. 3.4. Bottom surface of a microstrip signal conductor for t = 2 μm, w = 10 μm, h = 4 μm, (a) Current distribution for H_{SR} = 0.5 μm and f = 1 GHz, (b) current distribution for H_{SR} = 1 μm and f = 50 GHz.

Case 2: In the first case, the roughness was neglected. In the second case, it can no longer be neglected but it can be broadly approximated. When the skin-depth $\delta > 0.75H_{SR}$ and the current propagates almost exclusively through one roughness profile, then an analytic technique can be separately applied to analyze the conductor losses. In this case, the skin and proximity effects can be modeled in a traditional way, either with analytical equations or a numerical solver. The

surface roughness can then be accounted for with a correction factor formula like the Hammerstad or Groiss models. The correction factors are designed to work when skin-depth δ is larger than $0.75H_{SR}$ because this is the point where the surface roughness correction factors begin to saturate [119]. When $\delta << 0.75H_{SR}$, this can lead to significant inaccuracies. The current can only travel through one roughness profile because the roughness is being modeled separately from the current distribution in the conductor.

An example of this case is shown in Fig. 3.5 (the diagrams are generated with a filament model programmed in Matlab). To approximate roughness, the conductivity of the conductor is randomly increased around the conductor surface. Fig. 3.5(a) shows the current density in a microstrip transmission line. If we disturb the current flow along the top surface, to approximate roughness distributed only on the top surface, as in Fig. 3.5(b), there is almost no difference from the ideal case in Fig. 3.5(a). However, when the current flow is disturbed along the bottom surface, there is a significant difference. In this example, we could apply an analytical correction factor to the ideal line resistance using only the bottom surface roughness height (neglecting the roughness on the top surface altogether) because a large majority of the current flows on the bottom surface.

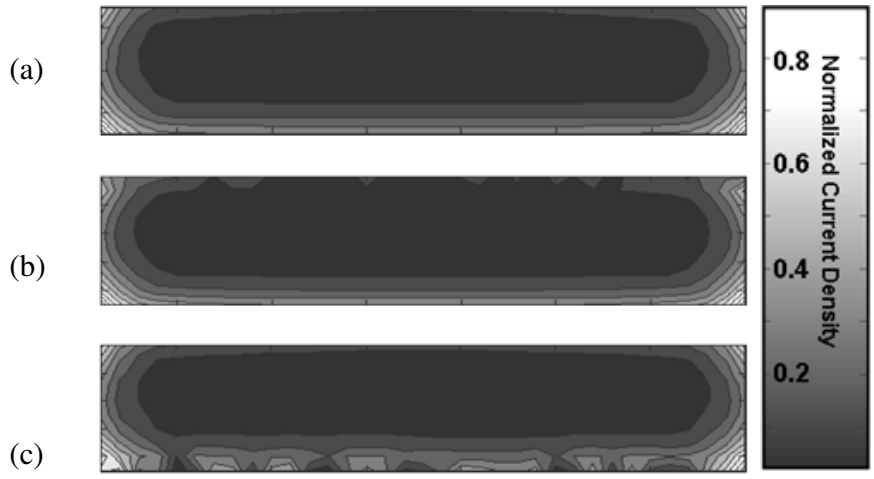

Fig. 3.5. (a) Current distribution in the signal conductor of a microstrip with substrate height = 5 μm, conductor width = 10 μm, and conductor thickness = 2 μm, f = 50 GHz. (b) the same microstrip signal conductor with a disturbed current flow on the top surface, (b) the same microstrip signal conductor with a disturbed current flow on the bottom surface.

Another example where this applies is a symmetrical stripline or coplanar line with the same roughness profiles, or similar roughness profiles, on the top and bottom of the line. In this case, the current is evenly distributed on the top and bottom surfaces, so only one roughness profile is necessary for analysis. Fabrication processes usually result in a different roughness on the bottom of the conductor compared to the top. Furthermore, higher permittivity dielectrics have led to narrower microstrips and asymmetric striplines and adjacent conductors are common in modern microelectric devices. Therefore, a third case for the analysis in these situations is necessary.

Case 3: In the final case, we must still make approximations to model the roughness but the approximations are more rigorous. When the environment inside the conductor is more complex (inhomogeneous roughness, arbitrary proximity effects, edge effects, etc.) and the frequencies are higher, other modeling techniques must be used. A modeling approach that models the roughness and the current density in a combined way would be necessary to model the transmission line non-idealities.

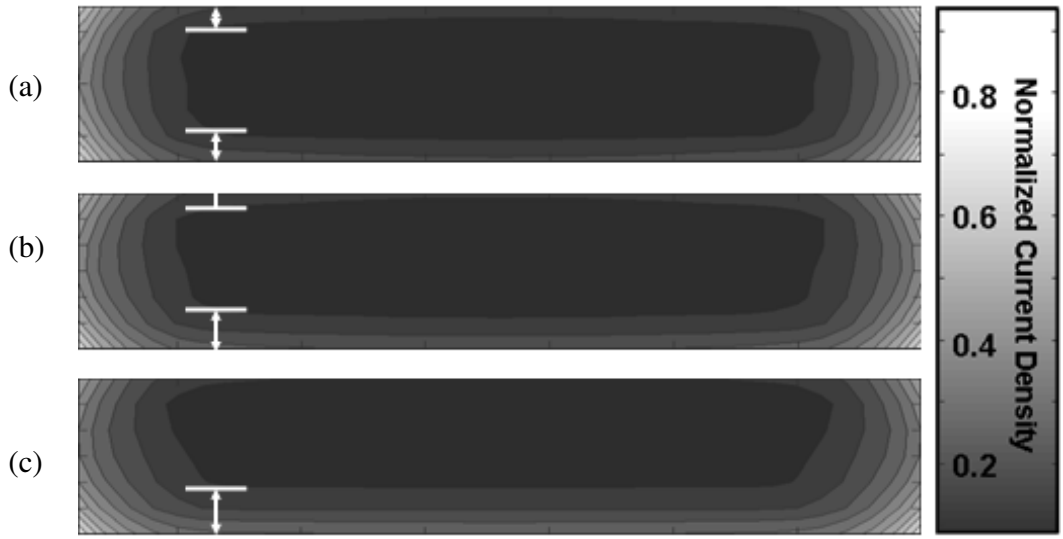

Fig. 3.6. The current density in a microstrip with different heights, (a) h/w = 1.5; (b) h/w = 0.5; (c) h/w = 0.33. (h = substrate height, w = signal conductor width).

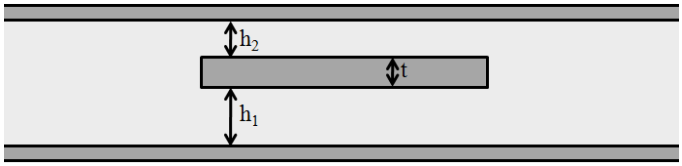

(a)

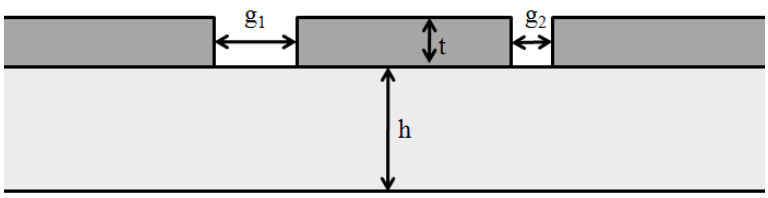

(b)

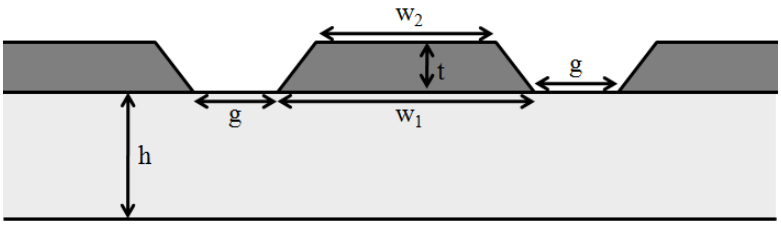

(c)

Fig. 3.7. Transmission lines requiring simultaneous roughness current density modeling; (a) uneven stripline; (b) asymmetric coplanar; (c) trapezoidal coplanar.

For example, the microstrip in Fig. 3.5 was a wide micristrip, and therefore the current was concentrated almost completely on the bottom surface. Fig. 3.6 shows microstrip current densities at different substrate heights. The largest height, Fig. 3.6(a), shows a more even distribution between the bottom and top surfaces. Therefore, in the case of a narrower microstrip line, when these different conductor surfaces (top and bottom faces) have different surface roughness heights, they must be separately considered and they must be considered together with the current density. Furthermore, until now we have only considered microstrip configurations. But, other structures like, but not limited to, Fig. 3.7(a), an asymmetrical stripline, Fig. 3.7(b), an asymmetrical coplanar line, or Fig. 3.7(c), a trapezoidal coplanar would also require a model that simultaneously models the current distribution and the roughness. There are a few different possibilities to do this.

In *Case A*, full-wave simulations can be used. Using a full-wave solver, a correction factor can be applied to the surface resistivity. In this case, a new correction factor should be applied to the surfaces separately wherever there are different roughness characteristics. The bandwidth limitations apply again, that the skin-depth $\delta > 0.75H_{SR}$, of the Hammerstad and Groiss formulas because they begin to saturate at these frequencies. An additional advantage with this technique is that a 3D full-wave solver can also evaluate the effects of surface roughness on discontinuities, reference conductors, and other passive components. The other modeling techniques do not have this capability. However, the simulation must be very carefully designed so that the conductor characteristics converge to a stable solution.

For transmission lines with large width to thickness ratios, for example, these simulations could last a very long time and still not produce results that are accurate over a broad frequency band. Additionally, when only the surface of the conductor is solved (and no mesh is generated inside the conductor) during a full-wave simulation, the conductor losses are not correctly modeled for lower frequencies (where $\delta > 0.5t$, t = conductor thickness). The frequency range under examination must lie in the region where skin-depth is smaller than the conductor thickness but that solution is only valid until the frequency where the correction factor begins to saturate – the technique only works inside that frequency window, which could be a narrow window for thin conductors with large surface roughness profiles. Solving inside the conductor will significantly extend the simulation time. In most cases, achieving a converged solution for the conductor attenuation while solving inside the conductor exceeds the computations capabilities of commercial solvers or results in computation times of days or months. In general, generating a mesh inside the conductor is not practical.

For *Case B*, when the transmission line structure lies outside the limitation of the full-wave modeling technique, the Adapted Filament Model is presented in the next section. One other attempt at solving this problem has been presented. A technique that partially models inhomogeneous roughness, combined with current distribution, was presented in [120]. This model, however, is only presented for stripline structures. The Adapted Filament Model is the first technique for arbitrary structures.

C. Validation and Development of Models Specific to a Technological Process or Electrical Structures

After the transmission line segment has been modeled, the predicted characteristics can be compared with s-parameter measurements. At this point a correction factor can be extracted for future applications. The Adapted Filament Model offers the flexibility to alter the model for different types of roughness profiles. The Hall roughness correction factor, for example, because it requires more information on the roughness that is normally available from a simple profile measurement, can only be applied as more geometrical information about the roughness is assembled and verified. These updated and refined models can then be adjusted and validated over time for a specific fabrication technology or for specific structures.

3.2. Calculating the Skin-Effect Resistance and Inductance Using the Adapted Filament Model

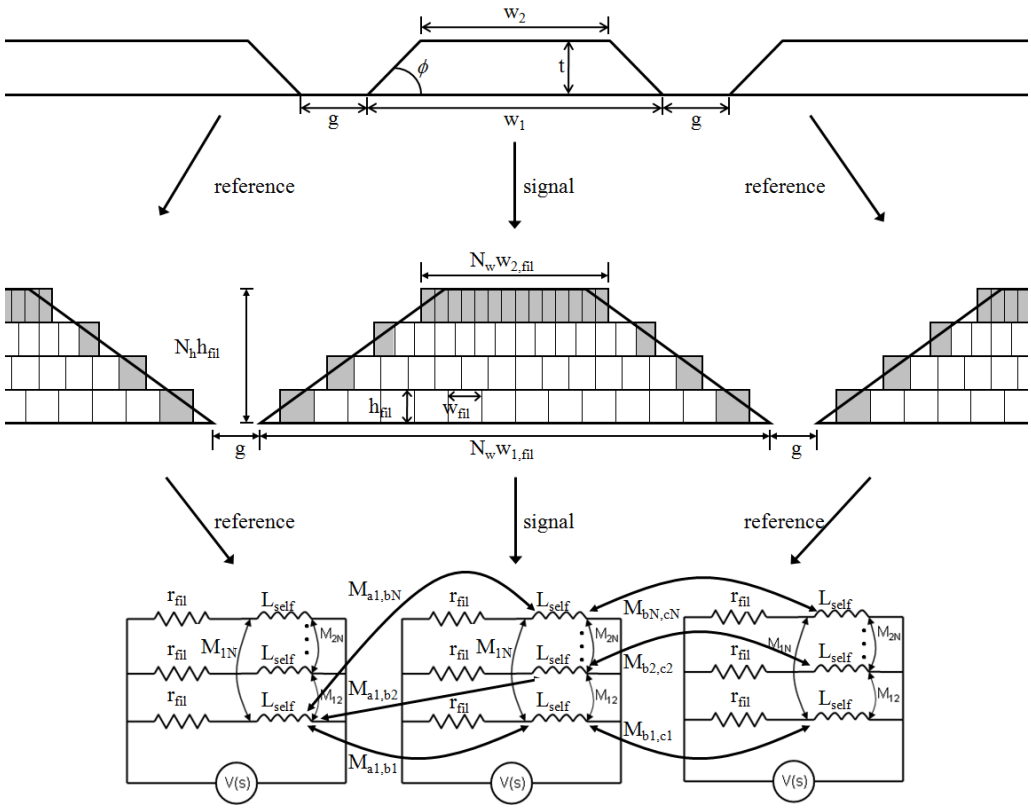

Fig. 3.8. Diagram of a filament model (top) and its corresponding ladder circuit (bottom).

The adapted filament model is proposed in this section in a response to the limitations of the state-of-the-art models. Filament models are commonly used to calculate the resistance and inductance of a conductor. Fig. 3.8 shows an implementation of the VuDinh model [16], slightly modified for a non-rectangular cross-section. Referring to Fig. 3.8 (middle), the cross-section of a trapezoidal conductor is discretized, where the total number of filaments in the discretization, $N_{tot} = N_h \text{ X } N_w$, and resistances, inductances, and mutual inductances are calculated for each filament. The same is done for the reference conductors, in this case the two coplanar flanks. Three different ladder circuits are constructed for the three different conductors as in Fig. 3.8 (bottom). Then, a mutual inductance matrix between each reference conductor and the signal conductor is created containing the mutual inductances between every filament in each conductor.

The mutual inductance was calculated with Eq. 3.3 published in [24] (variable *l* is the length of the conductor, *r* is the distance between the center points of two filaments). The same equation is used to determine the mutual inductances between the filaments in the different conductors. The self-inductances of the filaments were calculated with Eq. 3.2 published in [20]. The resistances were calculated with the traditional formula for the resistance of a prism, Eq. 3.4.

$$L_{self} = 0.2l\left[\ln\left(\frac{2l}{w_{fil}+h_{fil}}\right)+0.5+0.2235\left(\frac{w_{fil}+h_{fil}}{l}\right)\right]\mu H \qquad \text{Eq. 3.2}$$

$$M = 0.2l\left[\ln\left(\frac{l}{r}+\sqrt{1+\frac{l^2}{r^2}}\right)-\sqrt{1+\frac{r^2}{l^2}}+\frac{r}{l}\right]\mu H \qquad \text{Eq. 3.3}$$

$$r_{fil} = \frac{l}{\sigma h_{fil} w_{fil}} \qquad \text{Eq. 3.4}$$

The Adapted Filament Model proposed in this paper is based on the VuDinh model. For the Adapted Filament Model, to directly account for surface roughness, this resistance value is altered. In our case, to account for the surface roughness of the conductor, the resistances of the outside filaments (for example, the filaments shaded in Fig. 3.8(top)) were increased. A systematic approach for selecting the resistance of the filaments has been implemented in the model, which will be the focus of the next section. This leaves us with signal and reference

conductors with inhomogeneous conductivities over their cross-sections. The model is then solved with a computer (the author has used Matlab for the calculations in this chapter) using Eq. 3.5. In Eq. 3.5, subscripts *Ref1*, *Ref2*, and *Signal* refer to the coplanar reference conductors and the signal conductor. V_X, L_X, r_X and I_X refer to the voltage matrix, inductance matrix, resistance matrix and current matrix in conductor X. $M_{X,Y}$ refers to the mutual inductance between conductors X and Y.

$$\begin{bmatrix} V_{Ref1} \\ V_{Signal} \\ V_{Ref2} \end{bmatrix} = \begin{bmatrix} r_{Ref1} & 0 & 0 \\ 0 & r_{Signal} & 0 \\ 0 & 0 & r_{Ref2} \end{bmatrix} + s \begin{bmatrix} L_{Ref1} & M_{Ref1,Signal} & M_{Ref1,Ref2} \\ M^T_{Ref1,Signal} & L_{Signal} & M_{Signal,Ref2} \\ M^T_{Ref1,Ref2} & M^T_{Ref2,Signal} & L_{Ref2} \end{bmatrix} \begin{bmatrix} I_{Ref1} \\ I_{Signal} \\ I_{Ref2} \end{bmatrix} \quad \text{Eq. 3.5}$$

3.2.1. Accounting for Sawtooth Surface Roughness Profiles with the Adapted Filament Model

Fig. 3.9 is a view of the surface filaments with surface roughness. For standard applications, to approximate a nearly regular sawtooth roughness pattern, the resistance of the filaments in the region of surface roughness is increased in an exponential gradient (exponential to reflect both the horizontal and linear dimensions of the roughness). This concept is similar to the traditional Hammerstad surface roughness model, which assigns essentially a frequency dependent effective conductivity to the conductor. With the adapted filament model, however, the effective resistance is only applied to the part of the conductor with surface roughness. Then, the conductivity gradient stays constant over the frequency range while the current density in the conductor changes. As the current migrates to the outside, the higher resistance filaments, representing surface roughness, cause the resistance to increase above the ideal value. The surface roughness heights can be applied at random (with a random number generator) to each column of filaments to approximate random surface roughness with an average height. However, for a large number of filaments, this technique will average out to approximately the same as a constant resistance gradient. Therefore, a set of equations was developed to find the effective resistance of the filaments as a function of the layer in which they are located.

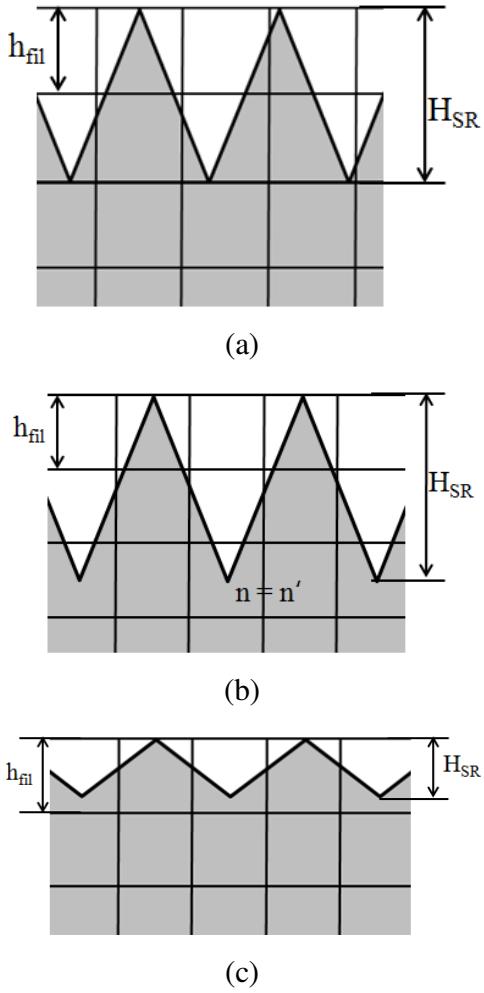

Fig. 3.9. Cross-sectional areas of the filaments for different surface roughness profiles, (a) Case 1, (b) Case 2, (c) Case 3.

The approximation is made that the surface roughness penetrates uniformly across the surface, with RMS peak-to-peak height of the surface roughness, H_{SR}, as it does in Fig. 3.9(a). The following equations, Eq. 3.6 and Eq. 3.7, describe what resistance the filaments are assigned. The variable $K_{FIL}(n)$ is the coefficient that determines the resistance of the filament. The variable N is the total number of layers that the peak-to-peak RMS surface roughness height penetrates, or the quotient of the surface roughness height (H_{SR}) and the filament height. For example, in the drawing in Fig. 3.9(a), N = 3. Essentially, $N = H_{SR}/h_{fil}$, which in case 1 is always an integer number. The variable n, is the layer that the filament occupies, starting with n = 1 at the layer on the surface, and increasing inward, until the average roughness height is reached. $R_{FIL,EFF}$ is then

the effective resistance of the particular filament.[121] In Eq. 3.6, the variable P represents the shape of the surface roughness. This will be discussed more in the next section. However, most surface roughness models view surface roughness as being sawtooth in shape, with lower inside angles of 60°. For this traditional view, P = 2, to represent the lateral and longitudinal dimensions of the roughness.

$$K_{fil}(n) = \left(\frac{2n-1}{2N} \right)^{P} \qquad \text{Eq. 3.6}$$

$$r_{fil,eff} = \left(\frac{\sigma l / w_{fil} h_{fil}}{K_{fil}(n)} \right) \qquad \text{Eq. 3.7}$$

Eq. 3.6 and 3.7 assume that the discretization can be made so that H_{SR} is equal to a discrete amount of filaments. While Eq. 3.6 remains the same, Eq. 3.7 can be expanded to include case 2, represented by Fig. 3.9(b). In this case, a new variable is introduced, *d*, which is defined in Eq. 3.8. The variable d is the same as N from case 1 except that *d* must not be an integer, it can be any positive real number. Eq. 3.9 is then the correction factor for the filament from $n = 1$, up to the last filaments where $n < d$. For the last filament, which is only partially penetrated by roughness, labeled as n' in Fig. 3.9(b) (in the case of Fig. 3.9(b) n' = 3), a different equation is necessary, Eq. 3.10.

$$d = \frac{H_{SR}}{h_{fil}} \qquad \text{Eq. 3.8}$$

$$K_{fil}(n) = \left(\frac{2n-1}{2d} \right)^{2} \qquad \text{Eq. 3.9}$$

$$K_{fil}(n) = \frac{1}{4}\left(\frac{n'-1}{d} \right)^{2} + \frac{1}{2}\left(\frac{n'-1}{d} \right) + \frac{1}{4} \qquad \text{Eq. 3.10}$$

The final case, case 3, is when $H_{SR} < h_{fil}$. In this case, only the first filaments directly on the surace must be modified. This can be done with Eq. 3.11, where *d* is defined by Eq. 3.7.

$$K_{fil}(n) = (1-d) + \frac{1}{4}(d)^{2} \qquad \text{Eq. 3.11}$$

The model will compute DC effects of surface roughness and the bandwidth should continue to the point where the skin-depth is approximately equal to the height of the discretized filaments.

(a) (b)

Fig. 3.10. The conductivity cross-section in the adapted filament model, (a) Homogeneous roughness across the entire cross-section, (b) roughness only on the top and sides of the conductor.

To better understand the modeling of the conductor, Fig. 3.10 shows the per-area resistance in the conductor cross-section. The white area in Fig. 3.10 (a) and (b) is a homogeneous resistance. In fact, it is the ideal resistance for that particular type of metallization material. The shaded parts show the resistance on the surfaces with surface roughness (the darker shades represent higher resistances and the lighter shades lower). Fig. 3.10 (a) shows a conductor with homogeneous surface roughness on all of its faces. In this case the resistance increases exponentially toward the surface on each face of the conductor. Fig. 3.10 (b) represents a conductor with surface roughness on the top and sides of the conductor but not on the bottom. In this case, the homogeneous conductivity extends down to the bottom of the conductor cross-section and the quadratic resistance gradient is constructed on the top and sides of the conductor only.

3.2.2. Accounting for Arbitrary Surface Roughness Profile Shapes by Customizing the Adapted Filament Model

It is not only the height of the surface roughness that affects the resistance; the shape and constitution will also play a role. Different technologies and treatments will create surface roughness profiles that affect the resistance in different ways. An example is that some printing processes will result in nanoparticle agglomerates on the surface of the conductor and different

sintering processes will, to a different extent, reduce the amount and size of nanoparticle agglomerates. This is an effect that will be shown during the verification chapter of this dissertation. Other chemical treatments, for example, will cause rounded roughness profiles instead of jagged profiles (as was discussed and referenced in Chapter 2).

The traditional approach to roughness modeling, which is demonstrated by Fig. 3.4, is that an effective length or conductivity is assigned to the conductor because the current must meander over the hills and valley of the conductor roughness. This is, however, not entirely true. One must see the roughness as discontinuities in the current flow, similar to transmission line bends. Magnetic fields outside the conductor, or eddy currents inside the conductor, will form positive or negative interference patterns as they navigate the periodic discontinuities. Because of this, the skin-depth cannot be thought of a homogeneous. This effect is demonstrated by the full-wave simulation in Fig. 3.11. It is clearly seen from the full-wave simulation that the current distribution is not homogeneous longitudinally over the roughness. A factor that additionally complicates this is that when different roughness shapes occur, for example rounded, spherical, angular, etc. This may cause the effect to change further.

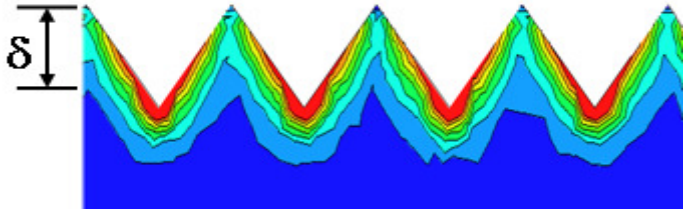

Fig. 3.11. Full-wave simulation of the skin-effect in a rough surface.

The Adapted Filament Model also has the flexibility to adjust to different technologies or treatments that result in different surface roughness shapes. One potential way of doing this in the adapted filament model is to use Eq. 3.6 with an exponent, P, other than 2. One can assume that the longitudinal and horizontal effects would both separately have a linear effect on the transmission line parameters because the horizontal component only affects the cross-sectional area and the longitudinal component only the electrical length. Their combined effect, multiplied together, would then be quadratic. For other surface roughness shapes, the components could be other than linear. This technique would not use a systematic analytic approach and instead would

be determined experimentally for a given technology. Fig. 3.12 shows how results vary when this exponent, assigned the variable P, is changed from 1.5 to 2.5.

The low frequency response does not change when this exponent is changed. This is important because the average surface roughness height, regardless of its shape, should not have an effect on the resistance until the skin-depth is on that same order. Then, the effect of the surface roughness becomes frequency dependent. The different surface roughness shapes have a different effect only above a certain frequency.

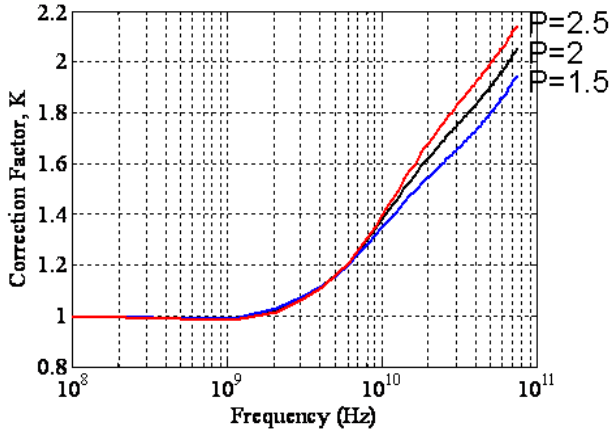

Fig. 3.12. Adjustments to the filament model to a technology.

3.3. Demonstration of the Adapted Filament Model for Various Configurations

The state-of-the-art filament model was programmed using a Matlab program. The model was validated by comparing its results to results presented in [20]. It was also validated with full-wave simulations that showed a deviation of less than 5% up to a frequency of 50 GHz (shown in Fig. 2.2) [122]. After the filament model was validated, the adjustments were made so that resistance gradients could be added on the different surfaces separately.

Here, the adapted filament model is used to observe the combined effects of surface roughness and proximity effects. We will consider a microstrip line. For the calculations, the line will be considered ideal, with an infinitely wide ground plane, and calculated using image theory. This

means that the return current path of the microstrip is approximated as an ideal ground plane by calculating an identical signal conductor as a mirror image over the location of the ideal ground plane. Image theory approximates the reference plane as infinitely wide and conductive. Theoretically, if surface roughness were only present on the bottom of the conductor, then its influence would be greater and if surface roughness were only on the top of the conductor then its influence would be less because the proximity effect would cause additional crowding on the bottom of the microstrip signal conductor. Also, theoretically, the height, h_s in Fig. 3.4, of the microstrip would play a role in this influence because, in a higher microstrip, the proximity effect would not be as strong.

3.3.1. Demonstration of the Adapted Filament Model for Microstrip Transmission Lines

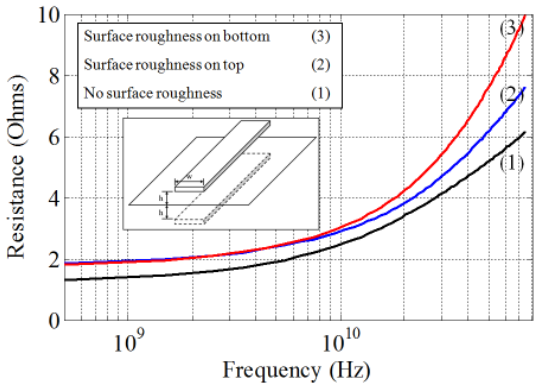

(a)

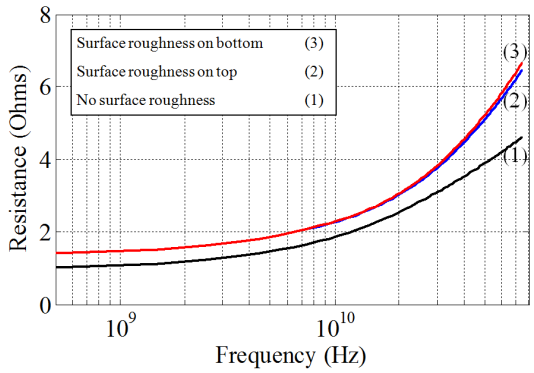

(b)

Fig. 3.13. 0.5 µm Surface Roughness on a microstrip line, (a) h/w = 0.5, (b) h/w = 4.

A conductor (w = 10 μm, t = 2 μm) was simulated in microstrip configuration two times, first with surface roughness only on the top face, and second with surface roughness only on the bottom face. This was done for two different heights. The results are shown in Fig. 3.13.

Fig. 3.13 shows that for a microstrip with h/w = 0.5, surface roughness on the bottom had a 33% stronger effect at 75 GHz than roughness on the top surface. When h/w = 4, the current is almost uniformly distributed around the conductor and the difference is only 3%.

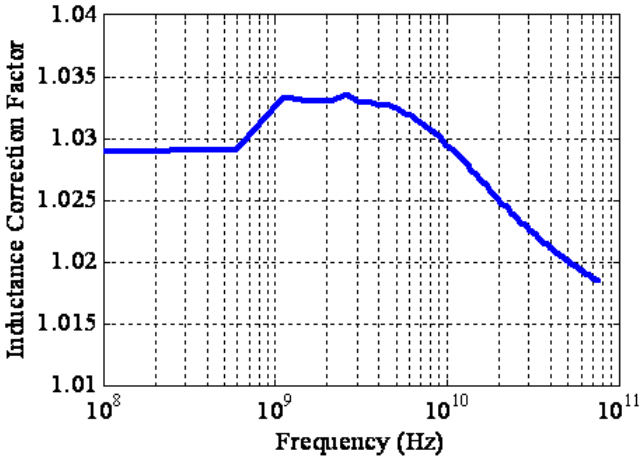

Fig. 3.14. Inductance correction factor for surface roughness.

The filament model also calculates the characteristic transmission line inductance. When we calculate the inductance with and without surface roughness (for w = 10 μm, t = 2 μm, h/w = 4) then find the ratio, we get the curve in Fig. 3.14, which is the inductance correction factor, K_{IND}, for this particular configuration. The inductance correction factor is particular to one transmission line structure. Inductance varies much less than the resistance, starting at around 3% and decreasing at higher frequencies.

3.3.2. Demonstration of the Adapted Filament Model for Coplanar Transmission Lines

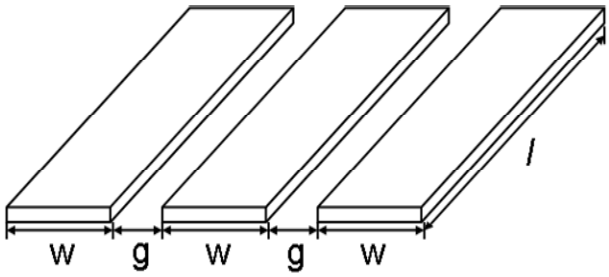

Fig. 3.15. Example of a coplanar transmission line.

For a second example, a coplanar transmission line, shown in Fig. 3.15, is modeled and the focus will be the geometry of the coplanar gap. The signal line and both ground lines will have the same dimensions as the signal line in the microstrip example (again, thickness, t = 2 μm, width, w = 10 μm, copper, $\sigma = 5.8 \times 10^7$ S/m, length = 1 mm). The gap of the coplanar line, g, will be kept very small at only g = 1 μm, as to exaggerate the proximity effect. For this example, $w = w_1 = w_2$ (referring to Fig. 3.8), meaning that the conductors are considered perfect rectangles.

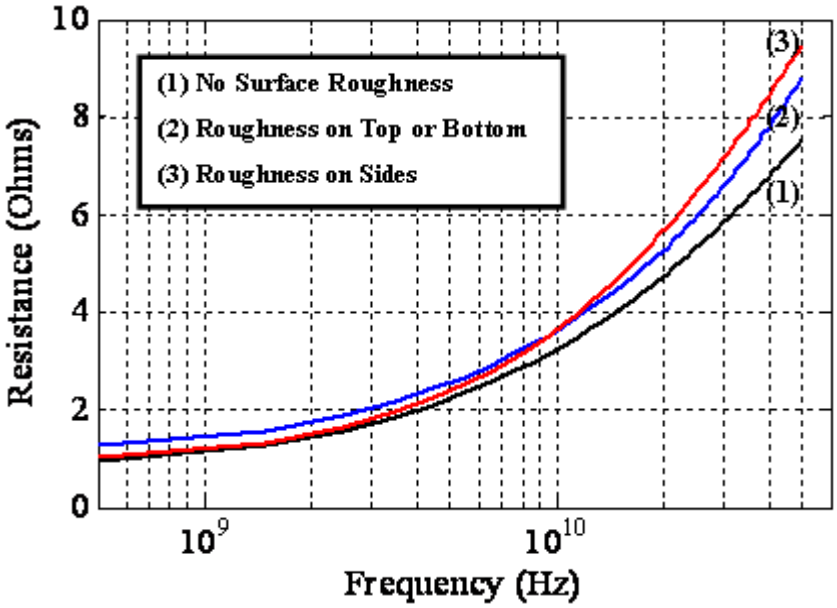

Fig. 3.16. Coplanar transmission line resistance with and without surface roughness.

For the example of the coplanar line, the resistance and inductance are calculated first without surface roughness. Then the parameters are calculated with surface roughness (h_{SR} = 0.8 μm) only on the top or bottom face of the signal conductor, then with surface roughness (h_{SR} = 0.8 μm) on conductor sides in the coplanar gap. Fig. 3.16 shows that adding surface roughness to the top or bottom face of the coplanar signal conductor has the exact same effect on the resistance of the line. The figure also shows that at DC and at lower frequencies, the effect of the surface roughness in the coplanar gap has very little effect. This is logical because this roughness occupies a smaller part of the cross-section area than the roughness on the top or bottom faces. At around 10 GHz, the roughness in the coplanar gap begins to have a very strong impact and actually increases above the curve representing the surface roughness on the top or bottom faces. At 50 GHz, the correction factor is K = 1.17 for the conductor with surface roughness on the top or bottom and K = 1.26 for the conductor with roughness on the sides. The roughness on the sides results in a 7.4% higher correction factor, even though the roughness is only present on 16% of the perimeter as opposed to 41%. This happens because the conductor reaches a point at that frequency that almost all of the current is flowing in the first micrometer in the coplanar gap.

3.4. Using the Filament Model to Determine the Source of Conductor Losses

Using the Adapted Filament model to determine the source of the losses in a structure is also a very valuable application for conductor characterization. With this technique, one can see the frequency ranges where the different loss mechanisms are introduced, which loss mechanisms are dominant, and how strongly dominant.

The ideal and non-ideal sources of losses in a transmission line include; (1) DC resistance, (2) Skin-effect resistance, (3) Proximity effects, (4) Edge effects caused by non-ideal cross-sections, and (5) Surface roughness. At a given frequency, one can determine, again with the filament model, the sources of the losses in a transmission line. The DC resistance is determined with the classical equation $R = l/(A\sigma)$. The skin-effect resistance can then be quantified with the basic filament model without proximity effects. The proximity effects can then be added by repeating

the calculations including the second ground plane conductor [122]. Then the effects of the non-ideal factors of a non-rectangular cross-section and surface roughness effects can be added.

An example is presented again in Fig. 3.16 using the coplanar line from Fig. 3.15. In this example, the width is, w = 20 μm, the thickness, t = 2 μm, and the gap, g = 5 μm, and l = 1 mm. The first curve shows only the DC resistance. The second curve is the skin-effect resistance without any proximity effect. The third curve includes the proximity effects. The fourth curve is the resistance when the coplanar lines are trapezoidal conductors with angles of 20° at the bottom corners. And, finally, the top curve includes a surface roughness factor of 0.5 μm on the top face of the conductor. The curves show that, based on the filament model and the models presented in this section, the resistance of a signal line can increase by more than 80% at frequencies above 10 GHz due to non-idealities like the non-rectangular cross-sections and surface roughness that can result from the technological tolerances associated with printing transmission lines. At low frequencies, below 500 MHz, the resistance experiences no increase as a result of skin-effect or proximity effect. The only low frequency increase in resistance comes from the change in the profile when the trapezoidal cross-section is considered and a slight increase when the surface roughness factor is considered. The changes in the model only change the values of the inductance within around 10%. Inductance calculations will be further discussed in Chapter 5.

It is also valuable to know that the proximity effect enters around 1 GHz, which is shown as curve (2), which can be thought of as the ideal transmission line. The edge-effects are introduced at about the same frequency as the proximity effect, because the trapezoidal conductor angles penetrate almost half the width of the conductor – when the proximity effect begins, there is simultaneous crowding into the narrower angle. The effect of surface roughness stay small and constant until about 5 GHz when it increases to a much more significant portion of the conductor losses.

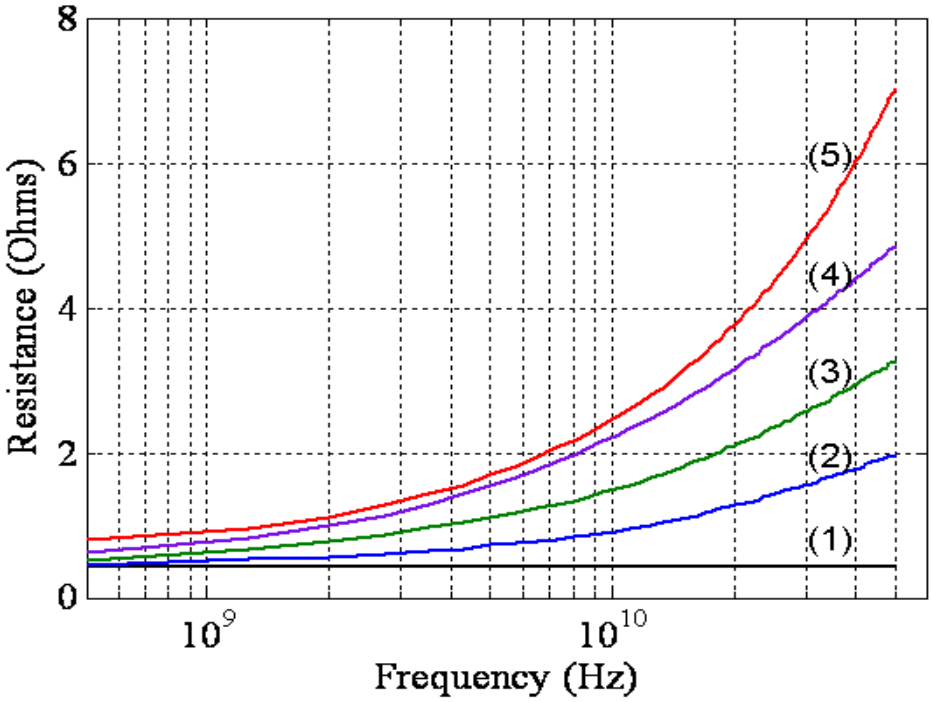

Fig. 3.17. Transmission line resistance for a coplanar line.

(1) DC Resistance

(2) Skin-Effect Resistance Only

(3) Skin-Effect and Proximity Effect Resistance

(4) Skin-Effect and Proximity Effect Resistance in a Trapezoidal Conductor

(5) Skin-Effect and Proximity Effect Resistance in a Trapezoidal Conductor with 0.5 μm Surface Roughness, H_{SR}, on the Top of the Conductor

3.5. A Lumped Element Equivalent Circuit for a Non-Ideal Conductor

As with ideal transmission lines, the CFE method can be used (which was discussed more in-depth in Chapter 2), without modification, to represent the resistance and the inductance in a non-ideal transmission line. In fact, a comparison of the results of the adapted filament method (for a transmission line that is presented in Chapter 5) is compared in Fig. 3.18 to its CFE representation. Both the resistance and the inductance are accurate within a few percent, with the highest variation around the corner frequency, near where skin-depth $\delta = t$.

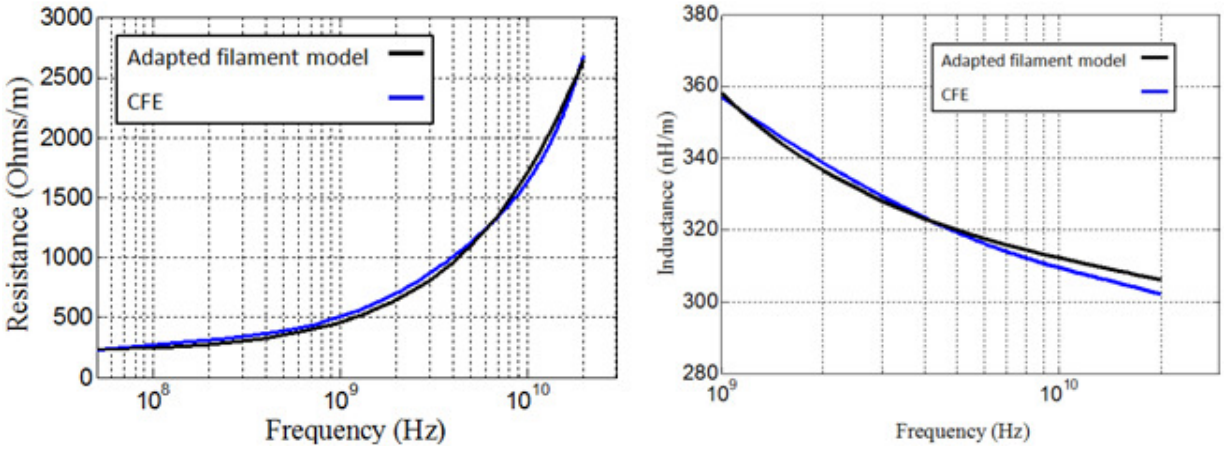

Fig. 3.18. (a) Comparison of the resistance and (b) the inductance of the adapted filament method and the CFE method.

Chapter 4: Modeling the Dielectric in Transmission Lines with Lossy and Conductive Dielectrics

As shown in Chapter 2, a great deal of state-of-the-art research is available for modeling the transmission line dielectric. Analytical and numerical quasi-static and full-wave simulation techniques have led to a comprehensive understanding of dielectric loss mechanisms in transmission line structures.

In Chapter 4, these modeling techniques are organized into a methodology, where their limitations are considered. During the methodology development, it will be shown that for composite lossy dielectrics, there is no fully developed state-of-the-art modeling technique available. Specifically, a method for the modeling of transmission line structures, where one or more of the dielectrics in the structure are composite dielectrics (meaning that it is a mixture of two dielectric materials), has not yet been proposed.

In this chapter, a modeling technique for transmission lines in this type of dielectric cavity will then be proposed to fill the gap in the methodology. The approach, and later its validation, uses a novel extension and combination of state-of-the-art theoretical, empirical, and experimental modeling and characterization techniques. Therefore, some of the techniques that were discussed in Chapter 2 will be further discussed and implemented in Chapter 4.

The case study used to demonstrate the methodology and modeling approach is the electrical modeling of organic dielectrics, particularly encapsulation and underfill materials that are typically used in plastic-encapsulated-circuits (PEMCs), which absorb moisture in humid environments. However, the approach is technology nonspecific and could be applied for other technologies, or can be extended for other passive structures.

4.1. State-of-the-Art Approach for Modeling the Dielectric in Transmission Lines with Lossy and Mixed Dielectrics

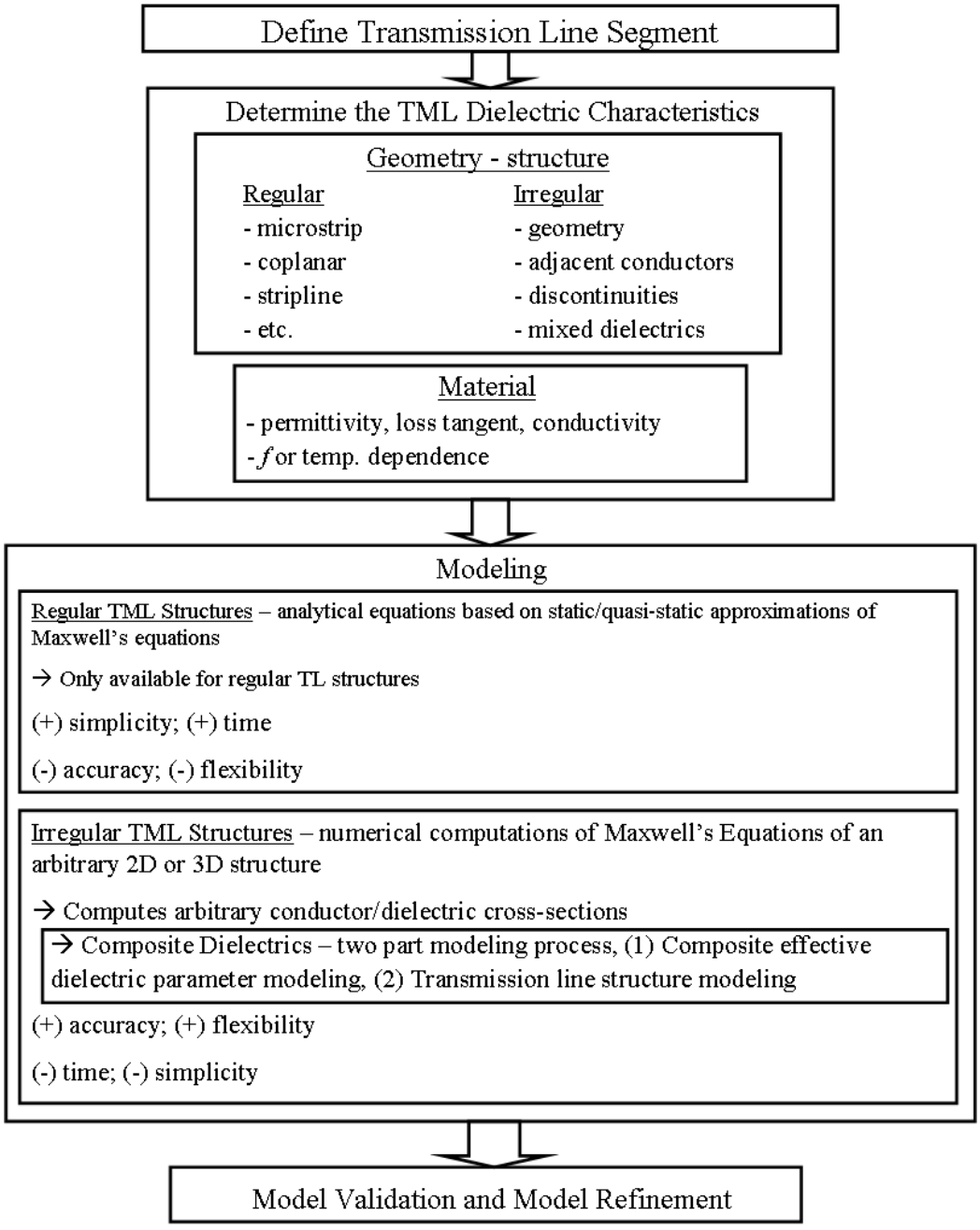

Fig. 4.1. Approach for the modeling of transmission lines with lossy and mixed dielectrics.

Traditionally, dielectric losses are examined as follows:

(A) Define Transmission Line Structure:

A segment of transmission line must first be defined and the geometric and material data for the dielectric materials must be determined. Geometrically, the structure can be divided into two different categories, (1) regular transmission line structures and, (2) irregular transmission line structures (the same categories as were used in conductor modeling). Both dielectric and conductor structure can make a transmission line regular or irregular. For dielectric modeling, a regular geometry has the additional requirement that the dielectric is homogeneous. For example, a coplanar waveguide with the same dielectric above and below, or with air on top and one dielectric below, is a regular dielectric structure because traditional analytical modeling techniques are available for their analysis. When a coplanar waveguide sits on a stack of several different dielectrics, then more complex models or numerical techniques are usually necessary.

The dielectric properties, both the permittivity and the loss characteristics, must also be known. Dielectric losses can be classified as either conductive losses or losses from dielectric loss mechanisms. Normally, the conductive losses are represented by σ, the conductivity of the material, and dielectric loss mechanisms are represented by the dielectric loss tangent, $\tan(\delta)$, which is the ratio of the imaginary part of the relative permittivity to the real part. The permittivity, conductivity, and dielectric loss tangents can also be represented by one frequency dependent complex permittivity.

(B) Transmission Line Modeling:

The modeling technique must be based on the information in Part (A) of the approach.

Regular transmission line structures can be modeled with traditional methods. Analytical equations are available to determine the effective relative permittivity for microstrip, coplanar, stripline, etc. configurations. With a known dielectric loss tangent, the losses can be computed from this information.

Irregular transmission line structures require other modeling techniques to predict losses. Usually, 2D or 3D simulation tools are used to model transmission lines with arbitrary cross-

sections. When all of the dielectric material information is available, these solutions are very accurate. The disadvantage is that simulation tools require a much longer solution time. However, if the dielectric is a composite, then these techniques are also not available. Therefore, a new approach is proposed in section 4.2 for solving this problem.

(C) Model Validation and Model Refinement:

The final part of the approach is to validate the model with measurements, refine the model parameters and apply the modeling for in time domain simulations when necessary.

4.2. Transmission Line Modeling with Dielectric Layers and Composites

When water is absorbed into a dielectric, the material becomes a composite. Different techniques have been used to model the electrical parameters of a composite material, as was discussed in Chater 2.

A very common technique is known as the Lichtenecker Mixing Equation, Eq. 4.4. The Lichtenecker Equation is very practical for investigating the relationship between water absorption and dielectric properties because (1) it is derived directly from Maxwell's Equations in [92] and (2), it includes an additional empirical factor, k (between -1 and 1), which can model a composite dielectric within the entire range of the Wiener Limits in [88]. For any mixture of two dielectric material volumes, regardless of how they are arranged, the effective dielectric parameters will fall between the Wiener Limits. One Wiener limit is when the two materials are arranged entirely in parallel, while the other limit is when the materials are entirely in series, as shown in Fig. 4.2. The limits Fig. 4.2 (a) and Fig. 4.2 (b) are represented by Eq. 4.1 and Eq. 4.2 respectively [88], where ε_1 and ε_2 are the permittivities of the two dielectrics and ε is the relative volume of the second dielectric. θ represents the volume ratio of the second dielectric. Fig. 4.2 (c) represents a homogenous mixture of two dielectrics and is represented by Eq. 4.3. The Lichtenecker Equation is Eq. 4.4, where k = 1 represents the Wiener Limit in Fig. 4.2 (b), k = -1 corresponds to Fig. 4.2 (a), and as k approaches 0, we have homogeneous absorption, Fig. 4.2 (c).

$$\varepsilon_{eff} = \frac{\varepsilon_1 \varepsilon_2}{(1-\theta)\varepsilon_1 + \theta\varepsilon_2} \qquad \text{Eq. 4.1}$$

$$\varepsilon_{eff} = (1-\theta)\varepsilon_1 + \theta\varepsilon_2 \qquad \text{Eq. 4.2}$$

$$\varepsilon_{eff} = \prod_{n=1}^{N} \varepsilon_n^{\alpha_n} \qquad \text{Eq. 4.3}$$

$$\varepsilon_{eff}{}^{k} = \theta\varepsilon_1{}^{k} + (1-\theta)\varepsilon_2{}^{k} \qquad \text{Eq. 4.4}$$

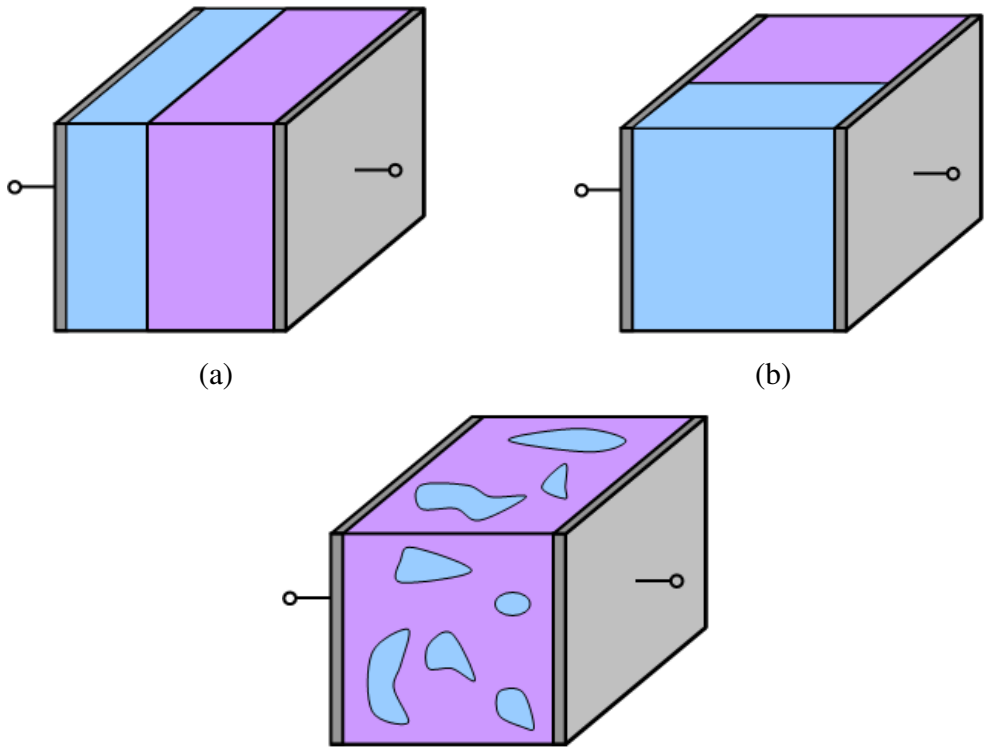

Fig. 4.2. (a) and (b) Distributions of two Wiener Limits, (c) Homogeneous composite distribution.

4.2.1. Modeling of Composite Properties

To model the effects of the moisture including the loss properties, the permittivities in Eq. 4.4 were examined in complex form, Eq. 4.5. The dielectric loss tangent, tan(δ), takes the form shown in Eq. 4.6, including the conductivity. It is, therefore, frequency dependent because the absorbed water has a finite conductivity (the second term of Eq. 4.6 makes it frequency dependent).

$$\varepsilon = \varepsilon_0 \varepsilon_r \left(1 - j \tan\left(\delta\right)\right) \qquad \text{Eq. 4.5}$$

$$\tan\left(\delta\right) = \tan\left(\delta\right)_d + \frac{\sigma}{\omega \varepsilon_0 \varepsilon_r} \qquad \text{Eq. 4.6}$$

In Eq. 4.6, the first term, $\tan(\delta)_d$, is the dielectric loss tangent dependent on dielectric loss mechanisms from polarization. The second term is dependent on conductivity, σ, and inversely proportional to the frequency. At very high frequencies, the second term in Eq. 4.6 becomes very small and the dielectric loss as a result of the polarization mechanism are dominant. At low frequencies, the second term in Eq. 4.6 becomes very large and the imaginary part of the permittivity becomes dominant in Eq. 4.5.

Because water is slightly conductive, the dielectric loss tangent at very low frequencies is dominated by the conductive part. As a result, the effective permittivity when calculated with the Lichtenecker mixing equation shows a drastic dispersion. At the low frequencies where the conductive term dominates, the effective relative permittivity of the composite is very high. The effective dielectric loss tangent is also very high. At higher frequencies, the effects decrease. The dispersion is also dependent on the distribution of the moisture. In Fig. 4.3, where 5% water ($\varepsilon_r = 80$, $\sigma = 0.25$ S/m) by mass is diffused into a polymer dielectric with a relative permittivity of 4.8, there is a large material dispersion in the composite dielectric characteristics. Both the permittivity and the dielectric loss tangent are much higher at low frequencies. For different distributions (where in the Lichtenecker Equation $k > 0$) representing a more parallel distribution, then the dispersion is still greater.

Fig. 4.4 shows the modeling of homogeneous diffusion of 5% water (by mass, $\varepsilon_r = 80$) into an epoxy polymer dielectric ($\varepsilon_r = 4.8$, $\tan(\delta) = 0.02$). In Fig. 4.4 the conductivity of the water is

treated as the variable. At low frequencies the tan(δ) of the composite is higher and then decreases for higher frequencies. Higher water conductivities show the decline at higher frequencies, with 4 S/m having a much higher loss tangent into the multi-gigahertz range. Meanwhile, the relative permittivity shows the same trend of starting very high and falling but stabilizing at higher frequencies. The permittivity curves are shifted to higher frequencies, meaning that the permittivity is higher in the lower frequencies, for higher conductivities.

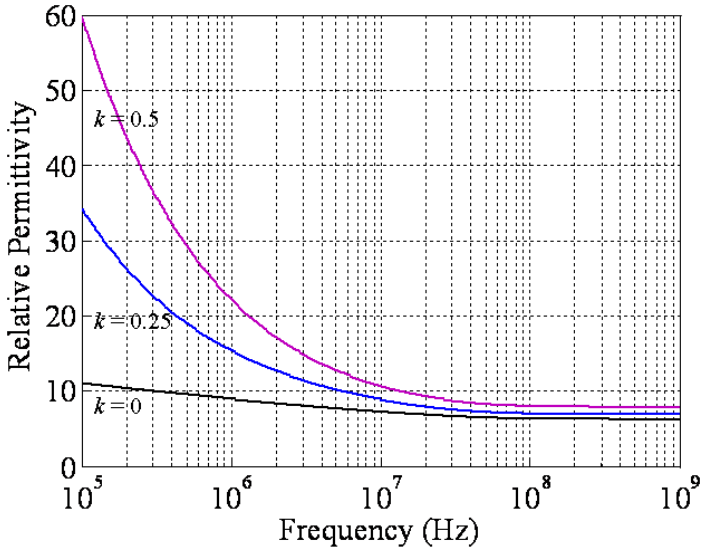

(a)

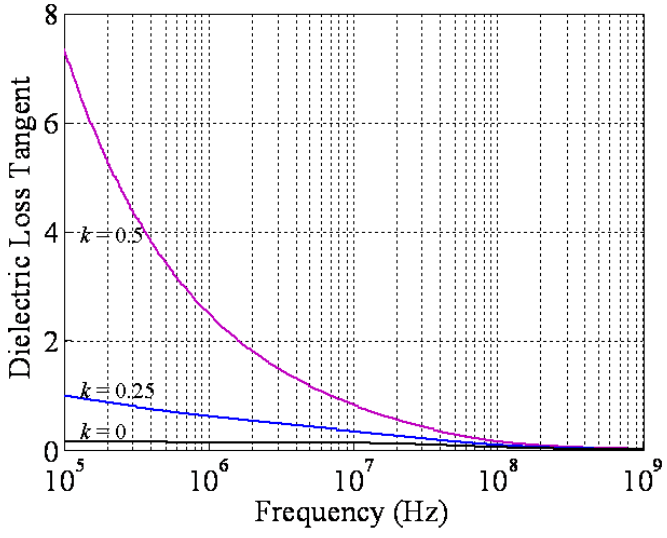

(b)

Fig. 4.3. Modeled dielectric characteristics for different composite distributions, σ = 1 S/m, (a) relative permittivity, (b) dielectric loss tangent.

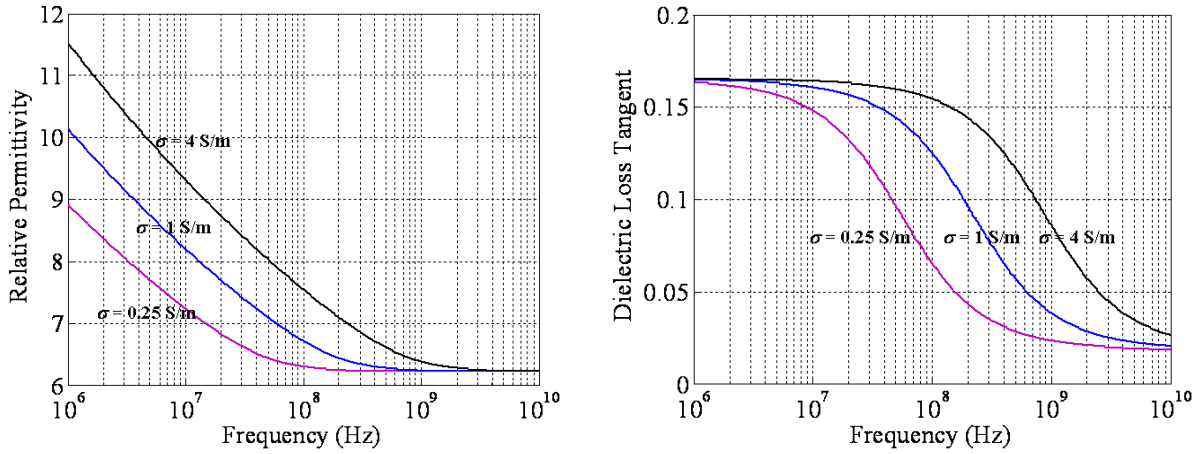

(a) (b)

Fig. 4.4. Modeled dielectric characteristics for different moisture conductivities, k = 0, (a) relative permittivity, (b) dielectric loss tangent.

Different technological tolerances could lead to these effects in a module. For example, adhesion loss or delamination could lead to moisture concentrating on an interface, leading to a more parallel distribution and more significant electrical effects. A crack in a dielectric could lead to anisotripic properties. Ions in the absorbed moisture or in an encapsulation material during encapsulation could lead to higher conductivity of the moisture absorbed into the encapsulation material.

4.2.2. Demonstration of the Composite Dielectric Modeling Approach for Coplanar Transmission Lines

In [123] Chen and Chou offer a model, based on conformal mapping techniques for modeling the capacitance of a coplanar waveguide. Then, using the theory of superposition of capacitances, Chen expands the model to include multiple dielectric layers above and below the metallization layer, similar to the structure in Fig. 4.5, which will be a focus of this chapter. In his paper, the model was theoretically investigated for dielectrics with three different layers under a coplanar transmission line and two layers above. The model was experimentally validated for dielectrics of two layers under the transmission line and one layer above. In fact, the model was validated for a Si/SiO_2 substrate cavity, which shows us that the model is valid for both lossless and lossy dielectric materials. When the capacitance and conductance are known, we can find the dielectric

attenuation using Eq. 4.7. Because we begin with a complex permittivity it is easier, in our case, to write the expression with a complex capacitance, as in Eq. 4.8, instead of a capacitance and a conductance.

$$\gamma = \sqrt{(R' + j\omega L')(G' + j\omega C')} \qquad \text{Eq. 4.7}$$

$$\gamma = \sqrt{(R' + j\omega L')(j\omega(C_R + jC_I))} \qquad \text{Eq. 4.8}$$

$$\alpha_d = \mathrm{Re}\sqrt{(j\omega L')(j\omega(C_R + jC_I))} \qquad \text{Eq. 4.9}$$

To find only the dielectric attenuation, the resistance, R′= 0, and therefore the L′ is approximated as constant and frequency independent. The inductance of the transmission lines were calculated using the 2D filament model shown in the previous section. So, the effective complex capacitance and the inductance are used to determine the dielectric attenuation with Eq. 4.9.

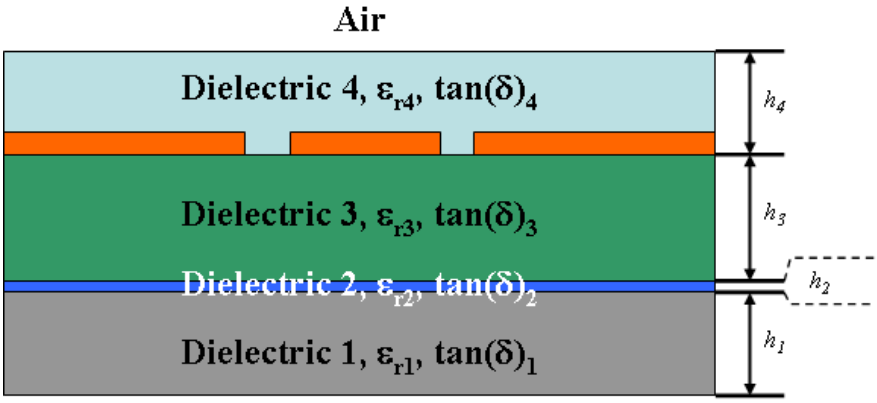

Fig 4.5. The dielectric structure simulated using the multilayer substrate model.

The Chen model was implemented using Matlab and its implementation was validated by comparison to the results published in the paper [123]. To simulate lossy dielectrics, where applicable, complex frequency dependent permittivities were constructed using Eq. 4.6. Material parameters have the properties shown in Table 4.1. The model approximates the conductor as infinitely thin.

TABLE 4.1. Material properties of the model in Fig. 4.6 and Fig. 4.9.

Material	Relative Permittivity	Dielectric Loss Tangent	Conductivity (S/m)
Silicon	11.9	0.02*	0.05*
Silicon dioxide	4	0	0
BCB	2.6	0.08	0
Encapsulation	4.8	0.02	0
Moisture	80	0.02	0.25 S/m
Glass	4	0.01	0

*These values are realistic values of commercially available high resistivity silicon used to demonstrate the model. Actual silicon electrical characteristics are dependent on the doping of the silicon.

The structure that will be initially investigated is shown in Fig. 4.6. It is a BCB redistribution layer, constructed on a glass substrate, with a thin SiO_2 layer between. Above the redistribution layer is a thin film coplanar transmission line with a polymer encapsulation material on top. The encapsulation material has saturation absorption of 5% water by mass (which is a realistic value for a silicon epoxy).

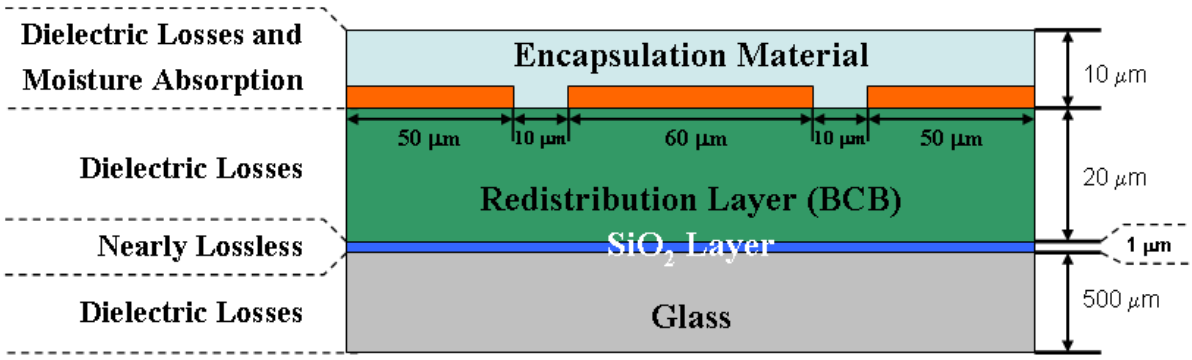

Fig. 4.6. Realistic dielectric buildup for 3D integration on a glass interposer.

First, the k variable in the Lichtenecker Equation was investigated. Three values were used, $k = 0$ was used to simulate an encapsulation with homogeneous moisture diffusion. To investigate moisture completely on an interface, $k = 1$. To simulate moisture partially diffused into the material and partially settled on the interface, $k = 0.5$ was assigned. The results are shown in Fig. 4.7. For this investigation, the loss characteristics for all of the materials were set to zero except

for the moisture. The goal of this investigation is to find the effects of only the moisture on the dielectric attenuation.

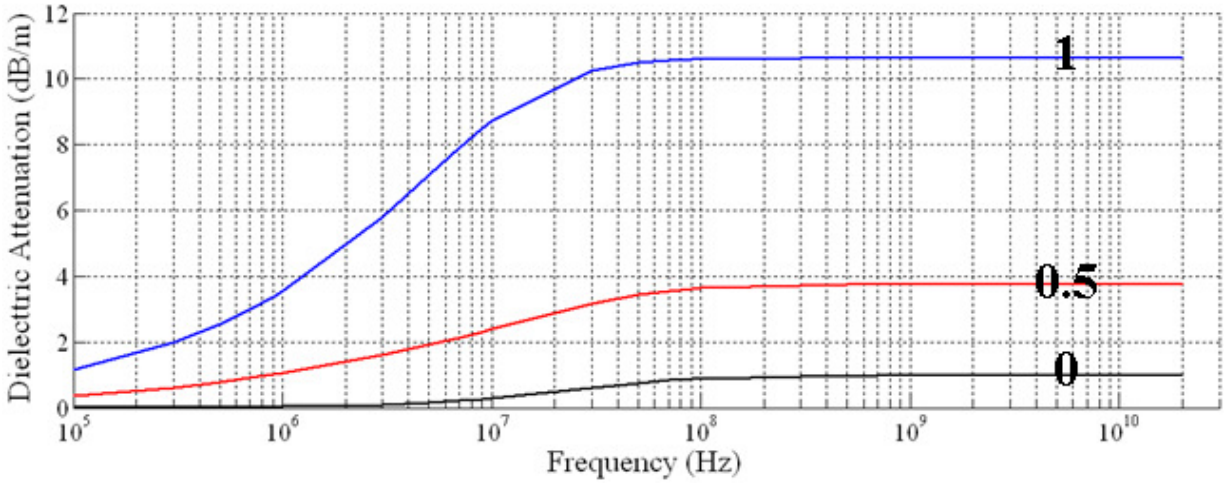

Fig. 4.7. Dielectric attenuation from moisture for three different mixing constants (σ = 0.25 S/m).

It becomes apparent looking at Fig. 4.7 that absorption that is parallel inhomogeneous, where the moisture contacts both the signal and ground metallization, results in much higher losses that moisture that is homogeneously absorbed. The losses begin in the MHz range and increase but then level off. Galvanic losses, as a result of conductivity in a dielectric, are usually frequency independent. However, in our case, the dielectric is a composite and the polymer dielectric material acts as a isolation layer. Until a certain frequency the polymer prevents the galvanic losses.

The second investigation looks at the conductivity of the moisture. Conductivity of water is related to the amount of ions present. If there are ions in the encapsulation material during fabrication, or if there are ions in the air or moisture during the absorption, then the conductivity of the moisture will vary. The results for three different conductivities are shown in Fig. 4.8.

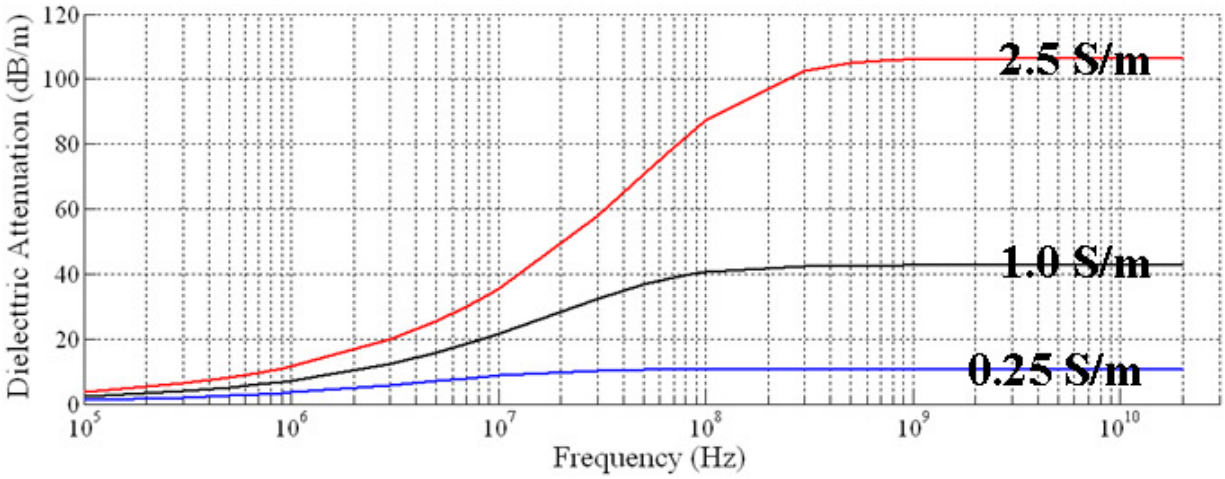

Fig. 4.8. Dielectric attenuation from moisture for three different moisture conductivities (k = 1).

The trend remains the same as the conductivity increases. At low frequencies, the dielectric losses from the moisture remain negligible. In the MHz frequency range they increase and level off. The higher the moisture conductivity value, the higher the losses. It is also a linear relationship. When the conductivity doubles, the stabilized value of the losses from the moisture also doubles. And for high conductivities, especially above 1 S/m, the losses become significant in comparison to conductor or dielectric losses from dielectric loss mechanisms.

The next investigations aim to show the dielectric losses in comparison to each other. The first structure that was investigated with this model was a coplanar line, packaged using thin-film technology, encapsulated with a polymer underfill. The specific dimensions are shown in Fig. 4.9.

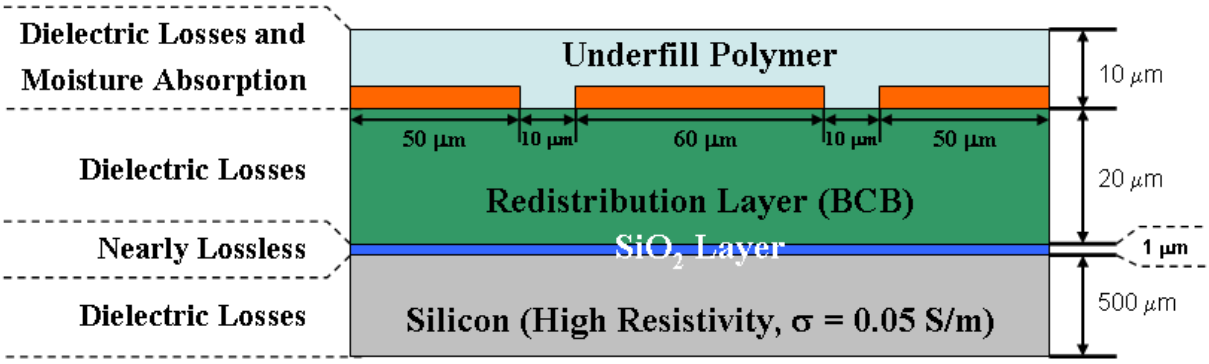

Fig. 4.9. Realistic dielectric buildup for 3D integration on a high resistivity silicon interposer.

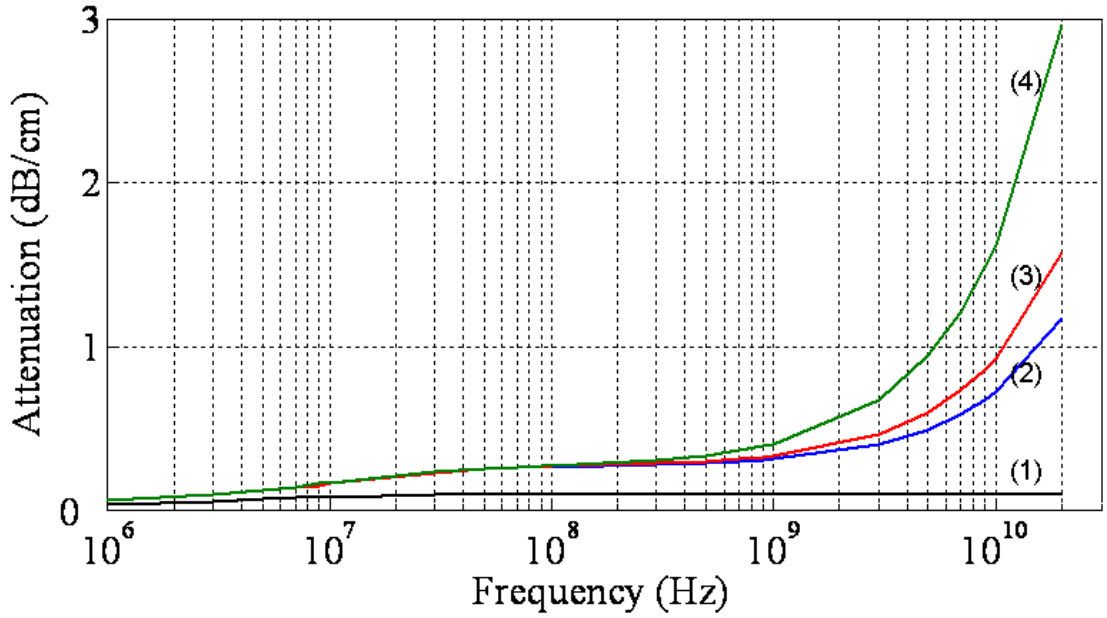

Fig. 4.10. Sources of the dielectric losses in the structure in Fig. 4.6. (1) Moisture (parallel isotropic), (2) Moisture and silicon, (3) Moisture, silicon, and Encapsulation, (4) Moisture, Silicon, Encapsulation, and BCB.

For the calculation of the dielectric losses, the underfill material is said to absorb 5% moisture and in the Lichtenecker Equation, $k = 1$. This is designed to simulate moisture settled onto the dielectric interface between the encapsulation material and redistribution layer. The conductivity value is an experimentally determined value for distilled water (determined in the second case study, something that will be discussed in chapter 5.2).

In this buildup we see that the galvanic losses for silicon and the losses for the moisture have similar trends, except that polarization losses in the silicon are introduced in the GHz frequency range. This makes sense because they are both semi-conductive dielectrics that are separated from the conductor with an isolation layer. For transmission lines on silicon, this has been referred to as the slow-wave effect, because the effective permittivity is very high at low frequencies causing a higher delay [124, 125].

Fig. 4.6 shows the same buildup that was used in Fig. 4.9, except that the interposer material has been changed from high resistivity silicon to glass. This is the buildup used to generate Fig. 4.11. Glass is non-conductive, which eliminates the slow-wave effect seen before with a silicon substrate. From 10 MHz up to 1 GHz, the moisture losses dominate. The losses, however, are

still very low, especially considering that this is for moisture concentrated along the interface which is the highest loss case. Above 2 GHz, the losses as a result of the dielectric loss tangents of the polymer dielectrics become strongly dominant, and at 20 GHz, the losses from moisture only accounts for about 6% of the total losses.

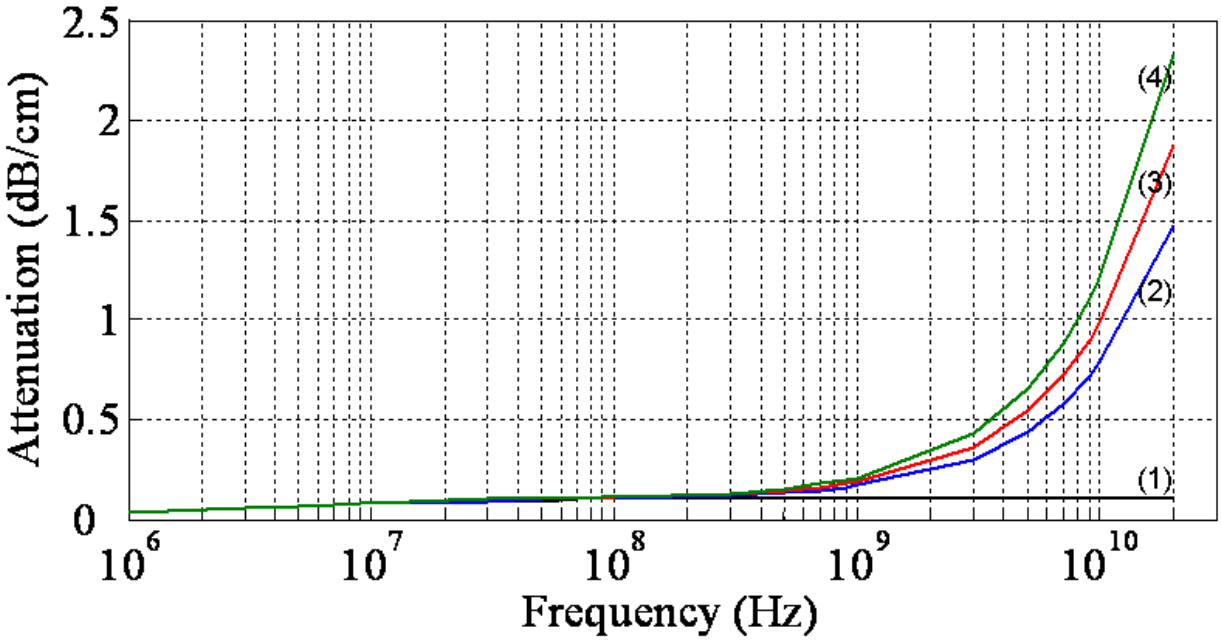

Fig. 4.11. Sources of the dielectric losses in the structure in Fig. 4.6. (1) Moisture (parallel isotropic), (2) Moisture and BCB, (3) Moisture, BCB, and Encapsulation, (4) Moisture, BCB, Encapsulation, and Glass.

Chapter 5: Experimental Validation of Signal Integrity Models for Non-Ideal Transmission Lines and Dielectrics

The models presented in Chapters 3 and 4 have been developed through theoretical electromagnetics and numerical methods. Therefore, these models will be validated with comparisons to measurements of sample structures.

5.1. Case Study 1: Modeling of Transmission Lines Printed with the M3-Process

In this section, we present an example of coplanar transmission lines with loss characteristics that are complex to characterize. Fig. 5.1 shows a 3-dimensional image of a coplanar transmission line segment printed using a modern printing process and Fig. 5.2 shows a photograph of the same structure. From the 3D image, one can see the roughness pattern on the top of the signal conductor, the center conductor section. The plane that is highlighted over the cross-section was the location where the transmission line dimensions and surface roughness characteristics were measured in Fig. 5.3.

For the fabrication of these transmission lines, a dispersion of nanoscaled silver particles was printed on a glass substrate with a CAD driven, maskless Aerosol Jet® printer from Optomec Inc. For this purpose, the dispersion was transferred in an aerosol stream by use of an ultrasonic source and then deposited on the substrate by a focused beam. The process resulted in small line widths of 25 µm and sharp edge definition. The lines were sintered afterwards in a convection furnace at 250°C for 120min. This maskless deposition technique is valuable for rapid

prototyping applications, e.g. for printed antennas, embedded passives and sensor structures, respectively [126].

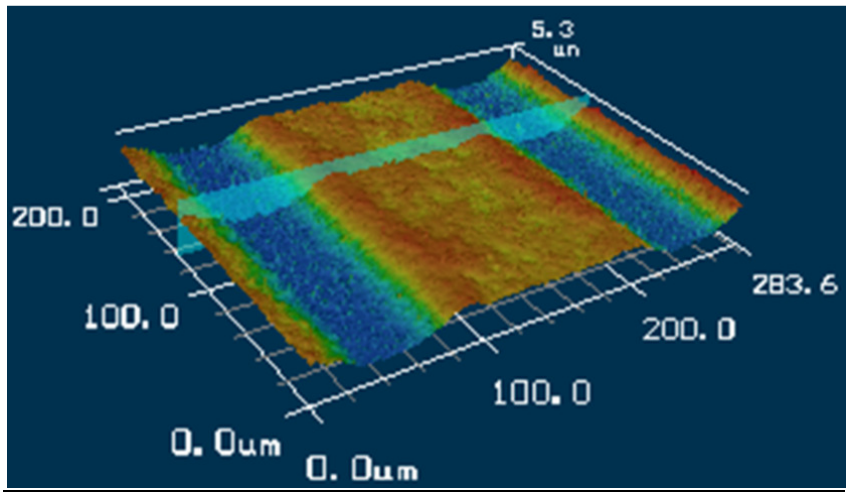

Fig. 5.1. 3-dimensional image of a coplanar transmission line.

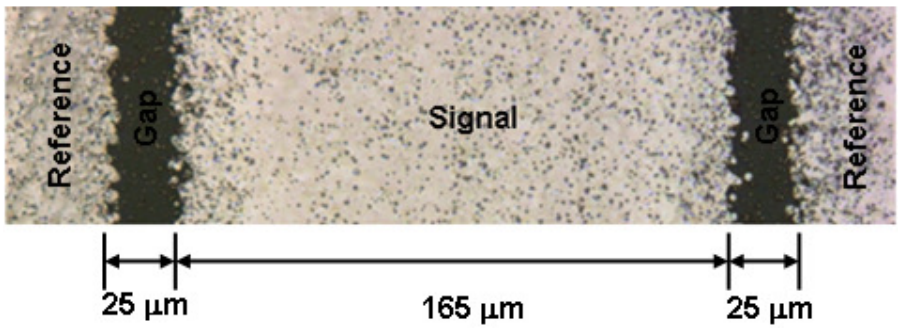

Fig. 5.2. Photograph of a printed coplanar transmission line.

5.1.1. Challenges Associated with Modeling Aerosol Printed Transmission Lines

The DC resistance of the transmission line is dependent on the cross-sectional area of the signal conductor. Fig. 5.3 (top) is a profile measurement of the signal line and Fig. 5.3 (bottom) is a profile measurement of the coplanar gap. The surface roughness of the conductor penetrates a significant amount into the surface of the conductor in comparison to the thickness of the conductor. In this case, the surface roughness will also play a role at low frequencies and the

impact will increase into the high frequency range. Because the surface roughness is 3-dimensional, the average cross-sectional area cannot be known from a single profile measurement and can only be assumed to be similar to that of the single cross-sectional profile. In the 3D image in Fig. 5.1, the roughness appears relatively uniform in the z-direction. Also, because the line is much wider than the RMS roughness height and because the fabrication technology remained constant, we will assume that the longitudinal direction has similar roughness characteristics to the lateral direction. At high frequencies, as the skin-depth decreases to a similar height as the surface roughness, the current must meander through the peaks and valleys of the roughness, increasing the resistance further. The edges of the conductors are very narrow angles – which have been referred to as edge-shape effects in this dissertation. This is further complicated by a strong proximity effect, as a result of adjacent conductors, which draws the current further into the edge of the conductor. As the frequency increases, the surface roughness effect will not only increase due to skin-effect, the proximity effect and edge-effects will also have an impact on its behavior. Furthermore, the surface roughness on the return current paths must also be analyzed because the proximity effects and edge effects will cause current crowding as well on the reference conductors.

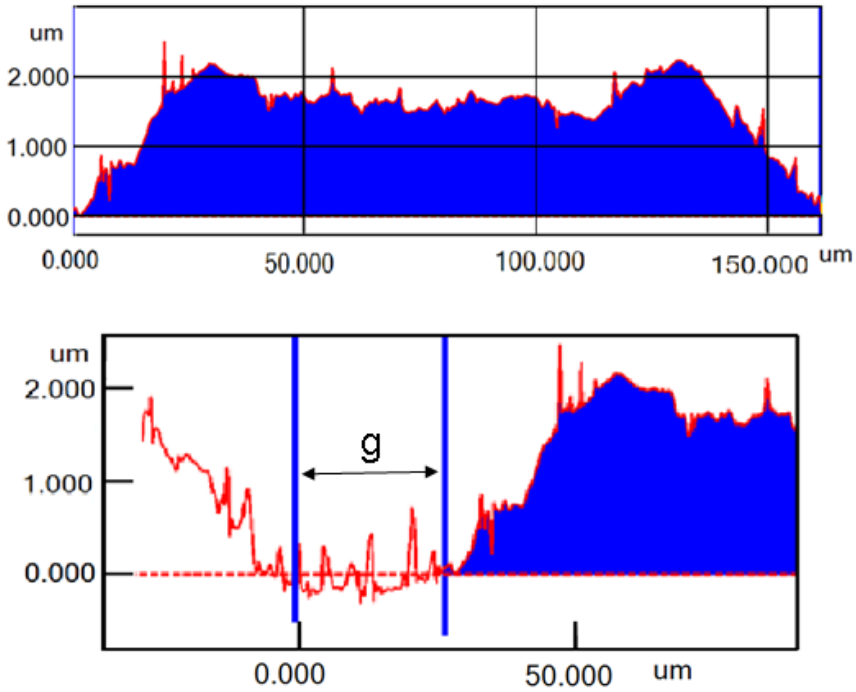

Fig. 5.3. Cross-sectional profile measurements of a coplanar transmission line, signal conductor (top), coplanar gap (bottom).

Fig. 5.4 shows Scanning electron microscope (SEM) photos of sintered and unsintered printed conductors. The image of the structure in Fig. 5.1, for example, was taken after sintering. This highlights another challenge of surface roughness modeling. The fabrication, as well as treatments after fabrication, can have a strong effect on the RMS roughness height and the form and constitution of the metallization.

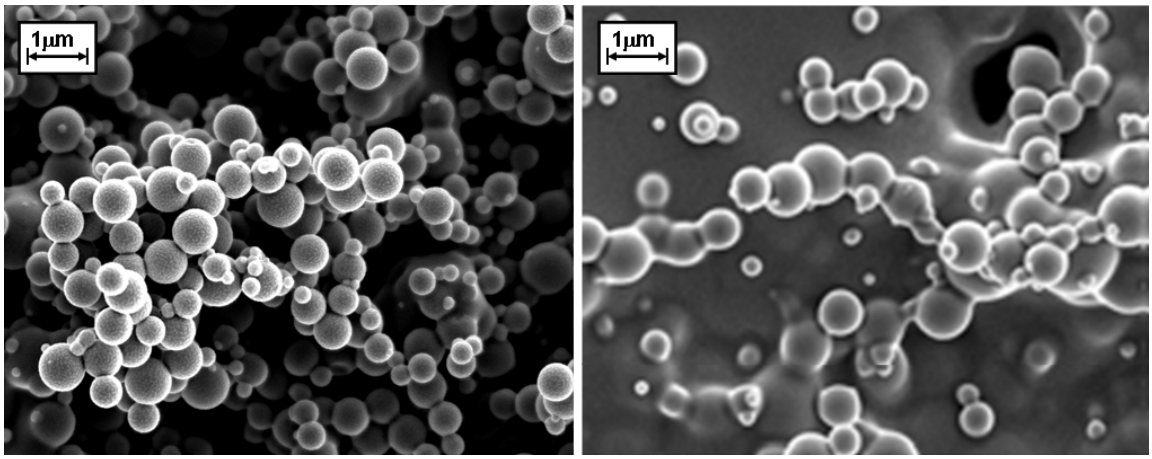

Fig. 5.4. SEM images of, unsintered silver conductor (left), sintered silver conductor (right).

5.1.2. Experimental Validation and Characterization of Transmission Line Samples

The first method used to validate the proposed model is to compare this to a traditional surface roughness model. This is only possible when we impose the limitations of the traditional model onto the proposed model. This means that, (1) the models are compared for a transmission line with heterogeneous roughness; (2) the results are normalized by subtracting the DC difference so that no DC effects are included; (3) no proximity effects are included; and (4) no return current path is included. These limitations are imposed because the traditional surface roughness models are limited and we hope to make a fair comparison between the adapted model and the traditional models. Essentially, we use the adapted filament model to model a conductor prism with a homogeneous surface roughness profile around the entire perimeter – an unrealistic case and valuable only as a comparison. The conductor, 10 µm wide and 5 µm thick copper, is simulated with and without roughness (0.45 µm RMS roughness height). To remove the DC effects in the

Adapted Filament Model, the results are scaled down by subtracting the small DC difference (which will cause no significant deviations at high frequencies because the DC difference is very small compared to the HF resistance) before dividing the curve with roughness by the curve without roughness. Fig. 5.5 shows the similarity. The two correction factors deviate from each other by less than 10% across the entire frequency range.

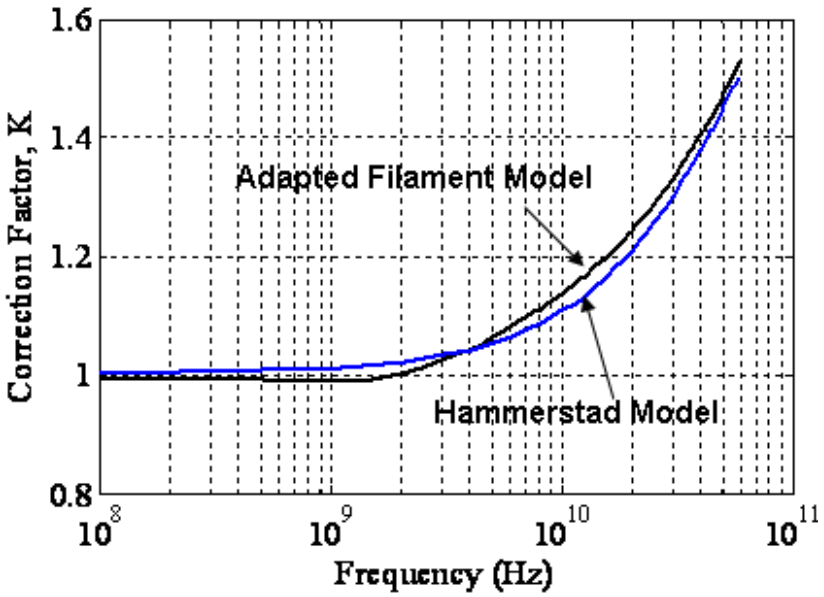

Fig. 5.5. Comparison of the Hammerstad and Adapted Filament Models for surface roughness modeling.

But, to accurately validate the Adapted Filament Model, because it is a much different technique than state-of-the-art methods, it must be compared with measurements. So, the adapted model was then used to model the transmission line in Fig. 5.1. The width of the line in the model was w = 165 μm, the average thickness was t = 1.7 μm, the gap distance was g = 25 μm, the modeled surface roughness on the top and angled surfaces was an average of 0.25 μm, and the surface roughness of the bottom surface was zero (the dimensions are also shown in Fig. 5.3). The bottom surface roughness was assumed to be the roughness of the glass substrate, which, with a separate measurement was less than 20 nm (this is the minimum surface roughness height that the machine could measure, so we only know that it is smaller than that height). The roughness in the gap in Fig. 3 is from overspray of nanopartical agglomerates, any effects of which are neglected. The measured surface roughness height was 0.44 μm RMS. The length of the measured line was l = 15 mm. The conductivity of the metallic ink was $\sigma = 2.5 \times 10^7$ S/m, in the

range of what the manufacturer specifies, but was determined by matching the lowest frequencies in the model and measurements (considered the quasi-DC case). The lower angles of the conductor trapezoids were 4.8°, which was calculated from the profile measurements (Fig. 5.3). The characteristic impedance was determined analytically to extract the attenuation from S-parameter measurements. In Fig. 5.6, the measurement was compared to the results of the model. The computation was done with a Matlab program and took approximately 20 minutes.

The discretization of the filament model was based on the highest frequency to be measured, 20 GHz. Based on the conductivity of the ink, the skin-depth δ at 20 GHz would be 0.7 μm. The cross-section was then discretized into 210 filaments horizontally, which means that w_{fil} is approximately equal to skin-depth, δ, for the bottom of the conductor, where the conductor width is the widest. The trapezoidal cross-section was accounted for by decreasing the w_{fil} of the row, and shifting the row to the center, as shown in Fig. 5.6 (a). The vertical measurement, t, was discretized into 4 filaments. This means $h_{fil} = 0.6\delta$. This was set smaller to better model the corner frequency as the skin-depth decreases below the conductor thickness and approaches the surface roughness height. Both return current conductors had the same discretizations. At lower frequencies, larger filaments were used to save computation time but the same guidelines with regard to skin-depth and filament dimensions were applied or exceeded.

The structure was built on a glass dielectric. Estimating for glass that the dielectric loss tangent, tan(δ), is 0.001, then based on a quick analytical estimate, from Eq. 5.1 (where q is the filling factor, λ_g is the guide wavelength, and tan(δ) is the dielectric loss tangent) the dielectric losses will be less than 3 dB/m at 20 GHz [16]. The substrate losses then compose approximately 1% of the overall losses. For this reason, they are neglected during the following calculations.

$$\alpha_d = \frac{q\varepsilon_r \tan\delta}{\varepsilon_{eff}\lambda_g} \qquad \text{Eq. 5.1}$$

S-parameters were measured with an Agilent VNA, using GSG probes with 150 μm pitch from Cascade. The analyzer was calibrated with a standard impedance substrate from Cascade using the LRRM method. The transmission lines were on a 1 mm thick glass substrate that was placed directly on the chuck. The resistance of the measured lines was extracted from the s-parameter measurements with Eq. 5.2. A moving average program was then applied to the measurements.

Accuracy of the model at high frequencies can be improved by increasing the discretization. Over the entire frequency range, the average deviation between measurement and modeling, shown in Fig. 5.6 (b), is less than 2%.

$$R = 2Z_0\alpha \qquad \text{Eq. 5.2}$$

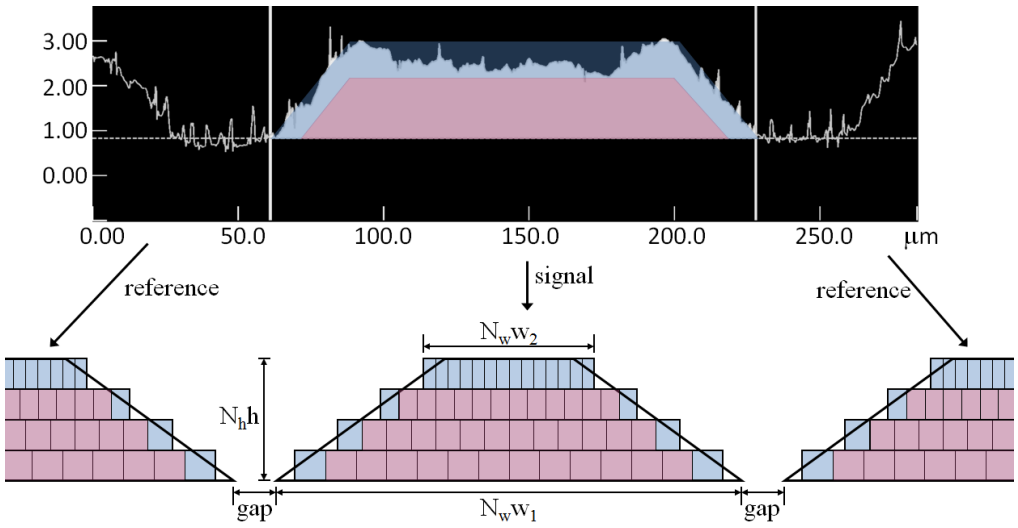

(a)

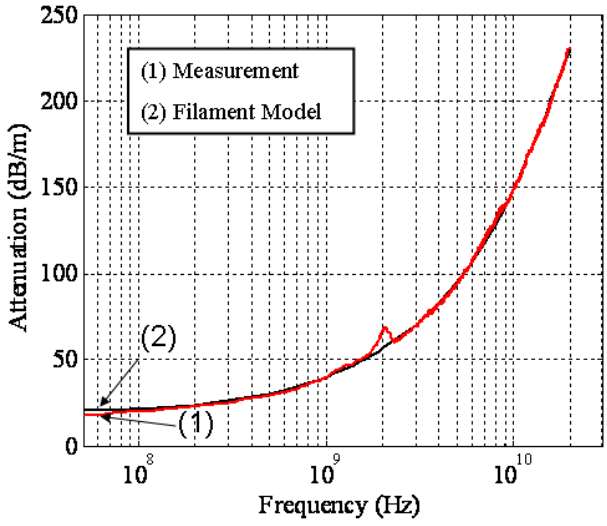

(b)

Fig. 5.6. (a) The conductor discretization from the conductor cross-section measurement, (b) Modeling and measurement results of the attenuation.

The transmission line used during this validation is unique because the skin-depth is first equal to half the conductor thickness around 15 GHz but roughness has an effect starting around 2 GHz. This means that an accurate full-wave simulation should generate a mesh inside the conductor

because the resistance will not be accurately computed for the lower frequencies. Generating a mesh inside the conductor, for a transmission line of this size and width to height ratio, will drastically increase computation times. This complicates the state-of-the-art approach of applying a correction factor to the surface resistivity during a full-wave simulation. Full-wave simulations also do not offer physical insight into the source of losses.

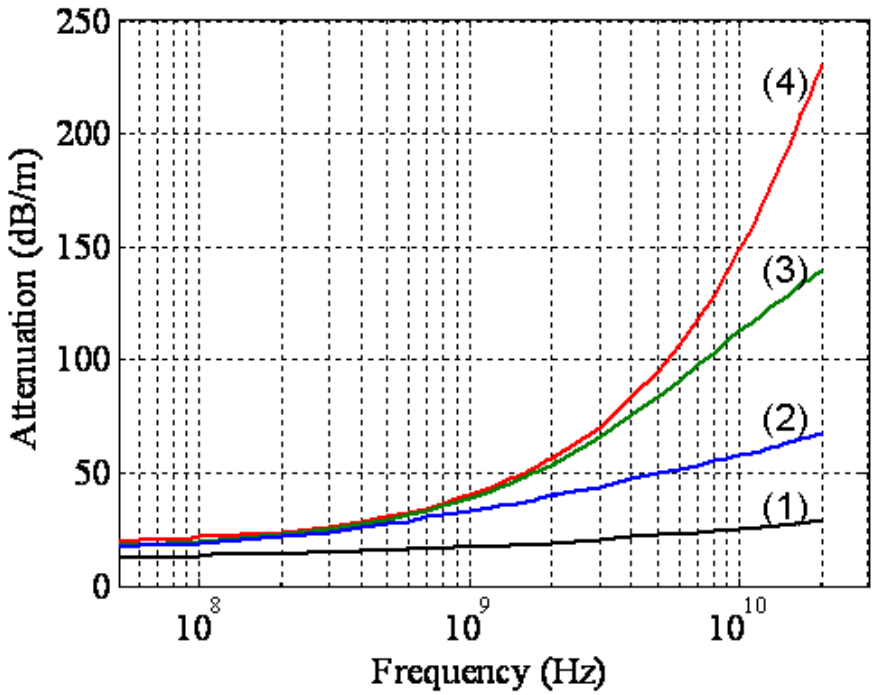

Fig. 5.7. Breakdown of losses in a coplanar line, (1) Skin-effect in ideal conductor slab, (2) Skin-effect and proximity effect in an ideal coplanar line, (3) Skin-effect and proximity effect in a coplanar line with angled edges, (4) A trapezoidal coplanar line with surface roughness.

Using the filament model, one can determine the source of the different losses. By eliminating the reference planes, the surface roughness correction, and the trapezoid angles, the attenuations as a result of a skin-effect in an ideal conductor is determined. Adding the reference conductors, the impact of the proximity effect is demonstrated – an ideal coplanar transmission line. Then the angles are added to the conductors to determine the impact of edge-effect on the losses. Then, finally, the Adapted Filament model is used. This breakdown of losses is shown in Fig. 5.7. The edge-effects begin to have an effect starting around 500 MHz and the surface roughness effect around 2 GHz. At 20 GHz, the modeled losses, with the non-idealities included, exceed the ideal rectangular coplanar transmission line by more than 300%. This breakdown offers an additional

advantage over traditional methods because the modeling can also be applied during the characterization phase of a transmission line to examine the magnitude and frequency ranges of different effects. This breakdown can also be used for optimization of conductor dimensions.

The previous technique was used with two other transmission lines to show the effects of various parameters, material and geometric, on the conductor losses. Fig. 5.8 shows the second coplanar waveguide that will be modeled. The measured conductivity, $\sigma = 1.5 \times 10^6$ S/m. The dimensions are reflected in the diagram. The thickness, $t = 3.0$ μm. The surface roughness on the top is 0.46 μm and the lower angles of the metallization are 25° (based on profile measurements).

The skin-depth at the highest frequency is $\delta = 1.6$ μm. It is much larger because the conductivity is much smaller. In this example, the model is used to investigate surface roughness effect where δ is several times larger than H_{SR}. Therefore, an especially large discretization was used to achieve a higher accuracy. At lower frequencies, larger filaments were used to save computation time but the same guidelines with regard to skin-depth and filament dimensions were applied or exceeded.

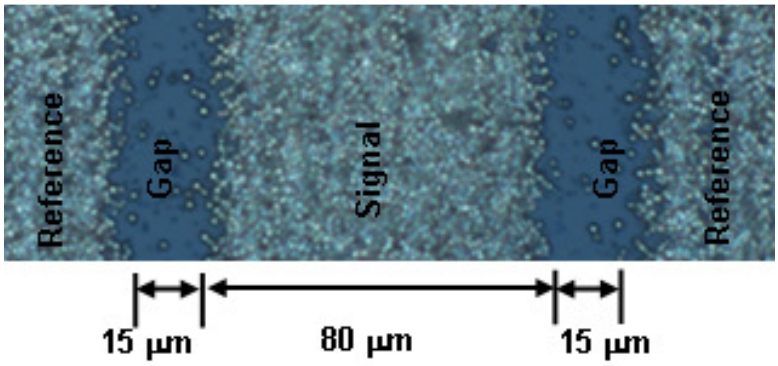

Fig. 5.8. First printed coplanar waveguide sample.

Fig. 5.9 shows the modeling and measurement of the first coplanar line. The modeling shows that, despite the fact that the surface roughness height is significant; the roughness has only a small effect, even into the multigigahertz range because the conductivity is smaller, meaning a larger skin-depth and a less significant proximity effect.

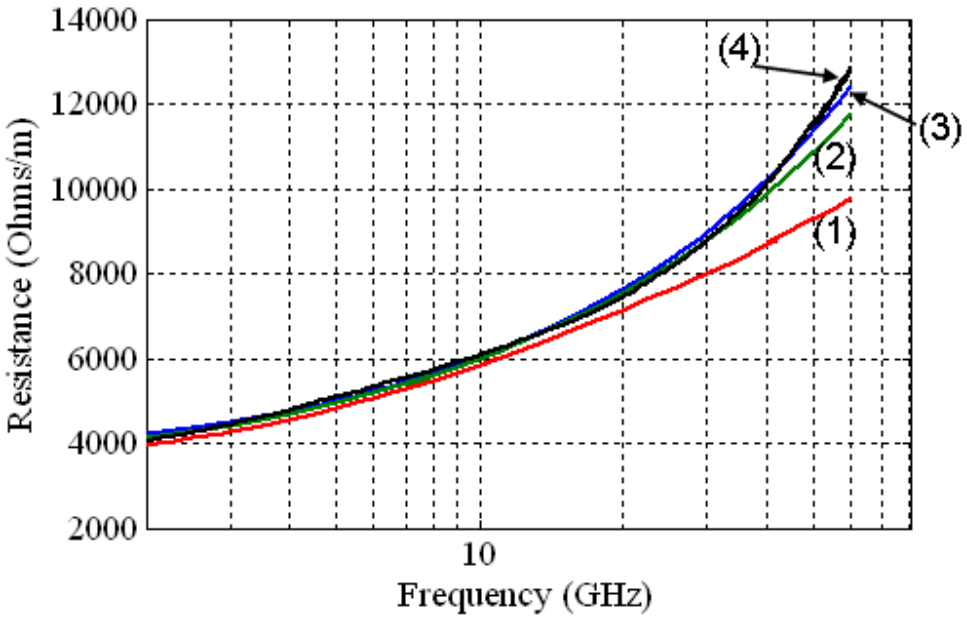

Fig. 5.9. Modeling and measurement of the coplanar waveguide from Fig. 8, (1) ideal transmission line, (2) trapezoidal transmission line, (3) trapezoidal line with roughness, (4) measurement.

In Fig. 5.9, the roughness begins to show an effect around 40 GHz. At 40 GHz, the skin-depth δ is approximately ¼H_{SR} (H_{SR} = peak-to-peak RMS surface roughness height). The edge-effects first play a role at 20 GHz.

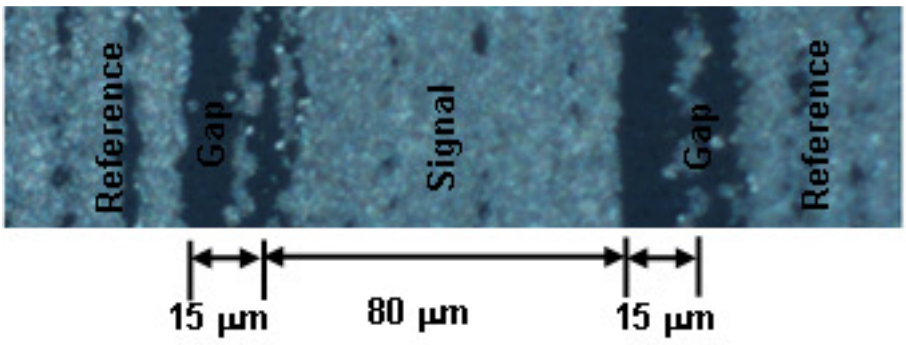

Fig. 5.10. Second printed coplanar waveguide sample.

The next sample, in Fig. 5.10, has similar dimensions to the previous sample in Fig. 5.8. The conductivity, however, is higher, $\sigma = 3.5 \times 10^6$ S/m. The thickness is smaller, t = 1.5 µm, but the surface roughness is also smaller, H_{SR} = 0.25 µm. The lower angles were approximated at 9°.

Additionally, the coplanar gap is not as well defined as in the previous transmission line. The same discretization was used for this conductor as was used for the previous conductor.

So, for this coplanar line, the conductivity is approximately doubled and the thickness is halved. Therefore, one would expect to see a very similar frequency response. Indeed, in Fig. 5.11, the frequency response is very similar to that of the coplanar waveguide modeled in Fig. 5.9.

The modeling of the coplanar waveguide in Fig. 5.10 shows that surface roughness has an effect first at around 30 GHz – also the multigigahertz range (where $\delta = 1/6\ H_{SR}$). The edge-effects also play a role earlier, less than 10 GHz – as expected because the angle is smaller.

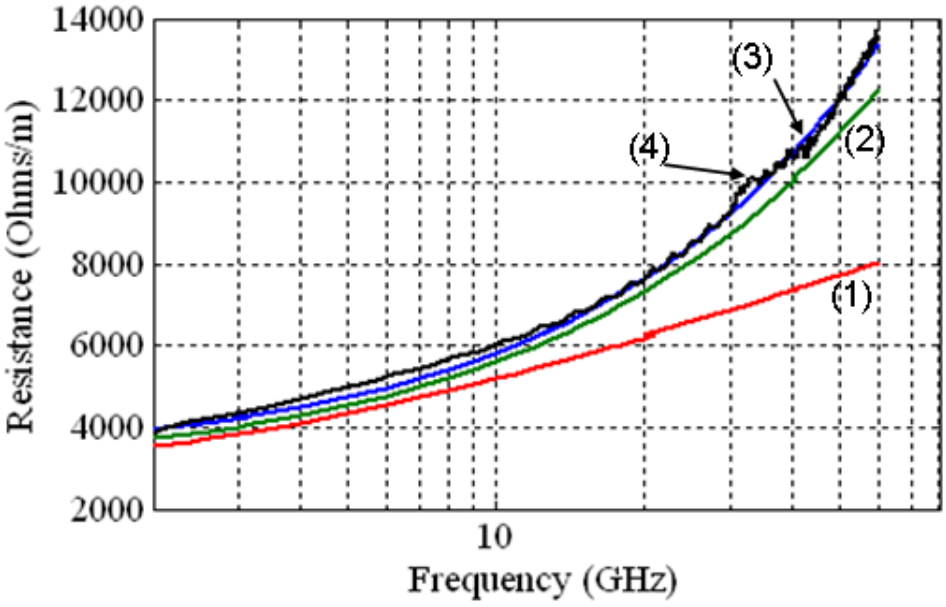

Fig. 5.11. Modeling and measurement of coplanar waveguide from Fig. 10, (1) ideal transmission line, (2) trapezoidal transmission line, (3) trapezoidal line with roughness, (4) measurement.

5.2. Case Study 2: The Influence of Moisture Absorption on the Electrical Parameters of Coplanar Transmission Lines

A application in electronics where composite dielectrics are common is in encapsulation materials. Encapsulation materials are common in electronic packaging to achieve hermetic packages. These materials are not completely hermetic, however, and absorb water or humidity

from the air. The saturation absorption usually lies between 2% and 5% by volume, but it can be higher in some cases. The absorption follows Fick's Law of Diffusion [93].

In this Chapter it will be shown that moisture absorption will not normally cause electrical failure in electronic modules. However, when moisture absorption is coupled with structural faults in the modules it can lead to electromagnetic reliability problems.

5.2.1. Design of Interdigital Capacitors

To validate the dielectric loss models in Chapter 4, an IDC is fabricated on FR4 that does not absorb a significant amount of moisture (<0.05% by mass, according to the technical data sheet, which will be neglected for the duration of the chapter). The structure was fabricated using a milling machine. The IDC was then encapsulated using an encapsulation material that absorbs 5.3% moisture at saturation. This saturation value was determined experimentally by examining the mass of a polymer disc. The mass of the disc was taken with a high tolerance scale before and after soaking the disc in water for 10 days. The IDC, shown in Fig. 5.12 has 80 fork tines (40 per electrode). The width, length, and separation distance of each tine is 220 μm, 20.75 mm, and 280 μm respectively. These dimensions, according to the schematic simulator in Agilent ADS, achieve a capacitance of approximately 80 pF, which can be accurately measured with an Agilent 4294A Precision Impedance Analyzer. According to the specification of the impedance analyzer, the measurements should be correct within 10% starting at 1 kHz, 3% starting at 1.5 kHz, and 1% at 20 kHz. They remain accurate to 3% up to 110 MHz, which is the maximum frequency that can be measured with the device [127].

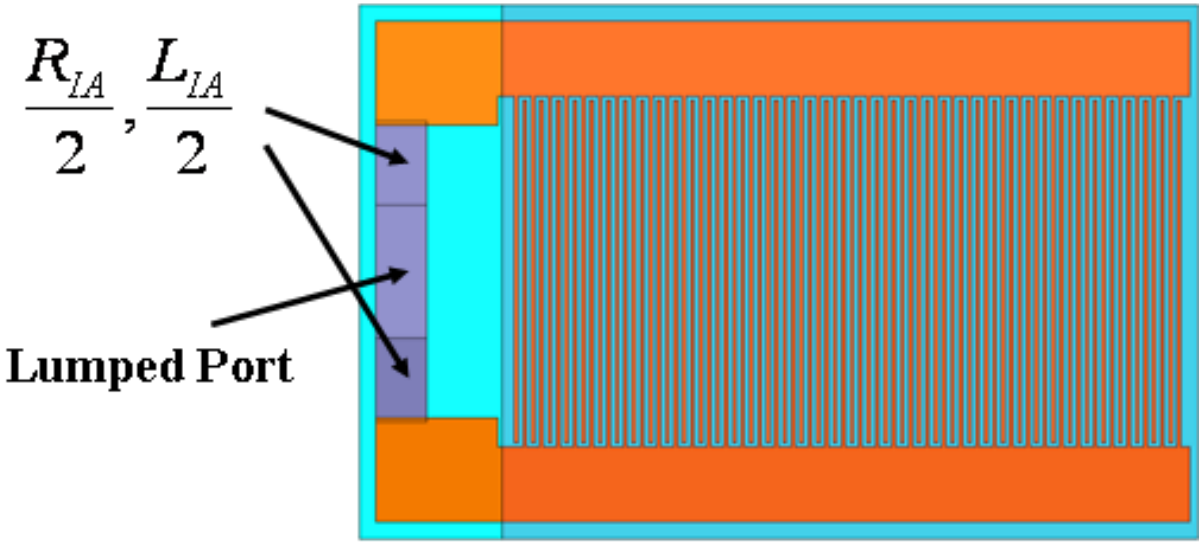

(a)

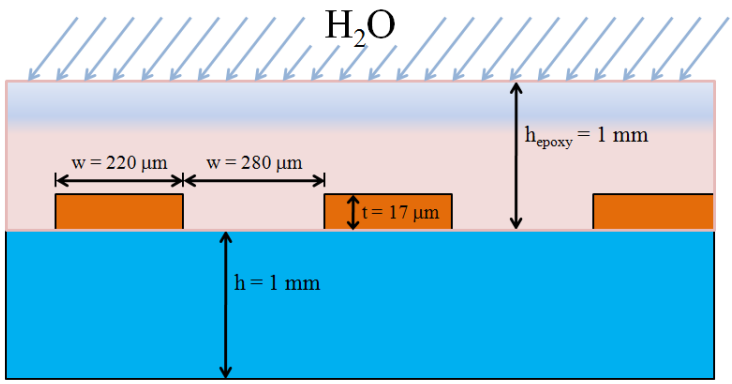

(b)

Fig. 5.12. Diagram of an IDC used for material characterization of polymer encapsulation material, (a) top view, (b) cross-sectional view.

5.2.2. High Frequency Measurement and Characterization

The IDC was first measured with the encapsulation material shortly after encapsulation. It had not been exposed to water and had been stored in a low humidity environment up to the time of measurement. The IDC was also modeled in Ansys HFSS (formerly Ansoft). The model was simulated using a convergence technique to achieve stable results. A lumped port was used, as shown in Fig. 5.12 with an inductance and resistance in series to represent the internal impedance of the impedance analyzer. This simulation and measurement act as a control sample, being used to validate the HFSS model and measurement technique for dry dielectrics. When this model

provides accurate results, then the dielectric properties of the encapsulation dielectric can be changed using the approach shown in Chapter 4 and re-simulated.

The results of the capacitance modeling and measurement of the control are shown in Fig. 5.13. The capacitance starting around 1 MHz, up to 80 MHz show very close agreement (with only around a 3% average difference). The discrepancy is higher at the lowest frequency, which could be explained by a very small amount of ions in the encapsulation material, causing a very small conductivity. The resonance is around 100 MHz for the measured and 106 MHz for the modeled, also a small discrepancy.

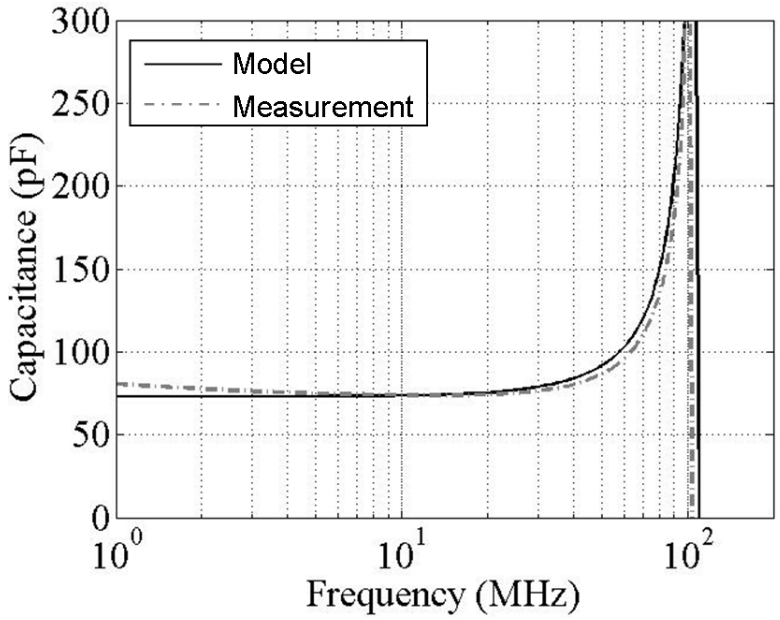

Fig. 5.13. Measurement and modeling of the capacitance of the encapsulated IDC before exposure to moisture.

After the control modeling and measurements were completed, the IDC was placed in direct contact with distilled water for ten days. The results are shown in Fig. 5.14. From previous investigations, we know that this particular encapsulation has the saturation moisture absorption of 5.3% by mass. After absorption, the capacitance is higher compared to the control in Fig. 5.13 over the entire frequency range. In fact, at around 20 MHz, the capacitance minimum, the sample with moisture absorption has a capacitance around 20% higher than the sample without. There is also greater capacitance dispersion in the measured and modeled sample when the water

absorption is considered. The dispersion is a result of the material dispersion. The effective dielectric permittivity is higher at lower frequencies because of the conductivity of the moisture.

At higher frequencies, from 1 MHz up to 100 MHz, there is also a very good agreement in the measured and modeled capacitance (within an average of 2%). However, there is a larger discrepancy between the measurement and modeling below those frequencies. The measured capacitance is higher than the modeled capacitance. The modeling of the effective dielectric parameters assumed, in Fig. 5.14, that the moisture absorption was perfectly homogeneous (k=0 in the Lichtenecker Mixing Formula). The absorption is, most likely, very close to homogeneous but not completely. As was discussed in the previous chapter, it is more likely that the absorption is slightly higher on the surface where the polymer was in contact with the water.

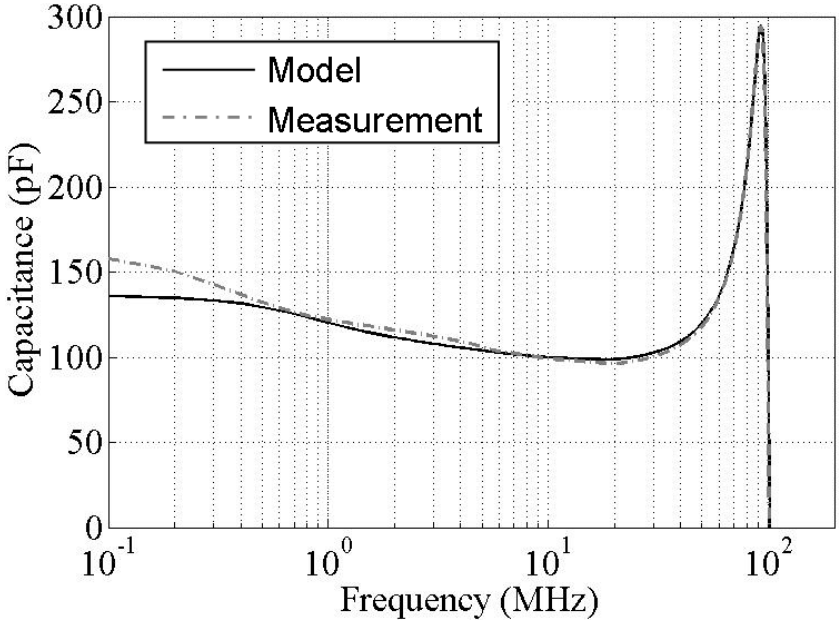

Fig. 5.14. Measurement and modeling (of homogeneous absorption) of the capacitance of the encapsulated IDC after saturation with moisture.

In Fig. 4.3 it was shown that even slightly inhomogeneous absorption can cause significant differences in the effective dielectric permittivity at low frequencies. Furthermore, it is shown that when the k variable in Lichtenecker's Mixing Formula (which represents the distribution of the composite dielectric) increases above zero but remains below 0.5, the dispersion in the effective permittivity can increase drastically in the kHz and MHz range. To explain the discrepancy between the modeling and measurement in Fig. 5.14, one could expect that, because

the water was only directly in contact with one surface of the encapsulation, that equilibrium was formed where the outside surface of the encapsulation polymer had a slightly higher concentration of moisture than the interface.

The *k* variable in the effective permittivity modeling was increased until the measured and modeled capacitance matched. To achieve the excellent agreement between the modeling and measurement shown in Fig. 5.15, $k = 0.05$. The variable was only changed 2.5% (on a spectrum from -1 to +1) to eliminate the difference. This confirms what was shown in the previous chapter that slight differences in the consistency of a composite dielectric can drastically change the effective permittivity at low frequencies.

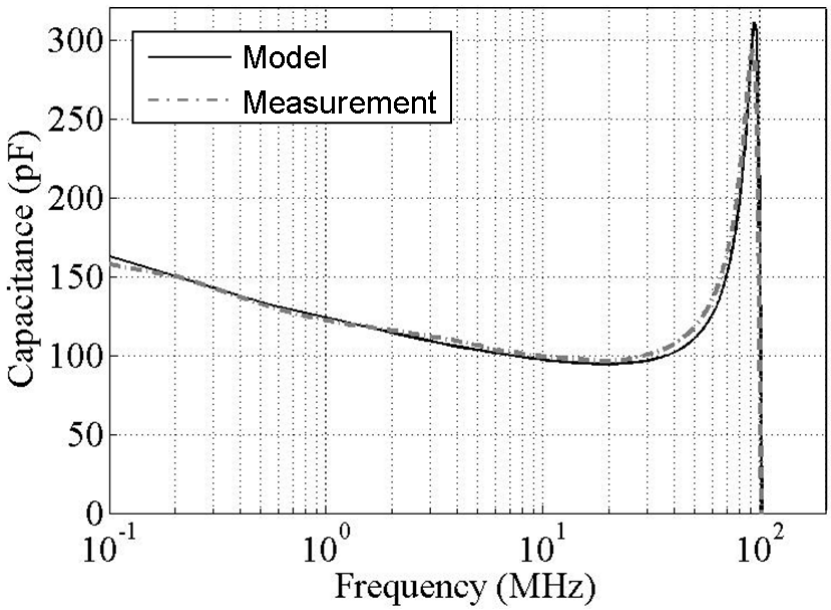

Fig. 5.15. Measurement and modeling (of slightly inhomogeneous absorption, k=0.05) of the capacitance of the encapsulated IDC after saturation with moisture.

Having achieved excellent agreement between the capacitance (which mostly represents the real part of the permittivity) of the modeled and measured IDC, the conductance, which mostly represents the imaginary part and the losses in the IDC, was also examined. In Fig. 5.16 the measured and modeled conductance were compared. The two curves also show a very good agreement. This shows that the dielectric modeling approach is also valid for determining dielectric losses in encapsulated structures.

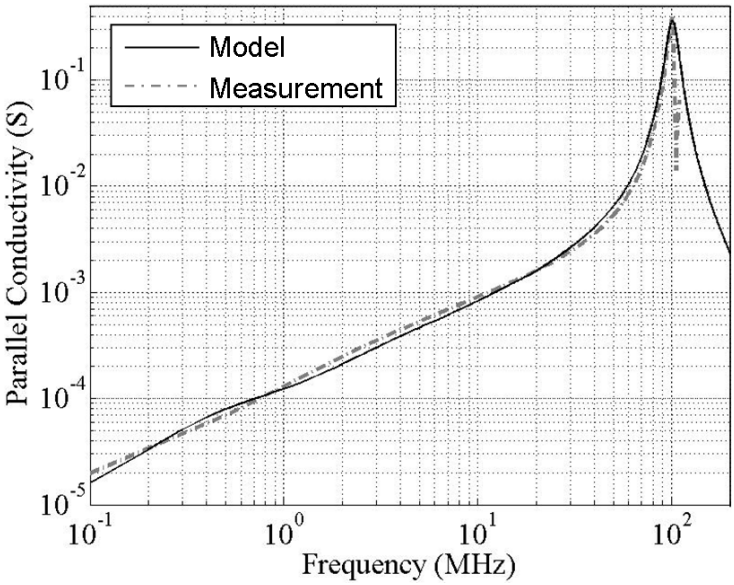

Fig. 5.16. Measurement and modeling (of slightly inhomogeneous absorption, k=0.05) of the conductance of the encapsulated IDC after saturation with moisture.

Chapter 6: Joint Modeling of Conductor and Dielectric Losses in a Coplanar Transmission Line

The conductor models from Chapter 4 and the dielectric models from Chapter 5 can now be combined to examine the transmission line parameters, considering all of the various effects. Rather than using Eq. 4.9 or Eq. 5.1 to determine the dielectric or conductor losses separately, the complex capacitance and non-ideal resistance and inductance can be determined with the proposed modeling approaches and used in Eq. 4.8 to determine the total attenuation of the transmission line.

The example presented in this section has the same dielectric characteristics and dimensions as the example shown in Fig. 4.12. The thickness of the conductor is 3 μm. The conductors are trapezoidal with lower angles set to 60°. A surface roughness profile on the top and angled surface of the conductors is assigned an RMS height of 0.5 μm.

The results for the attenuation of the transmission line are shown in Fig. 6.1. In Fig. 6.1 the trend for the dielectric losses changes from the trend that was seen in Chapter 4. At low frequencies, instead of beginning very low, it remains nearly constant from across the entire low frequency range. In Chapter 4, the dielectric losses were investigated with a lossless conductor (meaning the $R' = 0$). The conductor was, therefore, only a frequency independent inductance. The inclusion of the causality of the conductor changes the loss characteristics at low frequencies. The resistance and inductance was calculated using the adapted filament model in Chapter 3.

Eq. 6.1 uses the per-unit-length parameters to determine the characteristic impedance of the non-ideal transmission line. The calculated impedance is shown in Fig. 6.2.

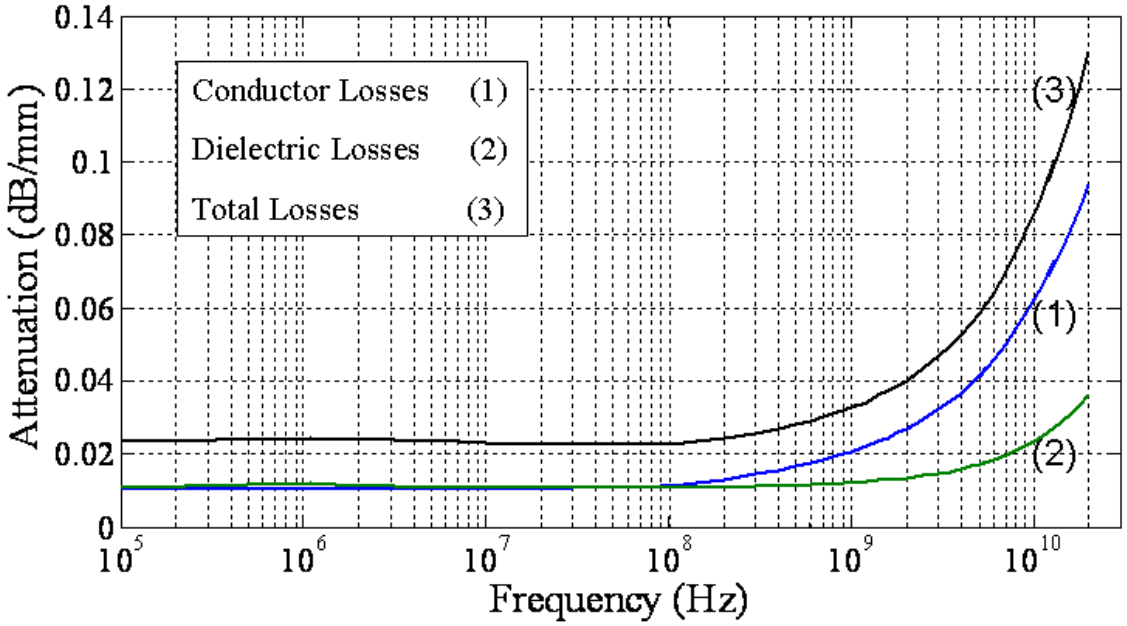

Fig. 6.1. Losses in a transmission line, considering non-ideal transmission line effects.

$$Z_o = \sqrt{\frac{(R' + j\omega L')}{j\omega(C_{\text{Re}} + jC_{\text{Im}})}} \qquad \text{Eq. 6.1}$$

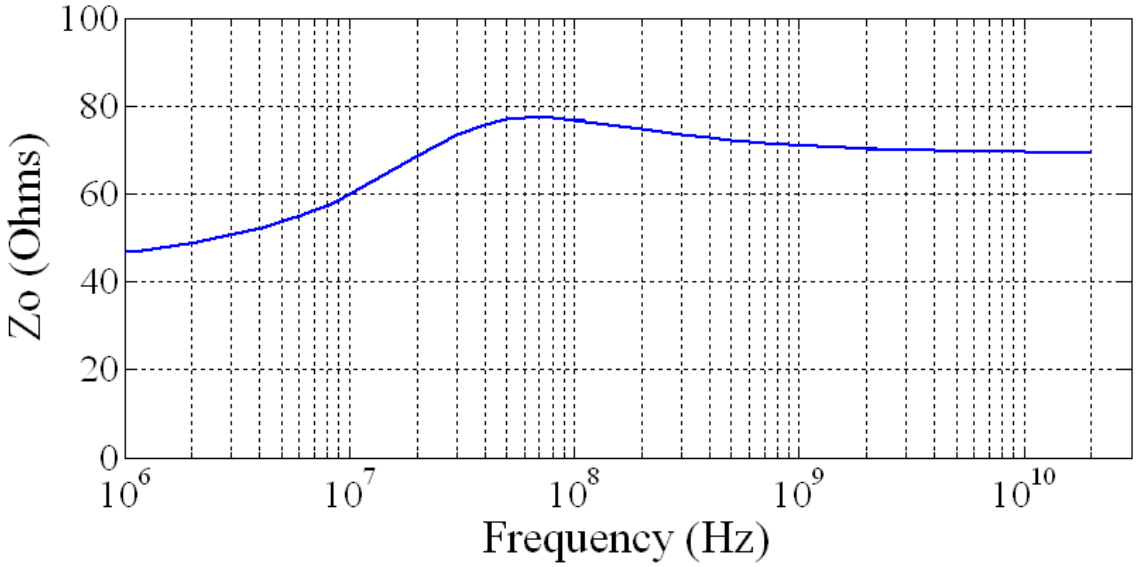

Fig. 6.2. Characteristic impedance of the transmission line, considering non-ideal effects.

The characteristic impedance shows an interesting trend that at lower frequencies it begins at around 45 Ω. It rises to nearly 80 Ω at 50 MHz before it falls again to 68 Ω at 20 GHz. The reason for this effect is that the material dispersion due to the mixed dielectric occurs at a lower frequency, which drives the impedance down. Then, the dielectric parameters stabilize but, due to the causality of the conductor, the inductance is still falling. This results in a frequency where the characteristic impedance peaks.

Phase velocity of the transmission line can also be determined from the imaginary part of the propagation constant γ, calculated with Eq. 4.9. Phase velocity, μ_p, is calculated by the expression Eq. 6.2.

$$\mu_p = \frac{\omega}{Im(\gamma)} \qquad \text{Eq. 6.2}$$

The ratio of the phase velocity to the speed of light in a vacuum for the transmission line configuration is shown in Fig. 6.3.

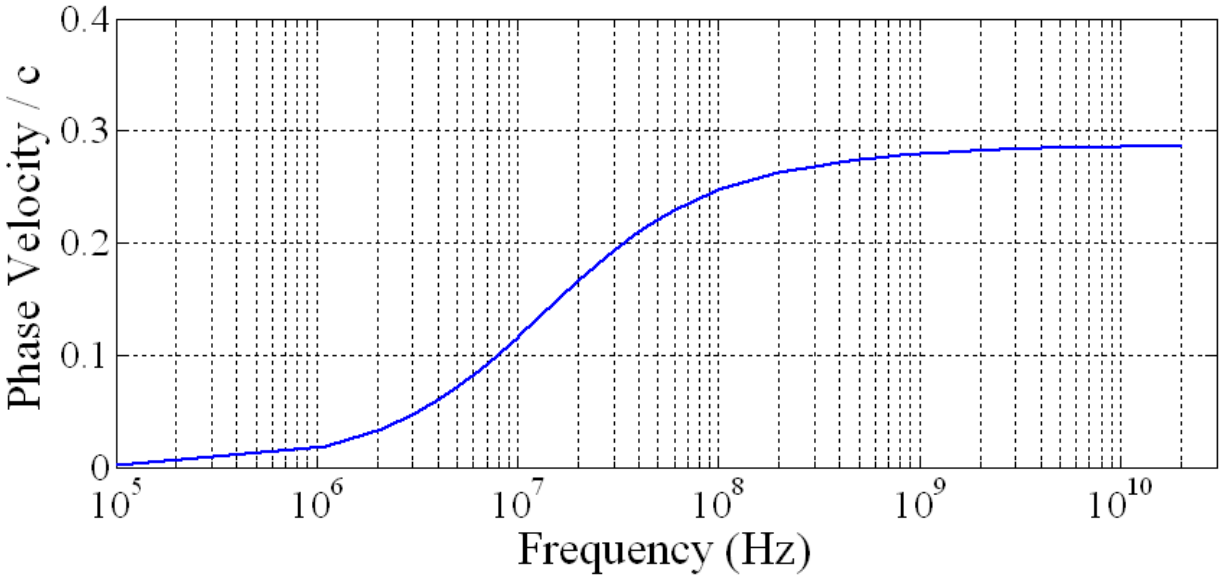

Fig. 6.3. Relative phase velocity of the transmission line, considering non-ideal effects.

Due to the material dispersion that was shown in Chapter 4, as a result of the composite dielectric, the phase velocity begins very low. Around the MHz frequency range it begins to increase and stabilizes in the GHz frequency range.

Chapter 7: Summary and Conclusions

7.1. Summary

A comprehensive review of state-of-the-art transmission line models has shown tremendous advancement and innovation in transmission line analysis. Many techniques are available to predict TML parameters. Very simple analytical formulas have been developed and refined for several decades and are very helpful for transmission line analysis. The most modern and advanced techniques are complex full-wave numerical techniques. Despite the multitude of available techniques, points have been identified where there are still significant modeling challenges. These points are:

(1) Surface roughness and edge effects, particularly over large frequency bands, with proximity effects and non-uniform roughness distribution.

(2) Modeling transmission lines with multiple dielectrics, particularly dielectric that include dielectric composites like moisture absorption in polymers.

For the modeling of surface roughness and edge effects, there are already existing models with very clear limitations. For this reason, a methodology was presented in Chapter 3 that identifies the specific case where the existing models fail. To compensate for this gap in the methodology, a novel modeling technique called the adapted filament model was proposed. The adapted filament model is a 2D quasi-static numerical model that discretizes the cross-section of a conductor. Then, a systematic approach is applied that builds a inhomogeneous resistivity across

the conductor cross section that represents the surface roughness. The novel modeling technique has several advantages over traditional techniques. (1) It analyzes the surface roughness and edge effects at the same time as the current density over an entire investigated frequency band. (2) The frequency dependent sources of the losses can easily be determined.

A methodology for dielectric modeling was proposed in Chapter 4. The methodology examines how various dielectric cavities must be modeled. For multiple dielectric layers, including dielectric materials that are composites, no modeling techniques were available for calculating transmission line parameters. Therefore, an approach was proposed that combines several models in a novel way to analyze a transmission line with a composite dielectric. This approach has been divided into two parts. (1) The Lichtenecker Mixing Formula is used to determine the effective frequency dependent dielectric material parameters for the dielectric composite. (2) Numerical or analytical techniques implement the frequency dependent material parameters to determine the transmission line characteristics. This approach was implemented for a polymer that is used to encapsulate transmission lines on PCBs, but also absorbs moisture from its environment (making it a composite dielectric).

In Chapter 5, the modeling approach and the methodology for conductor modeling were used to model conductor lines that were fabricated using a state-of-the-art aerosol ink-jet printing process. With the approach, a very good agreement between the modeled and measured attenuation has been achieved. Furthermore, the model identifies the dominant loss mechanisms at the different frequencies. The Lichtenecker Mixing Formula for the investigated encapsulation material was also validated using measurements of an IDC. For the first time, the Lichtenecker Equation was validated for complex permittivities, with excellent agreement between measured and modeled results. This is especially significant because one phase of the composite (the moisture) was conductive.

Chapter 6 combines the conductor and dielectric modeling approaches for a thin-film coplanar transmission line with realistic dimensions, dielectric buildup, dielectric moisture absorption, edge-shape effects, and surface roughness. The losses (broken down into dielectric, conductor, and total losses) are presented, as well as the frequency dependent characteristic impedance and frequency dependent phase velocity.

7.2. Conclusions

Several significant conclusions can be drawn from this work.

For conductor modeling, we can conclude:

(1) Analytical models for conductor and surface roughness modeling are significantly limited for accurately modeling the surface roughness in modern electronics packaging structures because of limitations in their bandwidths and flexibility.

(2) For examining narrow edge-effects and surface roughness effects, current full-wave modeling techniques have significant shortcomings. Those being that they require very long computation times and the accuracy of the results is difficult to evaluate.

(3) With the proposed adapted filament model it is possible to offer more accurate results than state-of-the-art surface roughness and edge-shape effect modeling techniques. Additionally, the model is applicable for transmission lines where other state-of-the-art models are not. And, the model is more straightforward, offering greater physical insight during the modeling process.

(4) The adapted filament model can accurate predict frequencies where proximity effect, edge-shape effects, and surface roughness effects are introduced in a transmission line structure. It can also predict which mechanisms are dominant across given frequency ranges. It is the first model to offer this capability.

Conclusions that can be made for dielectric modeling are:

(1) In the state-of-the-art research for dielectric modeling there is no comprehensive methodology for the modeling of dielectric parameters that includes composite dielectric modeling, were phases of the composite have various loss parameters. This deficiency is especially significant because polymer encapsulation and underfill materials absorb moisture and current models offer no way of evaluating the effect of moisture on the transmission line parameters.

(2) Through a novel combination of analytical and numerical models, a transmission line structure with a layered dielectric and/or a composite dielectric can be modeled. Both the real and imaginary part of the permittivity can be accurately modeled with a combination of models, including the Lichtenecker Equation and analytical or numerical transmission line models.

(3) Homogeneous water absorption into an encapsulation material with realistic moisture absorption characteristics will have little or no effect on the transmission characteristics of a transmission line above the MHz frequency range.

(4) Inhomogeneous water absorption, which could result from cracks, delamination, or adhesion loss of an encapsulation polymer, can have a much greater effect on the electrical parameters of a transmission line. Therefore, it is reasonable to assume that when structural faults exist in an encapsulated module, that those faults could contribute to electronic failure through water absorption.

Other Conclusions:

(1) The causality of the inductance has an effect on the low frequency losses of a dielectric. Therefore, at low frequencies, it is important to model the frequency dependence of both the inductance and the capacitance.

(2) The characteristic impedance and phase delay of the mixed and composite dielectrics have complex behavior that is dependent on the combined frequency dependency of the dielectric and the conductor.

References

[1] **H. Reichl, "3D Integration A European Perspective," presented at EPTC, Singapore, 2008.**

[2] **J. U. Knickerbocker, "Development of Next-generation System-on-package (SOP) Technology Based on Silicon Carriers with Fine-pitch Chip Interconnection," *IBM Journal of Research and Technology*, vol. IBM J. Res. & Dev. Vol. 49, 2005.**

[3] **I. Ndip, "Novel Methodologies for Efficient and Accurate Modeling and Optimization of System-in-Package Modules for RF/High-Speed Applications," in *Ph.D Thesis at the Department of Electrical Engineering*. Berlin: Technical University of Berlin, 2006.**

[4] **G. Q. Zhang, "The Changing Landscape of Semiconductors," presented at EPTC, Singapore, 2008.**

[5] **H. A. Wheeler, "Formulas for the Skin Effect," *Proceedings of the IRE*, vol. 30, pp. 412-424, 1942.**

[6] **R. A. Pucel, D. J. Masse, and C. P. Hartwig, "Losses in Microstrip," *IEEE Transactions on Microwave Theory and Techniques*, vol. 16, pp. 342-350, 1968.**

[7] **K. C. Gupta, Garg, R., Chadha, R., *Computer aided design of microwave circuits*: Artech House, 1981.**

[8] **J. He, N. S. Nahman, and S. M. Riad, "A causal skin-effect model of microstrip lines," presented at IEEE MTT-S International Microwave Symposium Digest, 1993.**

[9] **Z. Jianmin, M. Y. Koledintseva, J. L. Drewniak, D. J. Pommerenke, R. E. DuBroff, Y. Zhiping, C. Wheling, K. N. Rozanov, G. Antonini, and A. Orlandi, "Reconstruction of Dispersive Dielectric Properties for PCB Substrates Using a Genetic Algorithm," *IEEE Transactions on Electromagnetic Compatibility*, vol. 50, pp. 704-714, 2008.**

[10] **S. H. Hall, Garrett W., and McCall, James A., *High-Speed Digital System Design*. New York: Wiley Interscience, 2000.**

[11] **E. L. Barsotti, J. M. Dunn, and E. F. Kuester, "Strip edge shape effects on conductor loss calculations using the Lewin/Vainshtein method," *Electronics Letters*, vol. 26, pp. 983-985, 1990.**

[12] **E. L. Barsotti, E. F. Kuester, and J. M. Dunn, "A simple method to account for edge shape in the conductor loss in microstrip," *IEEE Transactions on Microwave Theory and Techniques*, vol. 39, pp. 98-106, 1991.**

[13] **C. L. Holloway and E. F. Kuester, "A quasi-closed form expression for the conductor loss of CPW lines, with an investigation of edge shape effects," *IEEE Transactions on Microwave Theory and Techniques*, vol. 43, pp. 2695-2701, 1995.**

[14] **G. Ghione, M. Goano, and M. Pirola, "Exact, conformal-mapping models for the high-frequency losses of coplanar waveguides with thick electrodes of rectangular or trapezoidal cross section," presented at 1999 IEEE MTT-S International Microwave Symposium Digest, 1999.**

[15] **J. Guo, Glisson, A. W., Kajfez, D., "Skin-effect resistance of conductors with a trapezoidal cross section," *Microwave and Optical Technology Letters*, vol. 18, pp. 387-389, 1998.**

[16] **T. Vu Dinh, B. Cabon, and J. Chilo, "New skin-effect equivalent circuit," *Electronics Letters*, vol. 26, pp. 1582-1584, 1990.**

[17] **T. Vu Dinh, B. Cabon, and J. Chilo, "Time domain analysis of skin effect on lossy interconnections," *Electronics Letters*, vol. 26, pp. 2057-2058, 1990.**

[18] **W. T. Weeks, Wu, L.L., McAllister, M.F., and Singh, A., "Resistive and inductive skin effect in rectangular conductors," *IBM J. Res. Development*, vol. 23, pp. 652-660, 1979.**

[19] **K. M. Coperich, A. E. Ruehli, and A. Cangellaris, "Enhanced skin effect for partial element equivalent circuit (PEEC) models," presented at Electrical Performance of Electronic Packaging, 1999, 1999.**

[20] **M. Shizhong, Amin, C., Ismail, Y.I., "Efficient model order reduction including skin effect," presented at Design Automation Conference Proceedings, 2003.**

[21] **M. Shizhong, C. Amin, and Y. I. Ismail, "Modeling skin and proximity effects with reduced realizable RL circuits," *IEEE Transactions on Very Large Scale Integration (VLSI) Systems*, vol. 12, pp. 437-447, 2004.**

[22] **H. Qi, M. Junfa, and Y. Wen-Yan, "Skin and proximity effects of curved microstrip interconnects," presented at Asia-Pacific Microwave Conference Proceedings, APMC05, 2005.**

[23] **D. De Zutter, H. Rogier, and L. Knockaert, "Surface current modelling of the skin effect," presented at IEEE 14th Topical Meeting on Electrical Performance of Electronic Packaging, 2005.**

[24] **T. Mido and K. Asada, "An analysis on VLSI interconnection considering skin effect," presented at Proceedings of the ASP-DAC '98, Asia and South Pacific Design Automation Conference, 1998.**

[25] **W. Chen, J. L. Drewniak, and L. Min, "FDTD modeling of skin effect," presented at 2002 3rd International Symposium onn Electromagnetic Compatibility, 2002.**

[26] **S. Celozzi, "On the finite element time domain solution of the skin effect equations in multiconductor lines," *IEEE Transactions on Magnetics*, vol. 30, pp. 3180-3183, 1994.**

[27] **G. I. Costache, "Finite Element Method Applied to Skin-Effect Problems in Strip Transmission Lines," *IEEE Transactions on Microwave Theory and Techniques*, vol. 35, pp. 1009-1013, 1987.**

[28] **G. I. Costache, M. V. Nemes, and E. M. Petriu, "Finite element method analysis of the influence of the skin effect, and eddy currents on the internal magnetic field and impedance of a cylindrical conductor of arbitrary cross-section," presented at Canadian Conference on Electrical and Computer Engineering, 1995, 1995.**

[29] **A. Konrad, M. Chari, and Z. Csendes, "New finite element techniques for skin effect problems," *IEEE Transactions on Magnetics*, vol. 18, pp. 450-455, 1982.**

[30] **M. J. Tsuk and J. A. Kong, "A hybrid method for the calculation of the resistance and inductance of transmission lines with arbitrary cross sections," *IEEE Transactions on Microwave Theory and Techniques*, vol. 39, pp. 1338-1347, 1991.**

[31] **W. Wlodarczyk and V. Besch, "Skin effect losses of interconnect lines in frequency and time domain," *Electronics Letters*, vol. 26, pp. 1237-1238, 1990.**

[32] **F. T. Ulaby, *Fundamentals of Applied Electromagnetics*. New Jersey: Prentice Hall, 1999.**

[33] **Y. Chu-Sun, Z. Fazarinc, and R. L. Wheeler, "Time-domain skin-effect model for transient analysis of lossy transmission lines," *Proceedings of the IEEE*, vol. 70, pp. 750-757, 1982.**

[34] **S. Kim and D. P. Neikirk, "Compact equivalent circuit model for the skin effect," presented at IEEE MTT-S International Microwave Symposium Digest, 1996.**

[35] **B. K. Sen and R. L. Wheeler, "Skin effects models for transmission line structures using generic SPICE circuit simulators," presented at IEEE 7th topical Meeting on Electrical Performance of Electronic Packaging, 1998.**

[36] **R. Griffith and M. Nakhla, "A new method for the time-domain analysis of lossy coupled transmission lines," presented at IEEE MTT-S International Microwave Symposium Digest, 1990.**

[37] **A. R. Djordjevic and T. K. Sarkar, "Analysis of Time Response of Lossy Multiconductor Transmission Line Networks," *IEEE Transactions on Microwave Theory and Techniques*, vol. 35, pp. 898-908, 1987.**

[38] **J. E. Schutt-Aine and R. Mittra, "Scattering parameter transient analysis of transmission lines loaded with nonlinear terminations," *IEEE Transactions on Microwave Theory and Techniques*, vol. 36, pp. 529-536, 1988.**

[39] **Y. D. S. Dawoud and D. Linton, "Skin effect modelling of the non-linear transmisssion line," presented at 25th European Microwave Conference, 1995.**

[40] **G. V. Kopcsay, B. Krauter, D. Widiger, A. Deutsch, B. J. Rubin, and H. H. Smith, "A comprehensive 2-D inductance modeling approach for VLSI interconnects: frequency-dependent extraction and compact circuit model synthesis," *IEEE Transactions on Very Large Scale Integration (VLSI) Systems*, vol. 10, pp. 695-711, 2002.**

[41] **T. Vu Dinh, B. Cabon, and J. Chilo, "SPICE simulation of lossy and coupled interconnection lines," *IEEE Transactions on Components, Packaging, and Manufacturing Technology, Part B: Advanced Packaging*, vol. 17, pp. 134-146, 1994.**

[42] **M. Kamon, N. Marques, L. M. Silveira, and J. White, "Generating reduced order models via PEEC for capturing skin and proximity effects," presented at IEEE 6th Topical Meeting on Electrical Performance of Electronic Packaging, 1997.**

[43] **M. Kamon, F. Wang, and J. White, "Generating nearly optimally compact models from Krylov-subspace based reduced-order models," *IEEE Transactions on Circuits and Systems II: Analog and Digital Signal Processing*, vol. 47, pp. 239-248, 2000.**

[44] **D. Kuznetsov and J. E. Schutt-Aine, "Difference model approach for the transient simulation of transmission lines," presented at IEEE International Symposium on Circuits and Systems, ISCAS '93, 1993.**

[45] **D. B. Kuznetsov and J. E. Schutt-Aine, "Optimal transient simulation of transmission lines," *IEEE Transactions on Circuits and Systems I: Fundamental Theory and Applications*, vol. 43, pp. 110-121, 1996.**

[46] **O. Kyung Suk, "Accurate transient simulation of transmission lines with the skin effect," *IEEE Transactions on Computer-Aided Design of Integrated Circuits and Systems*, vol. 19, pp. 389-396, 2000.**

[47] **H. Y. Lee and T. Itoh, "Phenomenological loss equivalence method for planar quasi-TEM transmission lines with a thin normal conductor or superconductor," *IEEE Transactions on Microwave Theory and Techniques*, vol. 37, pp. 1904-1909, 1989.**

[48] **S. D. Roy, "On the Realization of a Constant-Argument Immittance or Fractional Operator," *IEEE Transactions on Circuit Theory*, vol. 14, pp. 264-274, 1967.**

[49] **E. J. Tarasiewicz, A. S. Morched, A. Narang, and E. P. Dick, "Frequency dependent eddy current models for nonlinear iron cores," *IEEE Transactions on Power Systems*, vol. 8, pp. 588-597, 1993.**

[50] **M. Swaminathan, Engin, E., *Power Integrity and Design for Semiconductor and Systems*. Boston: Prentice Hall, 2007.**

[51] **E. Engin, "Modeling of Lossy Interconnections and Packages with Non-Ideal Power/Ground Planes," in *Department of Electrical Engineering*. Berlin: University of Hannover, 2004.**

[52] **E. Hammerstad and O. Jensen, "Accurate Models for Microstrip Computer-Aided Design," presented at MTT-S International Microwave Symposium Digest, 1980.**

[53] **S. Groiss, I. Bardi, O. Biro, K. Preis, and K. R. Richter, "Parameters of lossy cavity resonators calculated by the finite element method," *IEEE Transactions on Magnetics*, vol. 32, pp. 894-897, 1996.**

[54] **Ansoft_HFSS, "Help Files, Surface Roughness."**

[55] **S. Hall, S. G. Pytel, P. G. Huray, D. Hua, A. Moonshiram, G. A. Brist, and E. Sijercic, "Multigigahertz Causal Transmission Line Modeling Methodology Using a 3-D Hemispherical Surface Roughness Approach," *IEEE Transactions on Microwave Theory and Techniques*, vol. 55, pp. 2614-2624, 2007.**

[56] **M. V. Lukic and D. S. Filipovic, "Modeling of 3-D Surface Roughness Effects With Application to u-Coaxial Lines," *IEEE Transactions on Microwave Theory and Techniques*, vol. 55, pp. 518-525, 2007.**

[57] **S. Hall, Brist, G., Clouser S., Liang, T.,, "Non-classical conductor losses due to copper foil roughness and treatment," presented at ECWC Conference at IPC Printed Circuits Expo, 2005.**

[58] **L. Proekt and A. C. Cangellaris, "Investigation of the impact of conductor surface roughness on interconnect frequency-dependent ohmic loss," presented at Proceedings of the 53rd Electronic Components and Technology Conference, 2003.**

[59] **X. Chen, "EM Modeling of Microstrip Conductor Losses Including Surface Roughness Effect," *IEEE Microwave and Wireless Components Letters*, vol. 17, pp. 94-96, 2007.**

[60] **M. El-Shenawee, "Propagation characteristics of microstrip transmission line on rough dielectric substrate surface," presented at IEEE Antennas and Propagation Society International Symposium Digest, 1997.**

[61] **P. G. Huray, S. Hall, S. Pytel, F. Oluwafemi, R. Mellitz, D. Hua, and Y. Peng, "Fundamentals of a 3-D "snowball" model for surface roughness power losses," presented at IEEE Workshop on Signal Propagation on Interconnects 2007.**

[62] **C. Quan and W. Ngai, "A Stochastic Integral Equation Method for Resistance Extraction of Conductors with Random Rough Surfaces," presented at International Symposium on Intelligent Signal Processing and Communications, ISPACS '06, 2006.**

[63] **C. Quan and W. Ngai, "An efficient stochastic integral equation method for modeling the influence of conductor surface roughness on interconnect ohmic loss," presented at 50th Midwest Symposium on Circuits and Systems, MWSCAS'07, 2007.**

[64] **S. Normyle, McCarthy, T., Wynants, D., "The impact of conductor surface profile (Rrms) on total circuit attenuation in microstip and stripline transmission lines," presented at Taconic Advanced Dielectric Division, New York, 2006.**

[65] **Y. Lou and P. D. Christofides, "Feedback control of growth rate and surface roughness in thin film growth," presented at Proceedings of the 42nd IEEE Conference on Decision and Control, 2003.**

[66] **H. Dong-Ho, Y. L. Li, R. A. Vieweg, T. G. Ruttan, and L. A. Polka, "Dielectric material characterization using rough surface transmission lines," presented at 59th ARFTG Conference Digest, 2002.**

[67] **M. Henry, C. E. Free, Q. Reynolds, S. Malkmus, and J. Wood, "Electrical Characterization of LTCC Coplanar Lines up to 110 GHz," presented at 36th European Microwave Conference, 2006.**

[68] **J. E. Chan, K. Sivaprasad, and K. A. Chamberlin, "High-Frequency Modeling of Frequency-Dependent Dielectric and Conductor Losses in Transmission Lines," *IEEE Transactions on Components and Packaging Technologies*, vol. 30, pp. 86-91, 2007.**

[69] **T. Liang, S. Hall, H. Heck, and G. Brist, "A Practical Method for Modeling PCB Transmission Lines with Conductor Surface Roughness and Wideband Dielectric Properties," presented at IEEE MTT-S International Microwave Symposium Digest, 2006.**

[70] **W. H. Haydl, "Conductive Substrate Losses In Coplanar And Microstrip Transmission Lines," presented at 27th European Microwave Conference and Exhibition, 1997.**

[71] **K. C. Gupta, Garg, R., Bahl, I.J., *Microstrip Lines and Slotlines*. Norwood, Massachusetts: ARTEC, 1979.**

[72] **B. C. Wadell, *Transmission Line Design Handbook*. Boston: ARTEC House, 1991.**

[73] **K. Weide-Zaage, Horaud, W., Frémont, H., "Moisture diffusion in Printed Circuit Boards: Measurements ans Finite-Element-Simulations," *Microelectronics Reliability*, vol. 45, pp. 1662-1667, 2005.**

[74] **S. Yasufuku, Todoki, M., "Dielectric and Thermoanalytical Behavior of Moisture and Water in Aromatic Polyamide and Polyamide Films," presented at IEEE International Symposium on Electrical Insulation, Pittsburg, PA, USA, 1994.**

[75] **S. Yasufuku, Todoki, M., "Dielectric and Thermoanalytic Behavior of Moisture and Water in Aromatic Polyamide Paper," *IEEE Transactions on Electrical Insulation*, vol. 28, pp. 309-314, 1993.**

[76] **D. E. Pitkanen, Speerschneider, C.J., "Environmental Effects on Copper Thick Film Microcircuits," *IEEE Transactions on Compnenets, Hybrids, and Manufacturing Technology*, vol. CHMT-4, pp. 250-256, 1981.**

[77] **S. Ul-Haq, Raju, G.R.G., "Influence of Moisture Absorption in High Temperature Dielectrics," presented at Electrical Insulation and Dielectric Phenomena, 2002.**

[78] **J. M. Heinola, Lätti, K.P., Silventoinen, P., Ström, J.P., Kettunen, M., "A method to evaluate effects of moisture absorption on dielectric constant and dissipation factor of printed circuit board materials," presented at 9th** International **Symposium on Advanced Packaging Materials, 2004.**

[79] **Y. Zhao, Toyama, M., Kita, K., Kyuno, K., Toriumi, A., "Moisture-absorption-induced permittivity deterioration and surface roughness enhancement of lanthanum oxide films on silicon," *Applied Phsysics Letters*, vol. 88, 2006.**

[80] **W. Jujian, Zongshou, Z., "Regularity of Breakdown of Solid Dielectrics After Moisture Absorption," 1988.**

[81] **R. C. J. Vogels, Huang, M., van Driel, W.D., Zhang, G.Q., "Fast Characterization for Moisture Properties of Moulding Compounds: Influence of Termperature and Humidity," presented at 6th International Conference on Electronic Packaging Technology, 2005.**

[82] **S. Lee, Park, K.W., "Effect of fluorine on moisture absorption and dielectric properties of SiOF films," *Material Chemistry and Physics*, vol. 53, pp. 150-154, 1998.**

[83] **L. Xin, Gu, X., Hofstra, P.G., Bajcar, R.C., "Moisture-absorption, dielectric relaxation, and thermal conductivity studies of polymer composites," *Journal of Polymer Science B*, vol. 36, pp. 2259-2265, 1998.**

[84] **E. M. Mechvolodnova, Prut, E.V., Belgovskiy, I.M., Ponomarenko, A.T., Shevchenko, V.G., "The effect of moisture absorption on mechanical and dielectric properties of epoxy resins and composites," *Acta polymerica*, vol. 43, pp. 191-192, 1992.**

[85] **L. M. Zhu, D.; Lambird, G.; Holgado, W., "Moisture Diffusion Modeling and Application in a 3D RF Module Subject to Moisture Absorption and Desorption Loads," presented at 11th International Conference on Thermal, Mechanical, and Multiphysics Simulation and Experiments in Micro-electronics and Microsystems, EuroSimE, Bordeau, France, 2010.**

[86] **C. G. Regard, C.; Fremont, H., Poirier, P.; Xiaosong, M.A.; Jansen, K.M.B., "Fast reliability of SiP products," presented at 20th European Symposium on the Reliablility of Electron Devices, Failure Physics and Analysis, Bordeaux, France, 2009.**

[87] **H. B. C. Fan, K.Y.; Yuen, M.M.F., "Hydrophobic Self-Assembly Monolayer Structure for Reduction of Interfacial Moisture Diffusion," presented at Internation Conference on Electronic Packaging Technology & High Density Packaging (ICEPT-HDP), Beijing, China, 2009.**

[88] **P. S. C. Neelakantaswamy, B. V. R.; Rajaratnam, A., "Estimation of permittivity of a compact crystal by dielectric measurements on its powder: A stochastic mixture model for the powder-dielectric," *J. Phys. D: Appl. Phsy.*, vol. 16, pp. 1785-1799, 1983.**

[89] **B. V. R. N. Chowdari, P.S.; Akhter, S.K., "Application of the Logarithmic Law of Mixing for Estimation of Complex Permittivtiy and Electrical Conductivity of Fast Ion Conductors at Microwave Frequencies," *Solid State Ionics*, vol. 18, pp. 122-126, 1986.**

[90] **A. V. Goncharenko, Lozovski, V.Z., Venger, E.F., "Lichtenecker's equation: applicability and limitations," *Optics Communications*, vol. 174, pp. 19-32, 2000.**

[91] **T. Zakri, Laurent, J., Vauclin, "Theoretical evidence for 'Lichtenecker's mixture formulae' based on the effective medium theory," *J. Phys. D: Appl. Phys.*, vol. 31, pp. 1589-1594, 1998.**

[92] **R. Simpkin, "Derivation of Lichtenecker's Logarithmic Mixture Formula from Maxwell's Equations," *IEEE Transactions on Microwave Theory and Techniques*, vol. 58, pp. 545-550, 2010.**

[93] **H. C. Kärner, Schütz, A., "The Dielectric Properties of Fibre Reinforced Epoxies under the Influence of Humidity," presented at 4th International Conference on Properties and Applications of Dielectric Materials, Brisbane, Australia, 1994.**

[94] **J. E. Spanier, Herman, I.P., "Use of hybrid phenomenological and statistical effective-medium theories of dielectric functions to model the infrared reflectance of porous SiC films," *Physical Review B*, vol. 61, pp. 10437-10450, 2000.**

[95] **M. D. Auguelova, "Complex dielectric constant of sea foam at mocrowave frequencies," *Journal of Geophysics Research*, vol. 113, 2008.**

[96] **W. M. Merrill, Diaz, R.E., LoRe, M.M., Squires, M.C., Alexopoulos, N.G., "Effective Medium Theories for Artificial Materials Composed of Multiple Sizes of Spherical Inclusions in a Host Continuum," *IEEE Transactions on Antennas and Propagation*, vol. 47, pp. 142-148, 1999.**

[97] **D. A. Robinson, Friedman, S.P., "Effect of particle size distribution on the effective dielectric permittivity od saturated granular media," *Water Resources Research*, vol. 37, pp. 33-40, 2001.**

[98] **D. D. Smith, Fischer, G., Boyd, R.W., Gregory, D.A., "Cancellation of photoinduced absorption in metal nanoparticle composites through a counterintuitive consequence of local field effects," *Journal of the Optical Society of America B*, vol. 14, pp. 1625-1631, 1997.**

[99] **S. S. Kalarickal, Ménard, D., Das, J., Patton, C.E., Zhang, X., Sengupta, L.C., Sengupta, S., "Static and high frequency magnetic and dielectric properties of ferrite-ferroelectric composite materials," *Journal of Applied Physics*, vol. 100, 2006.**

[100] **R. Gehr, Fishcer, G., Boyd, R., "Nonlinear-optical response of porous-glass-based composite materials," *Journal of the Optical Society of America*, vol. 14, pp. 2310-2314, 1997.**

[101] **J. Gollub, Hand, T., Sajuyigbe, S., Mendonca, S., Cummer, S., Smith, D.R., "Characterizing the effects of disorder in metamaterial structures," *Applied Phsysics Letters*, vol. 91, 2007.**

[102] **L. Li, Ahmad, M., Brillhart, M., "Environmental Effects on Dielectric Films in Plastic Encapsulated Silicon Devices," presented at Electronic Components and Technology Conference, 2007.**

[103] **X. J. Ma, K.M.B.; Ernst, L.J., van Driel, W.D.; van der Sluis, O.; Zhang, G.Q., "Moisture Effects on a System in Package Carrier," presented at 10th Internatinal Conference on Thermal, Mechanical, and Multiphysics Simulation and Experiments in Micro-Electronics and Microsystems, Bordeaux, France, 2009.**

[104] **M. Jakob, Krupka, J., Mazierska, J., Bialkowski, M., "Temperature Dependence of Complex Permittivity of Planar Microwave Materials," presented at Asia-Pacific Microwave Conference, 2006.**

[105] **J. Hyun, Lee, S., Cho, S., Paik, K., "Frequency and Temperature Dependence of Dielectric Constant of Epoxy/BaTiO3 Composite Embedded Capacitor Films (ECFs) for Organic Substrate," presented at Electronic Components and Technology Conference, 2005.**

[106] **E. Li, Li, Z., Nie, Z., Zhang, Q., He, F., Guo, G., "Measurement of Complex Permittivity of Dielectric at High Temperatures by Using Cylindrical Cavity," presented at China-Japan Joint Microwave Conference, 2008.**

[107] **C. Guillermin, Rain, P., Rowe, S.W., "Characterization of Electro-thermal Aging of a Filled Epoxy Resin," presented at International Conference on solid Dielectrics, Toulouse, France, 2004.**

[108] **E. Bogatin, "Design rules for microstrip capacitance," *IEEE Transactions on Components, Hybrids, and Manufacturing Technology*, vol. 11, pp. 253-259, 1988.**

[109] **E. Bogatin, "A closed form analytical model for the electrical properties of microstrip interconnects," *IEEE Transactions on Components, Hybrids, and Manufacturing Technology*, vol. 13, pp. 258-266, 1990.**

[110] **W. Heinrich, "Quasi-TEM description of MMIC coplanar lines including conductor-loss effects," *IEEE Transactions on Microwave Theory and Techniques*, vol. 41, pp. 45-52, 1993.**

[111] **E. Carlsson and S. Gevorgian, "Conformal mapping of the field and charge distributions in multilayered substrate CPWs," *IEEE Transactions on Microwave Theory and Techniques*, vol. 47, pp. 1544-1552, 1999.**

[112] **G. Ghione and C. U. Naldi, "Coplanar Waveguides for MMIC Applications: Effect of Upper Shielding, Conductor Backing, Finite-Extent Ground Planes, and Line-to-Line Coupling," *IEEE Transactions on Microwave Theory and Techniques*, vol. 35, pp. 260-267, 1987.**

[113] **D. F. Williams, M. D. Janezic, A. R. K. Ralston, and R. S. List, "Quasi-TEM model for coplanar waveguide on silicon," presented at IEEE 6th Topical Meeting on Electrical Performance of Electronic Packaging, 1997.**

[114] **A. E. Engin, W. Mathis, W. John, G. Sommer, and H. Reichl, "Time-domain modeling of lossy substrates with constant loss tangent," presented at 8th IEEE Workshop on Signal Propagation on Interconnects Proceedings, 2004.**

[115] **K. M. Coperich, J. Morsey, A. C. Cangellaris, and A. Ruehli, "Physically consistent transmission line models for high-speed interconnects in lossy dielectrics," presented at Electrical Performance of Electronic Packaging, 2001, 2001.**

[116] **Y. Qingjian and O. Wing, "Computational models of transmission lines with skin effects and dielectric loss," *Asia-Pacific Conference Proceedings Circuits and Systems I: Fundamental Theory and Applications*, vol. 41, pp. 107-119, 1994.**

[117] **T. R. Arabi, A. T. Murphy, T. K. Sarkar, R. F. Harrington, and A. R. Djordjevic, "On the modeling of conductor and substrate losses in multiconductor, multidielectric transmission line systems," *IEEE Transactions on Microwave Theory and Techniques*, vol. 39, pp. 1090-1097, 1991.**

[118] **T. Vu Dinh, B. Cabon, and J. Chilo, "Modelling the capacitance of microstrip line using SPICE," *Electronics Letters*, vol. 28, pp. 194-196, 1992.**

[119] **B. Curran, Ndip, I., Guttowski, S., Reichl, H.;, "On the quantification and improvement of the models for surface roughness," presented at IEEE Workshop on Signal Propagation on Interconnects, SPI '09, Strasbourg, France, 2009.**

[120] **A. A. Koul, P.K.R.; Koledintseva, M.Y.; Drewniak, J.L.; Hinaga, S. , " Improved technique for extracting parameters of low-loss dielectrics on printed circuit boards," presented at IEEE International Symposium on Electromagnetic Compatability, Austin, Texas, Aug. 2009.**

[121] **B. Curran, Ndip, I., Guttowski, S., Reichl, H.;, "The Combined Modeling of Skin, Proximity, and Surface Roughness Effects with an Adapted Filament Model," presented at 7th International Workshop on Electromagnetic Compatibility of Integrated Circuits, Toulouse, France, 2009.**

[122] **B. Curran, Ndip, I., Guttowski, S., Reichl, H.;, "On the Quantification of the State-of-the-Art Models for Skin-Effect in Conductors, Including Those with Non-Rectangular Cross-Sections," presented at IEEE EMC Symposium 2009, Austin, TX, USA, 2009.**

[123] **E. C. Chen, S.Y., "Characteristics of coplanar transmission lines on multilayer substrates: modeling and experiments," *IEEE Transactions on Microwave Theory and Techniques*, vol. 45, pp. 939-945, 1997.**

[124] **H. B. Guckel, P.A.; Palocz, I., "A Parallel-Plate Waveguide Approach to Microminiaturized, Planar Transmission Lines for Integrated Circuits," *IEEE Transactions on Microwave Theory and Techniques*, vol. 15, pp. 468-479, 1967.**

[125] **H. F. Hasegawa, M.; Yanai, H., "Properties of Microstrip Line on Si-SiO2 System," *IEEE Transactions on Microwave Theory and Techniques*, vol. 19, pp. 869-881, 1971.**

[126] **V. R. C. Werner, M. Maiwald, V. Zöllmer, J. Bahr, G. Domann, and H. G. H. Wolf, B. Curran, I. Ndip, F. Oehler, "Design, direct write deposition and characterization of multilayer systems for customized electronic test applications," presented at European Congress and Exhibition on Advanced Materials and Processes, Glasgow, UK, 2009.**

[127] ***Agilent 4294A Precision Impedance Analyzer Data Sheet*****: Agilent Technologies Inc., 2008.**

Short Biography and List of Publications

Brian Curran received the B.S. degree in Electrical Engineering from the University of Rochester, New York, in 2001 and the M.Sc. degree in Electrical Communications Engineering from the University of Kassel, Germany, in 2008. Since 2008, he has been a Research Engineer in the RF and High-Speed System Design Group, Fraunhofer Institute for Reliability and Microintegration (IZM) Berlin. His main research interest is interconnect modeling, analysis and design for RF/high-speed applications. He has been an IEEE member since 2009 and an EuMA member since 2011.

Publications:

Journals

- Brian Curran, Ivan Ndip, Christian Werner, Veronika Ruttkowski, Marcus Maiwald, Heinrich Wolf, Volker Zoellmer, Gerhard Domann, Stephan Guttowski, Horst Gieser, Herbert Reichl, "An Adapted Filament Model for Accurate Modeling of Printed Coplanar Lines with Significant Surface Roughness and Proximity Effects", International Journal of Microwaves and Wireless Technologies, Special Issue for the European Microwave Week 2009, September, 2010.

- Brian Curran, Ivan Ndip, Stephan Guttowski, Herbert Reichl, "A Methodology for Combined Modeling of Skin, Proximity, Edge and Surface Roughness Effects", Microwave Theory and Techniques, IEEE Transactions on, September, 2010.

- Florian Ohnimus, Uwe Maaß, Gerhard Fotheringham, Brian Curran, Ivan Ndip, Thomas Fritzsch, Jürgen Wolf, Stephan Guttowski, Klaus-Dieter Lang, "Design and Comparison of 24 GHz Patch Antennas on Glass Substrates for Compact Wireless Sensor Nodes", International Journal of Microwave Science and Technology.

Conferences

- Brian Curran, Ivan Ndip, Jorg Bauer, Stephan Guttowski, Klau Dieter Lang, Herbert Reichl, "The Impact of Moisture Absorption on the Electrical Parameters of Organic Dielectric Materials", Thermal, Mechanical and Multiphysics Simulation and Experiments in Micro/Nanoelectronics and Systems, EuroSimE, April, 2011.

- Brian Curran, Ivan Ndip, Stephan Guttowski, Herbert Reichl, "The Combined Modeling of Skin, Proximity, and Surface Roughness Effects with an Adapted Filament Model", Poster Presentation: 7th International Workshop on Electromagnetic Compatibility of Integrated Circuits (EMCCompo), Toulouse, France, Nov. 2009.

- Brian Curran, Ivan Ndip, Christian Werner, Veronika Ruttkowski, Marcus Maiwald, Heinrich Wolf, Volker Zoellmer, Gerhard Domann, Stephan Guttowski, Horst Gieser, Herbert Reichl, "Modeling and Measurement of Coplanar Transmission Lines with Significant Proximity and Surface Roughness Effects", Oral Presentation: European Microwave Conference, Rome, Italy, Sept-Oct, 2009.

- Brian Curran, Ivan Ndip, Stephan Guttowski, Herbert Reichl, “On the Quantification of the State-of-the-Art Models for Skin-Effect in Conductors, Including Those with Non-Rectangular Cross-Sections”. Oral Presentation: Electromagnetic Compatibility (EMC), Austin, Texas, USA, Aug. 2009.

- Brian Curran, Ivan Ndip, Stephan Guttowski, Herbert Reichl, “The Impacts of Dimensions and Return Current Path Geometry on Coupling in Single Ended Through Silicon Vias”, Oral Presentation: Electronic Components and Technology Conference (ECTC), San Diego, California, USA, May 2009.

- Brian Curran, Ivan Ndip, Stephan Guttowski, Herbert Reichl, “On the Quantification of the State-of-the-Art Models for Surface Roughness Effect”, Oral Presentation: Signal Propagation on Interconnects (SPI), Strasbourg, France, May 2009.

- Brian Curran, Ivan Ndip, Stephan Guttowski, Herbert Reichl, “Modeling and Categorization of the Resistivity of Silicon Wafers For the Design of Silicon Based System Modules”, Oral Presentation: Semiconductor Conference Dresden (SCD), Dresden, Germany, Apr. 2009.

- Brian Curran, Ivan Ndip, Stephan Guttowski, Herbert Reichl, “Novel Multimodal High-Speed Structures Using Substrate Integrated Waveguides with Shielding Walls in Thin Film Technology”, Oral Presentation: Electronics Design of Advanced Packaging and Systems (EDAPS), Seoul, Korea, Dec. 12, 2008.

- Brian Curran, Ivan Ndip, Stephan Guttowski, Herbert Reichl, “Managing Losses in Through Silicon Vias with Different Return Current Path Configurations”, Oral Presentation: Electronic Packaging Technology Conference (EPTC), Singapore, Dec. 10, 2008.

- Brian Curran, Benjamin Wittwer, E.R. Srinidhi, Günter Kompa, “Highly Integrated Multi-Harmonic Tuner for Broadband High Power Source/Load-Pull System”, Oral Presentation: German Microwave Conference (GeMIC), Hamburg, Germany, March 11, 2008.